AD_____

Award Number: DAMD17-98-1-8278

TITLE: Analysis of the Role of Cortactin in Tumor Cell Invasion

PRINCIPAL INVESTIGATOR: Xi Zhan, Ph.D.

CONTRACTING ORGANIZATION: Holland Laboratory
American Red Cross
Rockville, Maryland 20855

REPORT DATE: July 2001

TYPE OF REPORT: Final

PREPARED FOR: U.S. Army Medical Research and Materiel Command
Fort Detrick, Maryland 21702-5012

REPORT DOCUMENTATION PAGE

Form Approved
OMB No. 074-0188

1. AGENCY USE ONLY (Leave blank)	2. REPORT DATE	3. REPORT TYPE AND DATES COVERED
	July 2001	Final (1 Jul 98 - 30 Jun 01)

4. TITLE AND SUBTITLE
Analysis of the Role of Cortactin in Tumor Cell Invasion

5. FUNDING NUMBERS
DAMD17-98-1-8278

6. AUTHOR(S)
Xi Zhan, Ph.D.

7. PERFORMING ORGANIZATION NAME(S) AND ADDRESS(ES)
Holland Laboratory
American Red Cross
Rockville, Maryland 20855
email - zhanx@usa.redcross.org

8. PERFORMING ORGANIZATION REPORT NUMBER

9. SPONSORING / MONITORING AGENCY NAME(S) AND ADDRESS(ES)
U.S. Army Medical Research and Materiel Command
Fort Detrick, Maryland 21702-5012

10. SPONSORING / MONITORING AGENCY REPORT NUMBER

11. SUPPLEMENTARY NOTES

12a. DISTRIBUTION / AVAILABILITY STATEMENT
Approved for Public Release; Distribution Unlimited

12b. DISTRIBUTION CODE

13. Abstract ***(Maximum 200 Words)*** *(abstract should contain no proprietary or confidential information)*

Cortactin is an actin cytoskeleton associated protein, frequently amplified and overexpressed along with the chromosome 11q13 in breast cancer, and acts as a prominent substrate of protein tyrosine kinase Src. We have hypothesized that cortactin plays a role in tumor progression by promoting metastasis. To test this hypothesis, we conducted a series of experiments aimed at characterizing the effects of cortactin and its mutant with a defect in tyrosine phosphorylation on cell motility *in vitro* and metastasis *in vivo*. These studies have eventually led to following conclusions: (1) cortactin is primarily implicated in actin cytoskeleton reorganization rather than DNA synthesis; (2) overexpression of wild type cortactin can increase cell motility and cell shape changes in response to growth factors and reactive oxygen species in a tyrosine phosphorylation dependent manner; (3) introduction of a cortactin mutant deficient in tyrosine phosphorylation can effectively inhibit cell motility and cell shape changes and depress tumor metastasis *in vivo*; and (4), the primary biochemical function of cortactin is to modulate actin polymerization by regulating the activity of Arp2/3 complex, a key machinery of actin polymerization. Our studies provide first evidence for the role of actin polymerization in tumor invasion and indicate a novel approach to suppress metastasis by targeting at actin polymerization.

14. Subject terms - breast cancer, cortactin, tyrosine phosphorylation	15. NUMBER OF PAGES 60
	16. PRICE CODE

17. SECURITY CLASSIFICATION OF REPORT	18. SECURITY CLASSIFICATION OF THIS PAGE	19. SECURITY CLASSIFICATION OF ABSTRACT	20. LIMITATION OF ABSTRACT
Unclassified	Unclassified	Unclassified	Unlimited

Table of Contents

Cover	1
SF 298	2
Table of Contents	3
Introduction	4
Body	5
Key Research Accomplishments	7
Reportable Outcomes	8
Conclusions	9
References	10

Introduction

Breast cancer is frequently associated with gene amplification of the chromosome 11q13, resulting in overexpression of cortactin, a cortical actin-associated protein and a prominent substrate of protein tyrosine kinase Src. Cortactin is accumulated in peripheral structures of cells including lamellipodia and membrane ruffles where cortical actin is enriched[1]. In MDA-MB-231 breast cancer cells plated on extracellular matrix cortactin is enriched in invadopodia, a type of membrane protrusions that participates in degradation of and invasion into the matrix[2]. While the precise role of cortactin in tumor progression remains unclear, amplification and overexpression of cortactin appear to be intimately associated with patients with poor prognosis or relapse[3], indicating that overexpression of cortactin may contribute to a late stage of tumor progression. The protein sequence of cortactin is featured by six and half tandem copies of a unique 37-amino-acid repeat and a Src homology 3 (SH3) domain at the carboxyl terminus. We have demonstrated that Src-mediated tyrosine phosphorylation primarily occurs at residues Tyr-421, Tyr-466 and Tyr-482, which lie between the repeat domain and the SH3. *In vitro*, cortactin binds to and cross-links F-actin into meshwork. The F-actin cross-linking activity of cortactin can be reduced upon tyrosine phosphorylation mediated by Src[4]. Inhibition of tyrosine phosphorylation of cortactin by a selective Src inhibitor reduces the response of endothelial cells to hydrogen peroxide-mediated cell injury[5]. While these studies suggest that cortactin may play a role in tumor metastasis, direct evidence is lacking. The support by this grant has allowed us to perform a series of experiments aimed at testing whether or not cortactin or its mutants can modulate tumor cell motility and metastasis *in vivo*. Our results provide evidence that cortactin is a suitable target to inhibit tumor metastasis.

Body

Experiments have been designed and performed in order to achieve the two tasks as proposed in the original grant. The results are summarized following. Detailed information about experimental procedures and results is described in the papers or manuscript attached in the Appendix.

Task 1. Develop cortactin mutants that can interfere with the function of endogenous cortactin within cells.

To achieve this task, we focused on a cortactin mutant where the tyrosine residues Tyr421, Tyr462 and Tyr482 are converted to Phe. In an early study, we demonstrated these three residues are the main targets by Src [6]. In the beginning of the funding period, we analyzed the response of the mutant carrying these mutated residues to tyrosine phosphorylation induced by fibroblast growth factor (FGF) in NIH3T3 cells. This study has led to the conclusion that these three tyrosine residues are essential for FGF-mediated phosphorylation of cortactin [7]. In a parallel experiment, we also introduced the mutant into human umbilical vein endothelial cells (HUVEC) through a retroviral vector [8]. Because HUVEC are very susceptible to changes in the presence of reactive oxygen species such as hydrogen peroxide, the cells were chosen to evaluate the activity of the cortactin mutant. As described in detail in the paper [8] attached in Appendix, HUVEC expressing wild-type cortactin enhanced the response to hydrogen peroxide mediated shape changes and the mutant deficient in tyrosine phosphorylation suppressed the shape changes. This result and the data from other studies have established that the mutation of cortactin at tyrosine phosphorylation can modulate the function of endogenous cortactin in a dominant negative manner.

Task 2. Analyze the effects of cortactin mutants on the invasive ability of breast cancer cells.

Having established the function of the cortactin mutant in tyrosine phosphorylation, we further analyzed the MDA-MB-231 breast tumor cells. Using the similar approach with retrovirus, we have successfully obtained 231 cells expressing wild type and the mutant cortactin deficient in tyrosine phosphorylation. These cells were evaluated for cell motility changes either *in vitro* or *in vivo*. The *in vitro* analysis was focused on cell migration and invasion through endothelial cells that were analyzed using a Transwell apparatus. The result of this analysis showed that the cells that overexpress wild type cortactin increased their motility whereas the cells expressing the cortactin mutant impaired the motility [9]. This result was consistent with the observation made in the analysis of shape changes in response to hydrogen peroxide. We also evaluated the cell proliferation potential of these cells and found that either wild type or mutant forms of cortactin did not have any effect on cell growth. Thus, cortactin appears to actin specifically in cell motility and cell shape changes rather than cell growth, in which most oncogenes are implicated.

To further confirm the function of cortactin in tumor progression, we also evaluated the metastatic potential of cortactin expressing tumor cells based on an experimental bone metastasis assay in mice [9]. This experiment resulted in a very similar conclusion to that obtained with *in vitro* assay: wild type cortactin enhances bone metastasis by 85% while the mutant suppressed

metastasis by 75%. Thus, these results provide first direct evidence showing that overexpression of wild type cortactin can potentiate tumor progression. In addition, they also indicate that cortactin is potentially suitable target to inhibit tumor metastasis.

Key Research Accomplishments

1. Established a cortactin mutant deficient in tyrosine phosphorylation that can act as a dominant negative mutant
2. Analyzed the function of tyrosine phosphorylation of cortactin in cell growth and cell motility
3. Established various assays to analyze the function of cortactin both *in vitro* and *in vivo*
4. Demonstrated that cortactin plays an important role in tumor metastasis

Reportable Outcomes

Presentation

1. Era of Hope Meeting in June 2000
2. American Cell Biology of Society, December, 2000

Publications

1. Src is required for cell migration and shape changes induced by fibroblast growth factor 1 (1999). Oncogene 18, 6700-6706.
2. Tyrosine phosphorylation of cortactin is required for H_2O_2-mediated injury of human endothelial cells (2000). J. Biol. Chem. 24, 37187-37193.
3. Activation of Arp2/3 complex mediated actin polymerization by cortactin (2001). Nature Cell Biology 3 259-266
4. Cortactin potentiates bone metastasis of breast cancer cells (2001). Cancer Research (in press)

Conclusions

Studies performed during this funding period have documented the important role of cortactin in tumor progression. Although the cortactin gene is frequently amplified in breast cancer, cortactin does not appear to be involved directly in the growth of tumors and unlikely to play a significant role in the early stage of tumor progression. Instead, cortactin is intimately involved in the actin cytoskeleton and its associated activities including shape changes and locomotion. Cortactin modulates the motility and metastatic potential of tumor cells in a tyrosine phosphorylation dependent manner. While overexpression of wild type cortactin enhances the migration and invasion of tumor cells *in vitro* and metastasis *in vivo*, a cortactin mutant deficient in tyrosine phosphorylation can impair both motility *in vitro* and metastasis *in vivo*. Thus, cortactin may be a suitable target for the future approaches aimed at inhibiting metastasis.

Reference:

1. Wu,H. & Parsons,J.T. Cortactin, an 80/85-kilodalton pp60src substrate, is a filamentous actin-binding protein enriched in the cell cortex. *J Cell Biol.* **120**, 1417-1426 (1993).
2. Bowden,E.T., Barth,M., Thomas,D., Glazer,R.I. & Mueller,S.C. An invasion-related complex of cortactin, paxillin and PKCmu associates with invadopodia at sites of extracellular matrix degradation. *Oncogene* **18**, 4440-4449 (1999).
3. Rodrigo,J.P., Garcia,L.A., Ramos,S., Lazo,P.S. & Suarez,C. EMS1 gene amplification correlates with poor prognosis in squamous cell carcinomas of the head and neck [In Process Citation]. *Clin. Cancer Res.* **6**, 3177-3182 (2000).
4. Huang,C. *et al.* Down-regulation of the filamentous actin cross-linking activity of cortactin by Src-mediated tyrosine phosphorylation. *J Biol. Chem.* **272**, 13911-13915 (1997).
5. Li,Y., Liu,J. & Zhan,X. Tyrosine phosphorylation of cortactin is required for H2O2-mediated of injury of human endothelial cells. *J Biol. Chem.* (2000).
6. Huang,C. *et al.* Down regulation of the F-actin crosslinking activity of cortactin by c-Src. *J. Biol. Chem.* **272**, 13911-13915 (1997).
7. Liu,J., Huang,C. & Zhan,X. Src is required for cell migration and shape changes induced by fibroblast growth factor 1. *Oncogene* **18**, 6700-6706 (1999).
8. Li,Y., Liu,J. & Zhan,X. The role of cortactin and Src in the H_2O_2-mediated injury of human endothelial cells. J.Cell Biol. 2000.
   Ref Type: Unpublished Work
9. Uruno,T. *et al.* Activation of Arp2/3 complex-mediated actin polymerization by cortactin. *Nat. Cell Biol.* **3**, 259-266 (2001).

Appendix

Oncogene (1999) 18, 6700–6706

http://www.stockton-press.co.uk/onc

Src is required for cell migration and shape changes induced by fibroblast growth factor 1

Jiali Liu[1], Cai Huang[1] and Xi Zhan*[,1,2]

[1]*Department of Experimental Pathology, Holland Laboratory of American Red Cross, 15601 Crabbs Branch Way, Rockville, Maryland, MD 20855, USA;* [2]*Department of Anatomy and Cell Biology, George Washington University 2300 I Street, Washington DC 20037, USA*

Fibroblast growth factor 1 (FGF-1) is a potent chemotactic factor and induces tyrosine phosphorylation of a cortical actin-associated protein (cortactin). The tyrosine phosphorylation of cortactin induced by FGF-1 requires the tyrosine residues 421, 482 and 466, which are targeted by the protein tyrosine kinase Src *in vitro*. Furthermore, FGF-1 is unable to induce tyrosine phosphorylation of cortactin within the cells derived from Src knockout mice ($Src^{-/-}$), indicating that Src is required for the tyrosine phosphorylation of cortactin induced by FGF-1. Although $Src^{-/-}$ cells are able to undergo rapid proliferation, they are impaired to respond to FGF-1 for the shape change and cell migration. Morphological analysis further reveals that FGF-1 fails to induce the formation of polarized lamellipodia and the translocation of cortactin into the leading edge of $Src^{-/-}$ cells. Consistent with the mitogenic response to FGF-1, the lack of Src does not affect the tyrosine phosphorylation of Snt (or Frs2), a FGF-1 early signaling protein that links to Ras. Therefore, our data support the notion that Src and cortactin participate in a FGF signal pathway for cell migration and shape change rather than mitogenesis.

Keywords: Src; FGF-1; cortactin

Introduction

The family of fibroblast growth factor (FGF) represents a large group of polypeptides that play important roles in embryonic development, tissue growth, wound healing, and angiogenesis (Burgess *et al.*, 1989). The prototypes of FGF, namely FGF-1 and FGF-2, are mitogenic and chemotactic for many mesenchyme-derived cells (Gospodarowicz, 1974; Maciag *et al.*, 1982). During the early response to FGF-1 or FGF-2, several intracellular proteins are phosphorylated at tyrosine residues (Huang *et al.*, 1986). These phosphotyrosyl proteins include phospholipase C γ (PLC-γ), Snt (or Frs2), Shc, Gab-1, and MAP kinases (Bogoyevitch *et al.*, 1994; Burgess *et al.*, 1990; Kouhara *et al.*, 1997; Ong *et al.*, 1997; Wang *et al.*, 1994, 1996). Whereas PLC-γ is important for FGF-mediated phosphatidylinositol turnover, it is not necessary for FGF-induced mitogenesis (Mohammadi *et al.*, 1992; Peters *et al.*, 1992). Snt encodes a protein that has an electrophoretic motility around 90 kDa (Kouhara *et al.*, 1997) and binds to FGF receptor 1 (FGFR-1) through its phosphotyrosine binding domain in a phosphotyrosine independent manner (Xu *et al.*, 1998). Snt functions as a lipid-anchored docking protein and targets the signaling adaptor Grb-2, either directly or through Sph-2 protein tyrosine phosphatase, to the plasma membrane (Hadari *et al.*, 1998; Kouhara *et al.*, 1997). Because Grb-2 binds to Sos, a Ras guanine nucleotide exchange factor (Buday *et al.*, 1993; Egan *et al.*, 1993; Rozakis-Adcock *et al.*, 1993), Snt is likely to be a primary component involved in the activation of the complexes of Ras/Raf/mitogen-activated protein kinase (MAPK), the major signal pathway from the plasma membrane to the nucleus. Likewise, Gab-1 (an IRS-related protein) and Shc act also as signaling adaptors and are likely involved in the similar pathway to the activation of Ras (Holgado-Madruga *et al.*, 1996; Rozakis-Adcock *et al.*, 1992). Although the exact roles of these molecules in the biological function of FGF are not fully elucidated, it is assumed that these factors may ultimately be important for the FGF's mitogenic activity.

It is less understood, however, how FGFs signal cell shape changes and migration. We have previously shown that FGF-1 requires a prolonged stimulation to reach a maximal mitogenic response (Zhan *et al.*, 1993a). Analysis of this late response (4–12 h) has revealed a series of tyrosine phosphorylated proteins that are not apparent during the early response. One of these proteins was characterized as cortactin, a prominent substrate of Src protein tyrosine kinase (Zhan *et al.*, 1993b). Cortactin is also a potent cross-linker for filamentous actin (F-actin) (Huang *et al.*, 1997) and co-localizes with F-actin in cell peripheral areas and punctate-like membrane structures (Wu *et al.*, 1993). We have recently described that the F-actin cross-linking activity of cortactin can be attenuated by Src-mediated tyrosine phosphorylation (Huang *et al.*, 1997). Furthermore, overexpression of a cortactin mutated at tyrosine phosphorylation sites impairs the migration of endothelial cells (Huang *et al.*, 1998). Therefore, these data indicate that cortactin acts as a modulator for the actin cytoskeleton.

The evidence for the role of Src in FGF signaling also begins emerging. In a previous investigation of FGF signaling, we described that the activated FGFR-1 is able to transiently associate with Src-like proteins in a manner dependent on tyrosine phosphorylation of FGFR-1 and the SH2 domain of Src (Zhan *et al.*, 1994). Overexpression of a normal Src can increase the response to FGF-1 mediated cellular scattering and motility (Rodier *et al.*, 1995). On the other hand, overexpression of a mutated form of Src inhibits the

*Correspondence: X Zhan, Department of Experimental Pathology, Holland Laboratory of American Red Cross, 15601 Crabbs Branch Way, Rockville, Maryland, MD 20855, USA
Received 7 December 1998; revised 1 July 1999; accepted 6 July 1999

scattering response without affecting mitogenesis induced by FGF-1 or EGF. In addition, the early withdrawal of FGF-1 from culture medium can induce cell migration without promoting DNA synthesis, this property is apparently correlated with a transient increase in Src kinase activity (LaVallee *et al.*, 1998). While these studies suggest that a Src-related activity may be involved in a FGF signaling independent on mitogenesis, neither the specific Src family members nor particular Src substrates have been defined. Furthermore, direct genetic evidence for the role of Src in the growth factor induced cell migration is still missing. In this report, we examined whether Src is required for the FGF-1 mediated tyrosine phosphorylation of cortactin within the cells derived from Src knockout mice. We found that a cortactin mutated at the tyrosine residues that are targeted by Src is impaired to respond to FGF-1 stimulation. In addition, cells lacking the Src gene are able to undergo proliferation in the presence of FGF-1, though these cells show fewer changes in morphology and have slower motility compared to normal cells. Furthermore, FGF-1 is able to induce tyrosine phosphorylation of Snt but not cortactin in Src knockout cells. These findings demonstrate that Src is the major kinase responsible for FGF-1-induced tyrosine phosphorylation of cortactin, and Src and cortactin are implicated in a signal pathway for cell migration and shape change, which is apparently distinct from that involved in the mitogenic response.

Results

Src is essential for the tyrosine phosphorylation of cortactin induced by FGF-1

In the attempt to verify that Src is required for the tyrosine phosphorylation of cortactin induced by FGF-1, we initially evaluated whether the tyrosine residues targeted by Src are necessary for FGF-1 mediated phosphorylation. In a previous study, we determined that the primary tyrosine residues targeted by Src reside at Tyr-421, Tyr-466 and Tyr-482 (Huang *et al.*, 1998). Thus, we analysed NIH3T3 cells expressing *myc*-Cort$_{F421F466F482}$, a cortactin mutant in which the three tyrosine residues are replaced with phenylalanines and the NH2-terminus is fused to the *myc* epitope (Huang *et al.*, 1998). As a control, a wild-type murine cortactin fused to the same *myc* epitope (*myc*-cortactin) was analysed in parallel. As shown in Figure 1, the level of tyrosine phosphorylated *myc*-cortactin significantly increased within 12 h after FGF-1 stimulation. In contrast, the mutant Cort$_{F421F466F482}$ failed to increase in its tyrosine phosphorylation in response to FGF-1. This result indicates that the tyrosine phosphorylation of cortactin induced by FGF-1 occurs at the same residues that are targeted by Src.

To further confirm the role of Src in the tyrosine phosphorylation of cortactin, we examined embryonic fibroblasts derived from the Src-knockout mice (Src$^{-/-}$) and fibroblasts derived from a normal mouse embryo (Src$^{+/+}$). The cells were maintained at near confluence in a serum-free defined medium supplemented with insulin (DMI) for 48 h and subsequently stimulated with FGF-1 for various times. The total cell lysates were prepared and analysed by immunophosphoty-rosine blot analysis. It appeared that Snt, which is a major FGF responsive protein and migrates at 90 kDa, was induced similarly in both types of cells (Figure 2a).

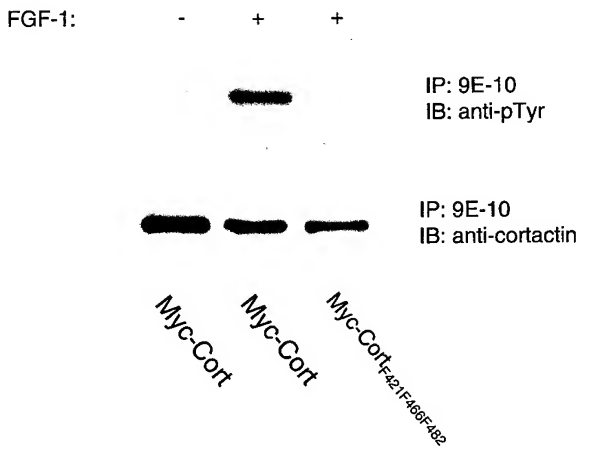

Figure 1 Tyrosine phosphorylation of cortactin induced by FGF-1 requires the tyrosine residues targeted by Src. Quiescent NIH3T3 cells expressing myc-Cort and myc-Cort$_{F421F466F466}$ were stimulated with FGF-1 for 12 h. The lysates from the stimulated cells were immunoprecipitated with a monoclonal cortactin antibody 9E-10 and further immunoblotted with a polyclonal phosphotyrosine antibody. The same blot was stripped and re-probed with the polyclonal cortactin antibody C001

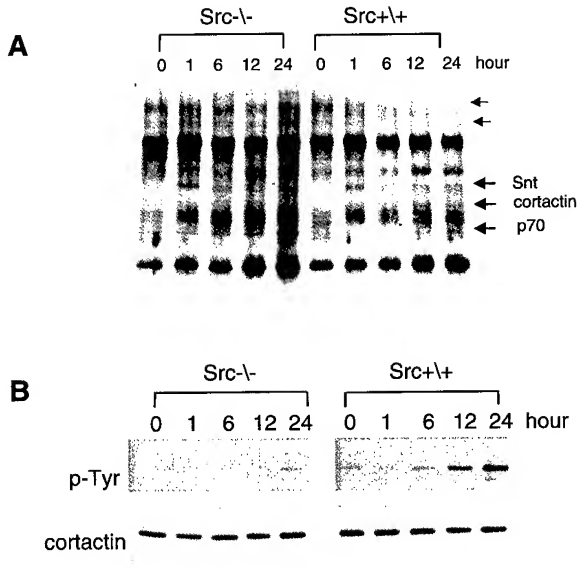

Figure 2 Tyrosine phosphorylation of cortactin in Src$^{-/-}$ cells. (**a**) Quiescent Src$^{-/-}$ and Src$^{+/+}$ cells were treated with FGF-1 for the times indicated. Total cell lysates were prepared by dissolving stimulated cells in SDS sample buffer. The lysates were then separated in SDS–PAGE and further blotted with monoclonal anti-phosphotyrosine antibody (4G10) as described in Materials and methods. (**b**) FGF-1 stimulated cell lysates were immunoprecipitated with a polyclonal cortactin antibody. The precipitates were immunoblotted with monoclonal anti-phosphotyrosine antibody 4G10

However, a phosphorylated band around 80 kDa was detected only in $Src^{+/+}$ but not in $Src^{-/-}$ cells (Figure 2a). The p80 band apparently co-migrated with cortactin (data not shown), which was further confirmed by immunoprecipitation with a cortactin antibody followed by immunophosphotyrosine blot analysis. As shown in Figure 2b, cortactin was hyperphosphorylated significantly in $Src^{+/+}$ cells after 12 h of FGF-1 stimulation. In contrast, it was weakly phosphorylated within $Src^{-/-}$ cells, although there was a slight increase in tyrosine phosphorylation of cortactin at 24 h of stimulation. This slight increase observed at 24 h was apparently due to a differential sample loading as indicated by analysing the same blot using a cortactin antibody (Figure 2b, the lower panel). Interestingly, we also observed several other phosphotyrosyl bands including one of 70 kDa and two bands between 130–200 kDa, which were actually enhanced in the FGF-1 stimulated $Src^{-/-}$ cells (Figure 2a). However, the identities of these bands are currently unknown. Taken together, these data demonstrated that Src is likely the primary kinase for FGF-induced phosphorylation of cortactin, and cortactin is apparently one of the major phosphotyrosyl proteins induced by FGF-1 in a Src-dependent manner.

Src is required for FGF-1-mediated cell shape change and migration

To elucidate the role of Src in the function of FGF-1, we also examined the morphological response of $Src^{-/-}$ and $Src^{+/+}$ to FGF-1. Under serum-starved culture conditions, both types of cells exhibited a typical quiescent morphology characterized by a flat monolayer (Figure 3). When the cells were exposed to FGF-

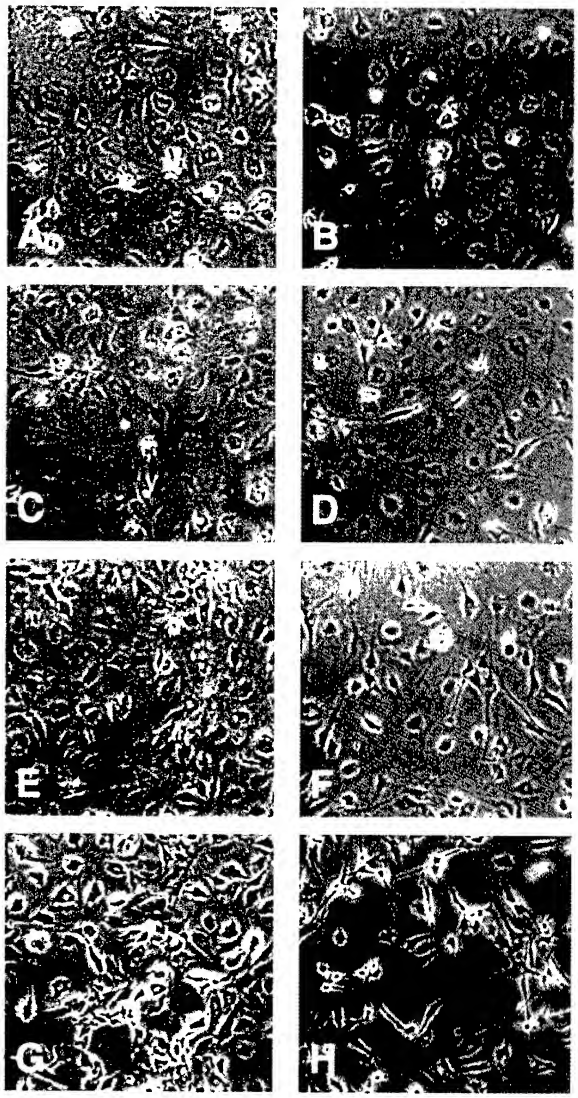

Figure 3 FGF-1 induces different morphological changes in $Src^{-/-}$ and $Src^{+/+}$ cells. Quiescent $Src^{-/-}$ (**a, c, e** and **g**) and $Src^{+/+}$ (**b, d, f** and **h**) cells were stimulated with FGF-1 for various times (**a** and **b**, 0 h; **c** and **d**, 6 h; **e** and **f**, 12 h; **g** and **h**, 24 h). Cells were inspected under a phase-contrast microscope

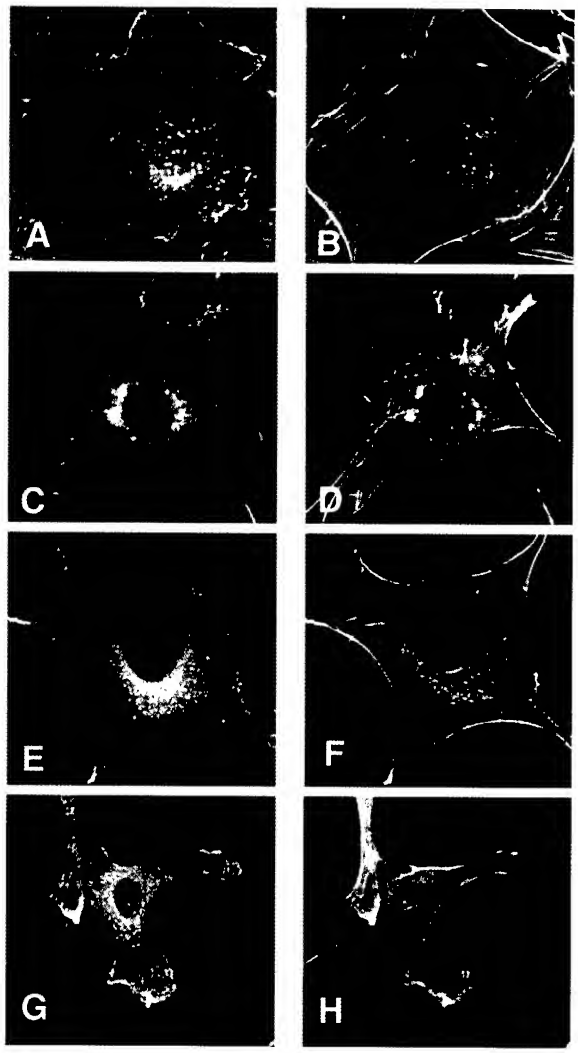

Figure 4 Redistribution of cortactin within $Src^{-/-}$ cells is impaired. Quiescent $Src^{-/-}$ (**a–d**) and $Src^{+/+}$ cells (**e–h**) were stimulated with or without FGF-1 for 15 h (**a, b, e** and **f**): untreated; **c, d, g** and **h**: FGF-1 treated). The cells were then double-stained with the polyclonal cortactin antibody C001 (**a, c, e** and **g**) and FITC-phalloidin (**b, d, f** and **h**) as described in Materials and methods. The stained cells were examined under a confocal microscope

1 for 12 h, $Src^{+/+}$ cells underwent a significant shape change typified by a greatly elongated cytoplasm (Figure 3). However, this change was not observed when $Src^{-/-}$ cells were analysed, although many of these cells round up after 12 h of FGF-1 stimulation. A close examination by confocal laser scanning microscopy also revealed a differential cortactin staining between these two types of cells. While cortactin was found within the areas around the periphery, the peri-nucleus, and punctate-like structures within the cytoplasm of both quiescent cells (Figure 4a,e), cortactin and F-actin co-stained abundantly within polarized lamellipodia, as defined by large intervening regions of the $Src^{+/+}$ cells at 12 h stimulation (Figure 4g,h). Concomitant with the association of more cortactin proteins with these polarized leading structures, less cortactin staining was detected in the peri-nucleus of FGF-1 treated $Src^{+/+}$ cells. In contrast, the $Src^{-/-}$ cells treated with FGF-1 did not show significantly polarized lamellipodia associated with cortactin and F-actin (Figure 4c,d). Instead, cortactin was more enriched at the peri-nucleus within those cells (Figure 4c).

The differential response of these cells to FGF-1 with respect to the morphological changes was apparently correlated with their motility as analysed by a wound-healing assay. As shown in Figure 5, both $Src^{-/-}$ and $Src^{+/+}$ cells did not show apparent migration within 6 h into the wounded areas generated by a rubber policeman when FGF-1 was absent (Figure 5a,c). In the presence of FGF-1, however, $Src^{+/+}$ cells displayed extensive elongation of their cytoplasm. Concomitant with the elongated morphology, many $Src^{+/+}$ cells were found in the wounded area (Figure 5d). In contrast, few $Src^{-/-}$ cells showed migration, although many of them exhibited rounding-up morphology (Figure 5b).

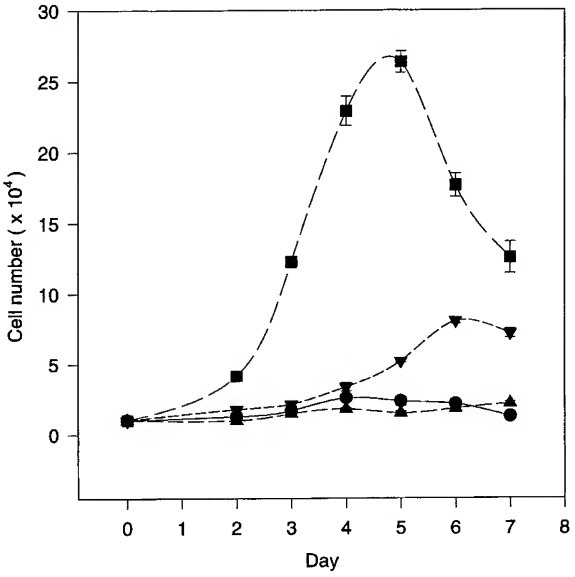

Figure 6 The lack of Src does not affect cell proliferation. $Src^{-/-}$ and $Src^{+/+}$ cells were seeded at 1×10^4 cells per well in a 24-well plate. At 8 h after plating, the culture medium was changed to DMI supplemented with FGF-1 (10 ng/ml) and heparin (10 units/ml). In the control samples, cells were maintained in DMI. At the times indicated, cells were trypsinized and counted using a hemocytometer. Each time point represents a mean of three independent experiments. Labels: ●, $Src^{-/-}$ in DMI only; ■, $Src^{-/-}$ in DMI plus FGF-1; ▲, $Src^{+/+}$ in DMI; and ▼, $Src^{+/+}$ in DMI plus FGF-1

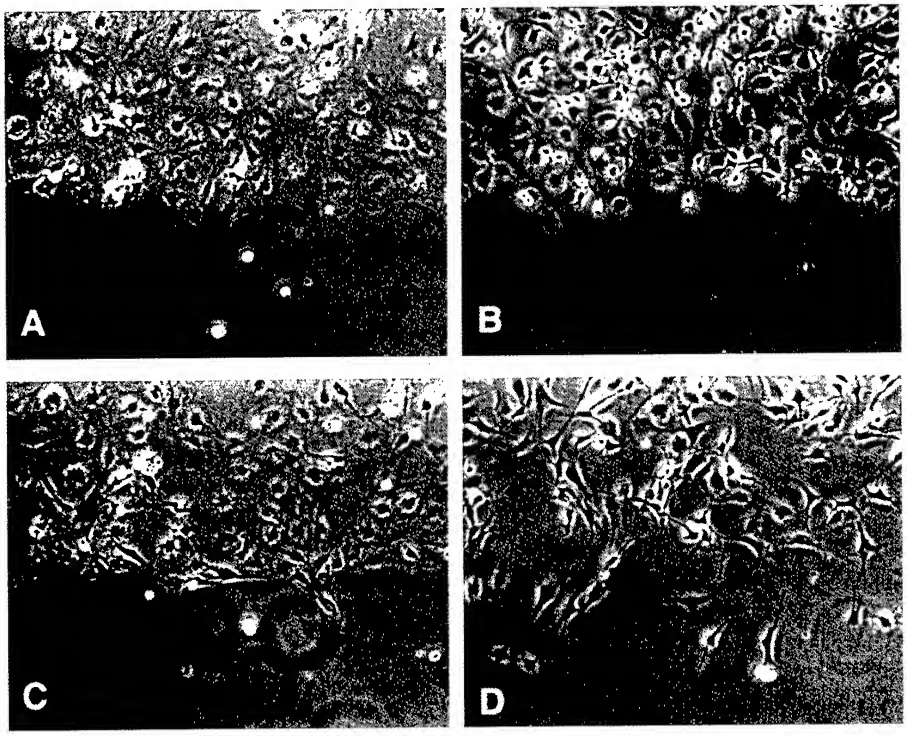

Figure 5 The lack of Src impairs cell migration. Quiescent $Src^{-/-}$ (**a** and **b**) and $Src^{+/+}$ cells (**c** and **d**) were stimulated with (**b** and **d**) or without FGF-1 (**a** and **c**). After 20 h of stimulation, the monolayers were wounded with a rubber policeman. The photographs were taken at 6 h after wounding

Src is not required for FGF-1 mediated cell proliferation

The rounding-up morphology exhibited by $Src^{-/-}$ cells in the presence of FGF-1 suggested that those cells were able to undergo mitosis. To further confirm this notion, we have measured their proliferative response to FGF-1. Both $Src^{-/-}$ and $Src^{+/+}$ cells were plated at approximately 5% confluence and maintained in DMI supplemented with FGF-1. As shown in Figure 6, both types of cells grew in a FGF-1-dependent manner. Interestingly, $Src^{-/-}$ cells appeared to grow even faster than $Src^{+/+}$ cells. The maximal number of $Src^{-/-}$ cells in the presence of FGF-1 was nearly four times higher than that of $Src^{+/+}$ cells (Figure 6). Thus, the lack of Src apparently does not inhibit but actually enhances the response to FGF-1 for proliferation.

Discussion

In this study, we provided evidence that Src is required for FGF-1-mediated shape change and cell migration. Our conclusion further supports the notion that Src plays a vital role in the signaling pathways for cell migration and shape change triggered by growth factors. However, our data also demonstrate that Src is not required for the FGF-1 mediated cell proliferation. In fact, the cells lacking Src grow much faster than normal cells (Figure 6). Consistent with the mitogenic response to FGF-1, the lack of Src does not impair the tyrosine phosphorylation of Snt (or Frs2). Snt has been shown to be a direct substrate for FGF receptors (Xu *et al.*, 1998). Because Snt shares homologous sequence with insulin receptor substrate 1, and binds to Grb-2 proteins, it is likely a major signaling molecule linking to the Ras/MAPK pathway and is essential for FGF's mitogenic activity. Thus, it appears that Src and cortactin are involved in a discrete signal pathway that primarily regulates the cytoskeletal changes. In support of this notion, transient FGF stimulation does not induce a maximum DNA synthesis but is able to induce the activation of Src and tyrosine phosphorylation of cortactin (LaVallee *et al.*, 1998). Furthermore, it is known that oncogenic Src (v-Src) transforms cells in a manner independent of MAPK, a key component for its mitogenic activity (Oldham *et al.*, 1998).

In light of the presence of many members in the Src family and other non-receptor tyrosine kinases (Thomas *et al.*, 1997), FGF-1 could utilize kinases other than Src to phosphorylate these molecules, as indicated by a recent report that FER, a non Src-related intracellular tyrosine kinases, is involved in a PDGF-mediated cortactin phosphorylation (Kim *et al.*, 1998). However, we found that the tyrosine phosphorylation of cortactin induced by FGF-1 is significantly impaired in the cells deficient in Src alone. Furthermore, the tyrosine residues targeted by Src are the same as those mediated by FGF-1 (Figure 1). These results reinforce the notion that cortactin is a preferred substate for Src compared to other Src-related kinases (Thomas *et al.*, 1995). It is also noteworthy that cortactin is the major tyrosine phosphorylated protein that is impaired in FGF-1-induced $Src^{-/-}$ cells (Figure 6a).

Cortactin is a cell periphery-associated protein that binds to and cross-links filamentous actin (Huang *et al.*, 1997; Zhan *et al.*, 1993b). In quiescent $Src^{-/-}$ or $Src^{+/+}$ cells, cortactin localizes evenly around the cell margins. This is consistent with our previous report that a mutant lacking tyrosine phosphorylation sites is still able to associate with cell peripheral structures in endothelial cells (Huang *et al.*, 1998). However, in FGF-stimulated $Src^{+/+}$ cells, the majority of cortactin was accumulated in the leading edges of the cells. This accumulation was apparently impaired within $Src^{-/-}$ cells, where cortactin is more concentrated around the nucleus. Thus, it appears that Src is required for the dynamic movement of cortactin within the cytoplasm. Interestingly, the rearranged cortactin co-localizes with F-actin either in newly formed lamellipodia in normal cells (Figure 4h) or around the nucleus (Figure 4d) in $Src^{-/-}$ cells, indicating that the movement of cortactin within cells is coupled with F-actin. A recent report has described that Rac is involved in the translocation of cortactin in PDGF-stimulated cells (Weed *et al.*, 1998). While Src can reportedly activate Ras-like GTPase (Chang *et al.*, 1995; Schieffer *et al.*, 1996), the lack of Src is unlikely to affect the activation of Rac in FGF treated cells because Src is not required for the activation of Snt, a primary signaling molecule that links to Ras, which in turn can activate Rac (Hall, 1998). Alternatively, the dynamic movement of cortactin requires its tyrosine phosphorylation, which apparently attenuates its F-actin cross-linking activity (Huang *et al.*, 1997). It has been suggested that the movement of cellular particles is due to a retrograde actin flow, a movement of newly formed actin filaments from the front of lamellipodia to the opposite direction of cell forward (Cramer, 1997). One model for the driving actin retrograde flow is that disassociation of cross-linked actin network at the back of the lamellipodium will generate a tension gradient which can drive retrograde flow of actin (Mogilner *et al.*, 1996). Thus, it will be of interest to define whether cortactin is involved in a driving force for actin retrograde flow. Further experiments using mutants for each of these pathways should dissect the mechanism for the cortactin translocation induced by FGF-1.

Materials and methods

Reagents

All chemicals unless otherwise indicated were from Sigma-Aldrich Inc. (St. Louis, MO, USA). Cortactin antibodies C001 and 2719 were prepared from rabbit as previously described (Zhan *et al.*, 1994, 1993b). Monoclonal antibody against the myc epitope 9E-10 was a gift from Tom Maciag (Maine Medical Center, Portland, ME, USA).

Cell culture

Embryonic fibroblasts derived from a Src knockout mouse ($Src^{-/-}$, clone 1) and embryonic fibroblasts from a normal mouse ($Src^{+/+}$, clone 8) were obtained as gifts from Soriano Phillipo (Washington University, Seattle, WA, USA). Cells are cultured in Dulbecco's modified Eagle's medium (DMEM) (Fisher Scientific, Pittsburgh, PA, USA) supplemented with 10% fetal calf serum and antibiotics. Quiescent monolayer cells were achieved by growing nearly to

confluence in a serum free defined medium supplemented with 10 μg/ml insulin (DMI) for 48 h (Zhan *et al.*, 1986). The stimulation of FGF-1 was initiated by adding recombinant human FGF-1 (10 ng/ml) and heparin (10 units/ml) to the culture.

Cell migration

Quiescent $Src^{-/-}$ and $Src^{+/+}$ cells were stimulated with FGF-1 as described above. After 20 h of stimulation, monolayers of the cells were wounded with a rubber policeman (2 mm wide). The cultures were photographed after 6 h of wounding.

Cell growth assay

Cells were seeded at 1×10^4 cells per well in a 24-well plate containing DMEM supplemented with 10% calf serum. At 8 h after seeding, the medium was changed to DMI supplemented with FGF-1 (10 ng/ml) and heparin (10 units/ml). In the control samples, DMI without FGF-1 was applied. The treated cells were harvested by trypsinization at the times indicated and counted under a phase-contrast microscope using a hemocytometer. For each time point, three wells of culture were analysed.

Analysis of tyrosine phosphorylation of cortactin

Quiescent cells were stimulated with FGF-1 as described above. At the times indicated, cells were harvested and lysed in RIPA buffer (10 mM Tris-HCl, pH 7.5, 1.0 mM EDTA, 150 mM NaCl, 1% Triton X-100, 0.1% sodium dodecyl sulfate, 0.5% sodium deoxycholate, 1.0 mM sodium orthovanadate, 10 μg/ml aprotinin, 10 μg/ml leupeptin, 1.0 mM phenylmethylsulfonyl fluoride), and clarified by centrifugation in a microcentrifuge for 10 min. The supernatants were immunoprecipitated with anti-cortactin antibody 2719 (Zhan *et al.*, 1993b). The immunoprecipitates were then resolved in a SDS-polyacrylamide gel electrophoresis (PAGE) (7.5%, w/v), transferred to a nitrocellulose membrane and further probed with anti-phosphotyrosine antibody (4G10, Upstate Biotechnology Inc. Lake Placid, NY, USA). The blot membrane was stripped and re-probed with the monoclonal cortactin antibody 4F11 (Upstate Biotechnology Inc. Lake Placid, NY, USA) (Wu *et al.*, 1993).

Analysis of cortactin mutants in NIH3T3 cells

The plasmid pMyc-cortactin (encoding a murine cortactin tagged by the *myc* epitope at its NH_2-terminus) and p-Myc-$Cort_{F421F466F482}$ (encoding a murine cortactin where tyrosine residues 421, 466 and 482 were changed to phenylalanine) were previously described (Huang *et al.*, 1998). The two plasmids were transfected into NIH3T3 cells with the Transfection MBS Mammalian Transfection Kit according to the manufacturer's recommended procedure (Stratagene, La Jolla, CA, USA). Stable transfectants were subsequently selected in DMEM containing 10% calf serum and 0.8 mg/ml G418 (Life Technologies, Gaithersburg, MD, USA). Quiescent transfected cells were stimulated with FGF-1 for 12 h and the cell lysates were immunoprecipitated with 9E-10 antibody against the *myc*-epitope. The precipitates were then subjected to immunoblot with a polyclonal phosphotyrosine antibody (Zhan *et al.*, 1993a). The blot was stripped and then re-probed with cortactin antibody C001.

Immunofluorescent analysis

$Src^{-/-}$ and $Src^{+/+}$ cells were grown on fibronectin-coated glass cover slips and maintained in DMI for 48 h. Cells were then stimulated with FGF-1 for overnight, double stained with cortactin antibody C001 and fluorescein-isothiocyanate-phalloidin, and examined by confocal laser microscopy as previously described (Huang *et al.*, 1998).

Abbreviations

F-actin, filamentous actin; FGF, fibroblast growth factor; DMI, defined serum-free medium supplemented with insulin; PAGE, polyacrylamide gel electrophoresis; FITC, fluorescein-isothiocyanate; PLC, phospholipase C.

Acknowledgements

We thank Dr Soriano Phillipe for providing Src knockout and normal mouse embryonic fibroblasts. We acknowledge the help of Dr Christian Haudenschild in confocal image analysis. We also thank Ms Yamei Gao and Ms Diana Norman for the photography, and Ms Donna Sobieski for the critical reading of the manuscript. This work was supported by National Institutes of Health grant R29 HL52753 and US Army grant DAMD17-98-8278 (X Zhan).

References

Bogoyevitch MA, Glennon PE, Andersson MB, Clerk A, Lazou A, Marshall CJ, Parker PJ and Sugden PH. (1994). *J. Biol. Chem.*, **269**, 1110–1119.

Buday L and Downward J. (1993). *Cell*, **73**, 611–620.

Burgess WH, Dionne CA, Kaplow J, Mudd R, Friesel R, Zilberstein A, Schlessinger J and Jaye M. (1990). *Mol. Cell Biol.*, **10**, 4770–4777.

Burgess WH and Maciag T. (1989). *Annu. Rev. Biochem.*, **58**, 575–606.

Chang JH, Gill S, Settleman J and Parsons SJ. (1995). *J. Cell. Biol.*, **130**, 355–368.

Cramer LP. (1997). *Front. Biosci.*, **2**, d260–d270.

Egan SE, Giddings BW, Brooks MW, Buday L, Sizeland AM and Weinberg RA. (1993). *Nature*, **363**, 45–51.

Gospodarowicz D. (1974). *Nature*, **249**, 123–127.

Hadari YR, Kouhara H, Lax I and Schlessinger J. (1998). *Mol. Cell. Biol.*, **18**, 3966–3973.

Hall A. (1998). *Science*, **279**, 509–514.

Holgado-Madruga M, Emlet DR, Moscatello DK, Godwin AK and Wong AJ. (1996). *Nature*, **379**, 560–564.

Huang C, Liu J, Haudenschild CC and Zhan X. (1998). *J. Biol. Chem.*, **273**, 25770–25776.

Huang C, Ni Y, Gao Y, Wang T, Haudenschild CC and Zhan X. (1997). *J. Biol. Chem.*, **272**, 13911–13915.

Huang SS and Huang JS. (1986). *J. Biol. Chem.*, **261**, 9568–9571.

Kim L and Wong TW. (1998). *J. Biol. Chem.*, **273**, 23542–23548.

Kouhara H, Hadari YR, Spivak-Kroizman T, Schilling J, Bar-Sagi D, Lax I and Schlessinger J. (1997). *Cell*, **89**, 693–702.

LaVallee TM, Prudovsky IA, McMahon GA, Hu X and Maciag T. (1998). *J. Cell Biol.*, **141**, 1647–1658.

Maciag T, Hoover GA and Weinstein R. (1982). *J. Biol. Chem.*, **257**, 5333–5336.

Mogilner A and Oster G. (1996). *Biophys. J.*, **71**, 3030–3045.

Mohammadi M, Dionne CA, Li W, Li N, Spivak T, Honegger AM, Jaye M and Schlessinger J. (1992). *Nature,* **358,** 681–684.

Oldham SM, Cox AD, Reynolds ER, Sizemore NS, Coffey Jr RJ and Der CJ. (1998). *Oncogene,* **16,** 2565–2573.

Ong SH, Lim YP, Low BC and Guy GR. (1997). *Biochem. Biophys. Res. Commun.,* **238,** 261–266.

Peters KG, Marie J, Wilson E, Ives HE, Escobedo J, Del Rosario M, Mirda D and Willliams LT. (1992). *Nature,* **358,** 678–681.

Rodier JM, Valles AM, Denoyelle M, Thiery JP and Boyer B. (1995). *J. Cell Biol.,* **131,** 761–773.

Rozakis-Adcock M, Fernley R, Wade J, Pawson T and Bowtell D. (1993). *Nature,* **363,** 83–85.

Rozakis-Adcock M, McGlae J, Mbamalu G, Pelicci G, Daly R, Li W, Batzer A, Thomas S, Brugge J and Pelicci PG. (1992). *Nature,* **360,** 689–692.

Schieffer B, Paxton WG, Chai Q, Marrero MB and Bernstein KE. (1996). *J. Biol. Chem.,* **271,** 10329–10333.

Thomas SM and Brugge JS. (1997). *Annu. Rev. Cell Dev. Biol.,* **13,** 513–609.

Thomas SM, Soriano P and Imamoto A. (1995). *Nature,* **376,** 267–271.

Wang JK, Gao G and Goldfarb M. (1994). *Mol. Cell. Biol.,* **14,** 181–188.

Wang JK, Xu H, Li HC and Goldfarb M. (1996). *Oncogene,* **13,** 721–729.

Weed SA, Du Y and Parsons JT. (1998). *J. Cell Sci.,* **111,** 2433–2443.

Wu H and Parsons JT. (1993). *J. Cell Biol.,* **120,** 1417–1426.

Xu H, Lee KW and Goldfarb M. (1998). *J. Biol. Chem.,* **273,** 17987–17990.

Zhan X and Goldfarb M. (1986). *Mol. Cell Biol.,* **6,** 3541–3544.

Zhan X, Hu X, Friesel R and Maciag T. (1993a). *J. Biol. Chem.,* **268,** 9611–9620.

Zhan X, Hu X, Hampton B, Burgess WH, Friesel R and Maciag T. (1993b). *J. Biol. Chem.,* **268,** 24427–24431.

Zhan X, Plourde C, Hu X, Friesel R and Maciag T. (1994). *J. Biol. Chem.,* **269,** 20221–20224.

Activation of Arp2/3 complex-mediated actin polymerization by cortactin

Takehito Uruno*, Jiali Liu*, Peijun Zhang*†, Ying-xin Fan*, Coumaran Egile‡, Rong Li‡, Susette C. Mueller§ and Xi Zhan*¶#

*Department of Experimental Pathology, Holland Laboratory, American Red Cross, 15601 Crabbs Branch Way, Rockville, Maryland 20855, USA
†Institute of Oceanology, Chinese Academy of Sciences, Qingdao 266071, China
‡Department of Cell Biology, Harvard Medical School, 240 Longwood Avenue, Boston, Massachusetts 02115, USA
§Department of Oncology, Georgetown University School of Medicine, Washington DC 20007, USA
¶Department of Cell Biology and Anatomy, The George Washington University, Washington DC 20037, USA
#e-mail: zhanx@usa.redcross.org

Cortactin, a filamentous actin (F-actin)-associated protein and prominent substrate of Src, is implicated in progression of breast tumours through gene amplification at chromosome 11q13. However, the function of cortactin remains obscure. Here we show that cortactin co-localizes with the Arp2/3 complex, a *de novo* actin nucleator, at dynamic particulate structures enriched with actin filaments. Cortactin binds directly to the Arp2/3 complex and activates it to promote nucleation of actin filaments. The interaction of cortactin with the Arp2/3 complex occurs at an amino-terminal domain that is rich in acidic amino acids. Mutations in a conserved amino-acid sequence of DDW abolish both the interaction with the Arp2/3 complex and complex activation. The N-terminal domain is not only essential but also sufficient to target cortactin to actin-enriched patches within cells. Interestingly, the ability of cortactin to activate the Arp2/3 complex depends on an activity for F-actin binding, which is almost 20-fold higher than that of the Arp2/3 complex. Our data indicate a new mechanism for activation of actin polymerization involving an enhanced interaction between the Arp2/3 complex and actin filaments.

Gene amplification at chromosome 11q13 constitutes an important genetic mechanism for the progression of several cancers, including breast cancer and head and neck carcinomas[1]. This amplification often results in overexpression of cortactin, an F-actin-associated protein[2,3]. Although overexpression of cortactin is usually correlated with poor prognosis[4], presumably because of enhanced metastasis, its biochemical and biological functions remain unclear.

Cortactin is known to be a prominent substrate for several non-receptor protein tyrosine kinases, including Src, Fer and Syk[2,5–7]. Increased tyrosine phosphorylation of cortactin is a common cellular response to growth factors, stress, cell shrinkage, and cell injury mediated by oxygen-reactive radicals[3,8–10]. *In vitro*, tyrosine phosphorylation mediated by Src reduces the F-actin-crosslinking activity of cortactin[11]. Cortactin has a unique structure that features 6.5 tandem repeats of a 37-amino-acid sequence and a carboxy-terminal SH3 domain (Fig. 1a). Between the repeat and the SH3 domain lie a proline-rich sequence, an α-helical region and three tyrosine residues that are targeted by Src-related kinases[12]. Cortactin also contains an N-terminal domain, the sequence of which is conserved across species and in HS1, a cortactin-related protein that is exclusively expressed in the haematopoietic lineage[13]. In cultured fibroblasts, cortactin is mainly distributed within the leading edges of cells, for example in lamellipodia and punctate-like structures[2,12]. In MDA-MB-231 cells, an invasive breast cancer cell line, cortactin is associated with the invadopodium, a cortical structure that penetrates into and degrades the extracellular matrix during invasion[14]. In addition to tumour cells, cortactin is also implicated in the phagocytosis of several invasive bacteria, including *Shigella flexneri*, *Chlamydia trachomatis* and enteropathogenic or enterohaemorrhagic *Escherichia coli*[15–17]. Upon contact with the host cell, these invasive bacteria induce subcortical actin polymerization, which leads to their uptake by the host. Cortactin is accumulated either at the attachment sites or around the macropinocytic vacuole. However, the exact function of cortactin in the formation of the invasive structure is currently unknown.

Over the past few years, considerable effort has been devoted towards the identification of factors involved in the *de novo* assembly of actin-rich structures. Among them, the Arp2/3 complex has emerged as a key regulator of actin-filament nucleation that is conserved from yeast to humans[18]. The complex is composed of seven subunits, including two actin-related proteins, Arp2 and Arp3, and five further subunits. It is concentrated in dynamic actin structures such as the leading edges of motile cells and cellular structures[19]. The Arp2/3 complex is able to bind to the pointed ends and to the sides of actin filaments, and these activities are thought to be involved in the formation of the branched structures observed both *in vivo* at the leading edges of motile cells[20] and *in vitro*[21]. The purified complex exhibits a low-level actin-nucleation activity that can be enhanced by cellular proteins such as members of the Wiskott–Aldrich-syndrome protein (WASP) family[22–26] or by bacterial proteins such as *Listeria* ActA[19,27].

Here we show that cortactin binds to the Arp2/3 complex through its N-terminal domain and stimulates its actin-nucleation activity. Association with the Arp2/3 complex is also essential and sufficient for cortactin to localize within actin-rich patches. Furthermore, we show that the F-actin-binding activity of cortactin is essential for cortactin to stimulate the Arp2/3 complex. Our results imply a new mechanism for the regulation of actin polymerization nucleated by the Arp2/3 complex.

Results

Cortactin interacts directly with the Arp2/3 complex. The N terminus of cortactin is remarkably conserved from humans to *Drosophila* as well as in HS1 (Fig. 1a). This sequence contains ten

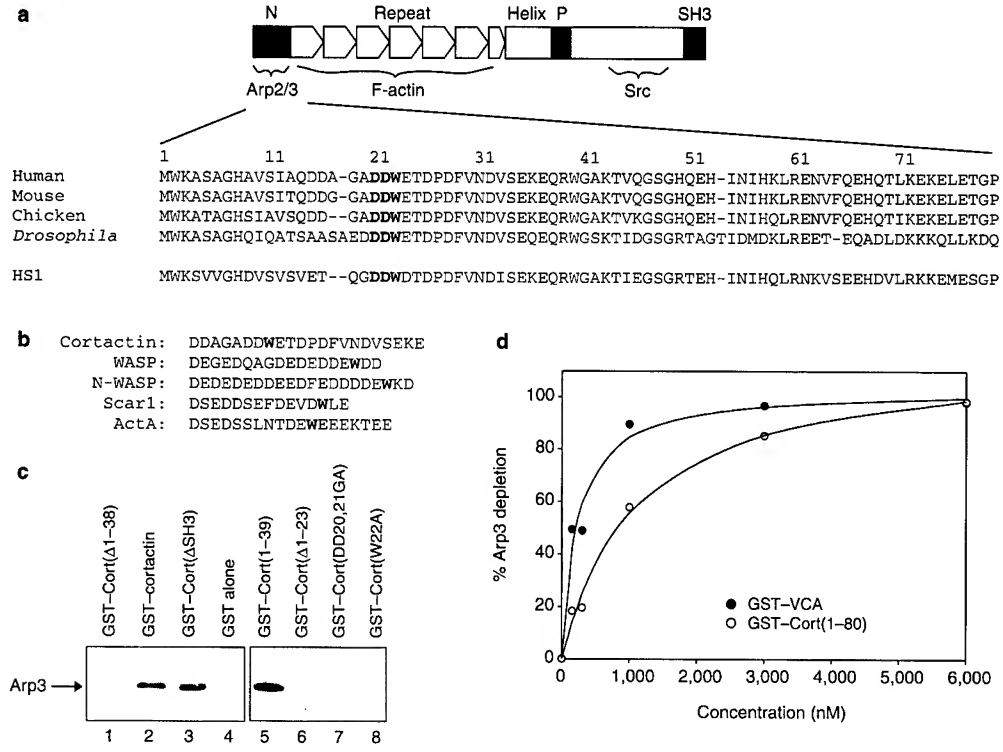

Figure 1 **Characterization of the interaction of cortactin with the Arp2/3 complex. a**, Schematic representation of the structural domains of cortactin. The domains that are targeted by the Arp2/3 complex, F-actin and Src are labelled. The amino-acid sequence of the N-terminal domain (residues 1–80) was compared across species and with HS1. N, N terminus; P, proline-rich sequence; SH3, Src-homology 3 domain. **b**, Comparison of the N-terminus of human cortactin with the acidic domains of human WASP, N-WASP, Scar and *Listeria* ActA. Conserved tryptophan residues are shown in bold. **c**, Interaction of recombinant cortactin proteins with purified Arp2/3 complex. Recombinant GST-tagged cortactin derivatives (5 μg) were incubated with 10 pmol of purified bovine Arp2/3 complex. The resulting protein complexes were precipitated with glutathione–sepharose and immunoblotted with anti-Arp3 antibody. **d**, Estimation of the affinity of the N-terminus of cortactin for the Arp2/3 complex. Purified Arp2/3 complex (4 nM) was incubated with the indicated amounts of immobilized GST–Cort(1–80) or GST–VCA for 90 min at 4 °C. After incubation, samples were centrifuged at 800*g* for 10 s. The presence of Arp3 in the supernatants was detected by SDS–PAGE followed by immunoblotting with anti-Arp3 antibody. Amounts of Arp3 were quantified by digital scanning and were normalized to percentage depletion. The resulting data were used to fit a rectangular hyperbola, yielding apparent K_d values of 1,095 nM and 222 nM for GST–Cort(1–80) and GST–VCA, respectively.

acidic amino acids and a tryptophan residue. Similar sequences are also present in WASP-like proteins and in ActA (Fig. 1b) and have been shown to be required for the interaction of these proteins with the Arp2/3 complex[19,24,27,28]. To determine whether cortactin physically interacts with the Arp2/3 complex, we examined the association of glutathione-*S*-transferase (GST)-tagged cortactin with purified bovine Arp2/3 complex in an *in vitro* pull-down assay. As shown in Fig. 1c, lane 2, the Arp2/3 complex was pulled down by GST–cortactin but not by GST beads (lane 4), indicating that the Arp2/3 complex can interact directly with cortactin.

To identify the cortactin domain that binds to the Arp2/3 complex, we generated a series of cortactin mutants and analysed their interactions with the Arp2/3 complex in pull-down assays using GST–cortactin beads. As shown in Fig. 1c and summarized in Fig. 2a, the N terminus of murine cortactin (residues 1–39) is essential and sufficient to bind to the Arp2/3 complex. To test whether the acidic amino-acid residues and the tryptophan located in the N terminus are important for cortactin to bind to the Arp2/3 complex, we prepared two cortactin variants bearing point mutations — one containing a DD20,21GA mutation and the other containing W22A. As summarized in Fig. 2a, both mutations abolished the interaction with the Arp2/3 complex.

These data indicate that cortactin may bind to the Arp2/3 complex in a manner similar to that of WASP-related proteins and of ActA. However, the affinity of cortactin for the Arp2/3 complex seemed to be weaker than that of WASP proteins. On the basis of the cortactin N-terminal peptide GST–Cort(1–80), we estimated that the dissociation constant (K_d) of cortactin for the Arp2/3 complex is ~1 μM (Fig. 1d). Under the same conditions, we estimated the K_d for a GST-tagged peptide encoding a verprolin-cofilin-acidic homology domain (GST–VCA), a constitutively active peptide derived from N-WASP[25], as 220 nM (Fig. 1d).

Cortactin activates the nucleation activity of the Arp2/3 complex. We examined the effect of cortactin on the activity of the Arp2/3 complex in more detail using an *in vitro* actin-polymerization assay with pyrene-labelled monomeric actin (G-actin). Cortactin alone had no apparent effect on spontaneous actin polymerization, which is consistent with our previous findings[11], whereas the Arp2/3 complex alone at 250 nM increased moderately the rate of actin polymerization (Fig. 3a). However, combination of the Arp2/3 complex and cortactin significantly reduced the initial lag phase. The half-time to reach a steady state of actin polymerization in the presence of both the Arp2/3 complex and cortactin was roughly two- to threefold less than that for the Arp2/3 complex alone. This activity was found to be about four- to fivefold lower than that of GST–VCA when both were analysed in the presence of 100 nM Arp2/3 complex (Fig. 3c). Cortactin also enhanced the rate of actin polymerization. In the presence of 100 nM Arp2/3 complex and 1.5 μM G-actin, cortactin generated ~0.95 nM barbed ends at half-maximal polymerization, which is about 2.4-fold more than that generated by the Arp2/3 complex

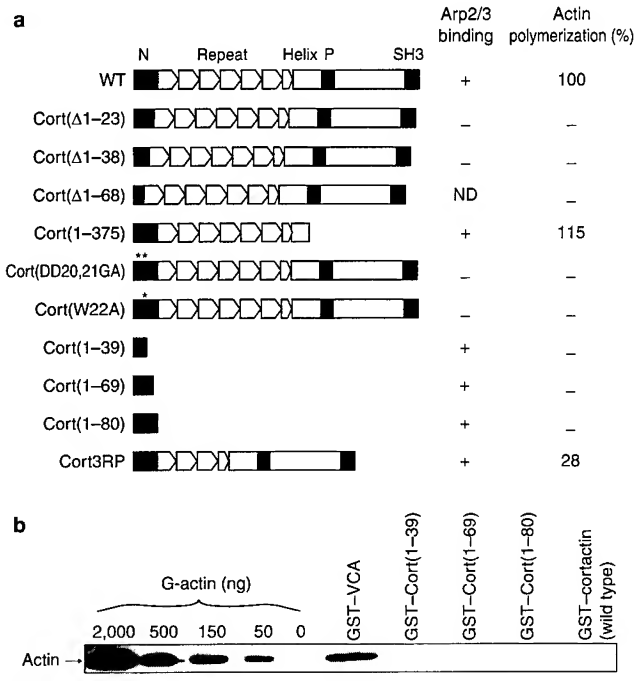

Figure 2 **Correlation between binding to the Arp2/3 complex and cortactin-mediated stimulation of actin polymerization. a**, Mapping of the structural motifs of cortactin for the binding to and activation of the Arp2/3 complex. Arp2/3-binding activities were determined on the basis of GST-tagged proteins (see Fig. 1c). Data for actin-polymerization activities were obtained on the basis of the results shown in Fig. 4. For analysis of actin polymerization, GST-tagged peptides (Cort(1–39), Cort(1–69), Cort(1–80) and Cort(1–375)) or GST-free peptides (other mutants) were used. The positions of the point mutations in Cort(DD20,21GA) and Cort(W22A) are indicated by an asterisk. The activity of each protein was calculated by comparing the time taken to yield a half-maximal actin polymerization with that for the Arp2/3 complex alone. This activity was further normalized by comparison with that of wild-type cortactin. Relative activities of <10% of the value for wild-type cortactin were considered insignificant are indicated by a minus sign. ND, not determined. **b**, Cortactin does not bind to G-actin. G-actin (1.4 μM) was incubated with 2 μM GST-tagged cortactin derivatives or VCA immobilized on glutathione beads at 4 °C for 1 h in 200 μl binding buffer (5 mM Tris–HCl pH 8.0, 0.2 mM $CaCl_2$, 0.5 mM dithiothreitol, 0.2 mM ATP, 2 mM $MgCl_2$ and 50 mM KCl). G-actin bound to beads was detected by immunoblotting using an anti-actin monoclonal antibody. As a quantitative control, different amounts of G-actin were loaded onto the same gel.

alone. The activity of cortactin for actin polymerization was also dependent upon the concentration of the Arp2/3 complex. The actin polymerization stimulated by cortactin came to a saturated level within ~250 s in the presence of 250 nM Arp2/3 complex, whereas it required 450 s to plateau in the presence of 100 nM Arp2/3 complex (Fig. 3a). At 10 nM, the intrinsic activity of the Arp2/3 complex was barely detected (Fig. 3d). Under these conditions, cortactin showed no significant stimulation of actin polymerization within 10 min. However, in the presence of small amounts of GST–VCA, cortactin was able to increase actin polymerization by <30%. In the presence of high concentrations of GST–VCA (such as 400 nM) the activity of GST–VCA became dominant, and no significant stimulation or inhibition by cortactin was observed. These results indicate that cortactin may potentiate GST–VCA-mediated actin nucleation only in a narrow range of concentrations. Cortactin also activated the Arp2/3 complex in a dose-dependent manner with a maximal activity at ~50 nM in the presence of 100 nM Arp2/3 complex (Figs 3b and 4c).

The activity of cortactin for actin assembly requires its ability to bind to the Arp2/3 complex, as either deletion or point mutation of the sequences for binding to the Arp2/3 complex abolished the activity to activate it (Fig. 4a). To ensure that the failure of these mutants to stimulate actin polymerization was not due to a gross structural alteration, such as unfolding, that may be introduced by mutations, we analysed Cort(Δ1–23), Cort(W22A) and Cort(DD20,21GA) by gel filtration. All mutants exhibited a Stokes' radius of ~5.8 nm, which is the same as that of wild-type cortactin (Fig. 4d). Because such a size is equivalent to a globular protein with a relative molecular mass of >300,000 (M_r 300K; ref. 29), which is significantly larger than the mass predicted for a cortactin monomer (61K), cortactin may either exit as an oligomer or have an unusual structural conformation. As a result, these data indicate that these mutants may maintain the same structural folding as wild-type cortactin.

Binding to F-actin, but not G-actin, is required for the ability of cortactin to activate the Arp2/3 complex. Binding to the Arp2/3 complex itself seems to be insufficient for cortactin to stimulate actin polymerization. Both GST–Cort(1–39) and GST–Cort(1–80), both of which bind to the Arp2/3 complex as efficiently as does full-length cortactin, were unable to stimulate actin polymerization (Fig. 4b). The truncated mutant Cort(1–375), which spans a region that includes the motifs for binding to both Arp2/3 and F-actin (the tandem repeats), showed a similar actin-polymerization activity to wild-type cortactin (Fig. 4b), indicating that binding to the Arp2/3 complex and F-actin is sufficient for its stimulation of actin polymerization. Consistent with this view is the observation that the cortactin mutant Cort3RP, which contains only the final three repeats but still maintains a large Stokes' radius (5.7 nm; Fig. 4d), had a significantly lesser affinity for F-actin, with an estimated K_d of 9.1 μM (Fig. 4c, inset). In keeping with its reduced F-actin binding, the activity of this mutant was also much less than that of wild-type cortactin. The ability of the mutant to activate actin nucleation, as calculated by measuring half-maximal stimulation, was ~28% of that of wild-type cortactin (Fig. 4c).

To activate the Arp2/3 complex, the VCA domain of WASP proteins must bind simultaneously to the Arp2/3 complex and to G-actin[25,30]. We therefore used pull-down assays to determine whether or not cortactin also binds to G-actin. As shown in Fig. 2b, neither full-length nor N-terminal derivatives of cortactin fused to GST showed any detectable G-actin-binding activity. This was the case even after prolonged exposure (data not shown). Under the same conditions, the association of G-actin with GST–VCA was readily detected (Fig. 2b).

We also compared the affinities of cortactin and the Arp2/3 complex for F-actin. As shown in Fig. 4c (inset), the K_d of cortactin for F-actin is ~230 nM, which is almost 20-fold lower than that of the Arp2/3 complex (4.5 μM) as measured under the same conditions. Because F-actin is known to be an important activator of the Arp2/3 complex[23], these data indicate that cortactin may activate the Arp2/3 complex by promoting its association with F-actin.

Interaction of cortactin with the Arp2/3 complex is required for their co-localization *in vivo*. The above results indicate that cortactin can interact with the Arp2/3 complex *in vitro* to promote actin assembly. To determine whether cortactin may function together with the Arp2/3 complex within the cell, we examined their subcellular localizations in human MDA-MB-231 breast cancer cells and in NIH 3T3 fibroblasts using antibodies against cortactin and against Arp3, a component of the Arp2/3 complex[31]. MDA-MB-231 cells contain few stress fibres, as shown by phalloidin staining, and instead deposit most F-actin into giant particulate structures that are associated with membrane (Fig. 5b). Within these particulate structures, endogenous cortactin or wild-type cortactin tagged with Myc epitope at its C terminus (WT-cortactin–Myc) accumulated (Fig. 5a, b). Arp3 was also enriched in these F-actin patches. Using image analysis, we estimated that ~80% of cortactin immunostaining was co-localized with that of Arp3 (Fig. 6c). In proliferating NIH 3T3 cells, Arp3 and cortactin co-localized in lamellipodia and membrane ruffles, as well as in

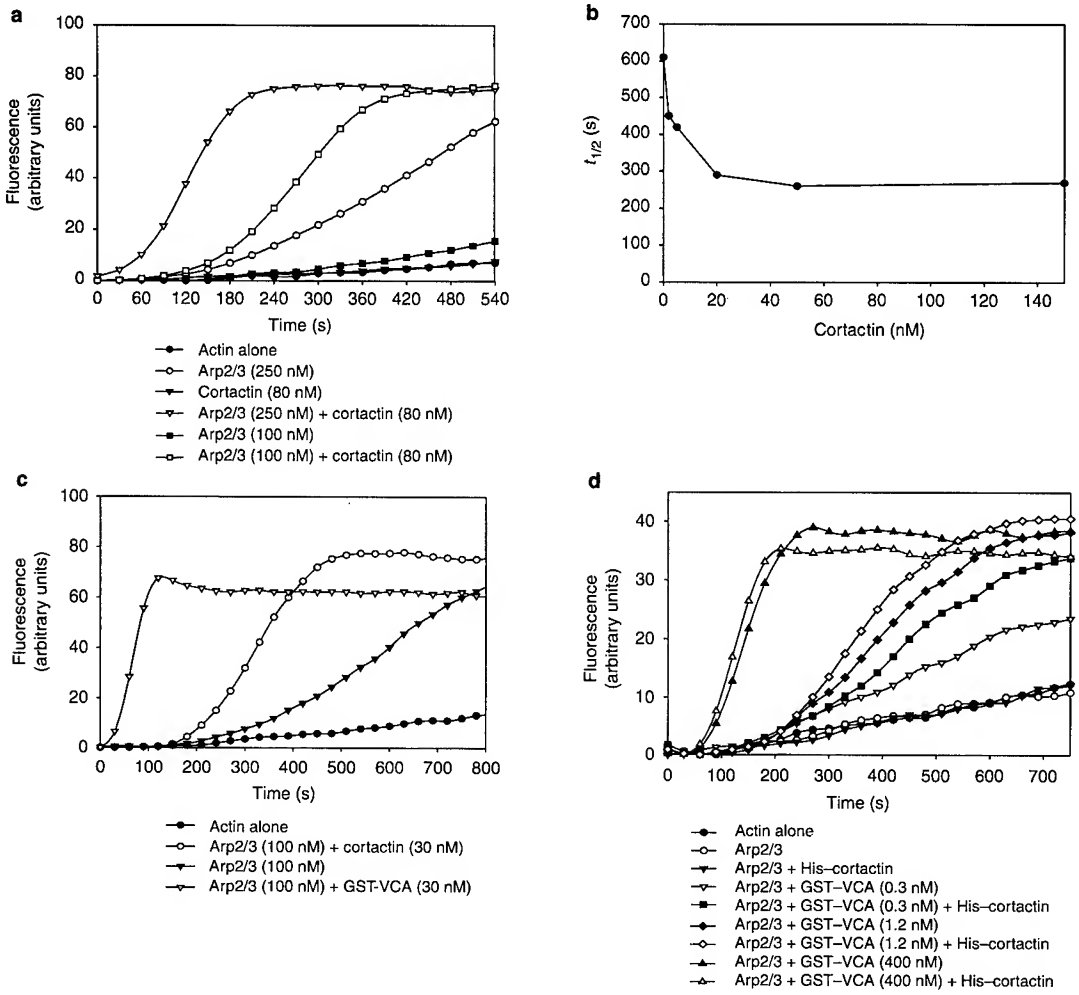

Figure 3 **Cortactin stimulates actin polymerization nucleated by the Arp2/3 complex. a**, Polymerization of 2.8 μM 10% pyrene-labelled actin monomers was initiated with 80 nM cortactin in the presence of 100 or 250 nM Arp2/3 complex as indicated. **b**, Dose-dependence of cortactin-mediated polymerization of 2.8 μM 10% pyrene-labelled actin monomers in the presence of 100 nM Arp2/3 complex. The activity of cortactin was determined on the basis of the time taken to induce half-maximal activity ($t_{1/2}$). **c**, Comparison of the activity of cortactin with that of GST–VCA. Polymerization of 1.5 μM pyrene-labelled actin was carried out in the presence of 30 nM cortactin or GST–VCA, and 100 nM Arp2/3 complex. **d**, Stimulation of actin polymerization by cortactin and GST–VCA. Conditions were as follows: 1.5 μM pyrene-labelled actin, 10 nM Arp2/3 complex, 50 nM His–cortactin, and 0.3, 1.2 or 400 nM GST–VCA.

small punctate structures (Fig. 5a). Thus, the Arp2/3 complex and cortactin seem to be associated with the same type of F-actin structures. In contrast with WT-cortactin–Myc, a cortactin mutant with deletion of amino acids 1–68 (Cort(Δ1–68)–Myc) was either diffusely distributed within the cytoplasm or was localized to peripheral ruffles (Figs 5b and 6b). To determine whether binding to the Arp2/3 complex is sufficient for the association of cortactin with particulate structures, we analysed MDA-MB-231 cells expressing Cort(1–80)–Myc. As shown in Fig. 5c, this mutant accumulated within Arp3-containing patches as efficiently as did wild-type cortactin. Quantification of the co-localization of Arp3 with wild-type and mutant cortactin proteins is shown in Fig. 6c. Whereas WT-cortactin–Myc and Cort(1–80)–Myc co-localized with Arp3 in the particular structures, binding of Cort(Δ1–68)–Myc to these structures was significantly reduced. Thus, interaction with the Arp2/3 complex is not only required but is also sufficient for the specific distribution of cortactin at particular structures within cells. However, Cort(1–80)–Myc appeared to be diffused within the cytoplasm of cells in which it was over-expressed (Fig. 5c), indicating that association with cortactin mutants that are deficient in Arp2/3 binding could also alter the function of the endogenous Arp2/3 complex.

Discussion

Activation of the nucleation of actin assembly is an important mechanism by which extracellular signals regulate the reorganization of the actin cytoskeleton[32]. Recent studies have shown that actin polymerization in the cell cortex is mainly nucleated by the Arp2/3 complex[18]. However, the activity of the Arp2/3 complex itself to nucleate actin assembly is inefficient and requires other cellular activators. In mammalian cells, all activators of the Arp2/3 complex identified so far belong to the WASP family. The ability of the VCA domain of WASP-family proteins to activate the Arp2/3 complex requires a G-actin-binding domain (WH2) as well as a cofilin-homology domain and an acidic domain at the C termini of these proteins. Here we have shown that a non-WASP-related protein, cortactin, can also promote the actin-nucleation activity of the Arp2/3 complex by two- to threefold. Although this activity seems to be at a lower level than that of the VCA domain of N-WASP, cortactin activates the Arp2/3 complex in a manner that is distinct from that of WASP proteins and may thus constitute a unique mechanism of actin organization mediated by the Arp2/3 complex within cells.

Like WASP, the activity of cortactin to promote actin

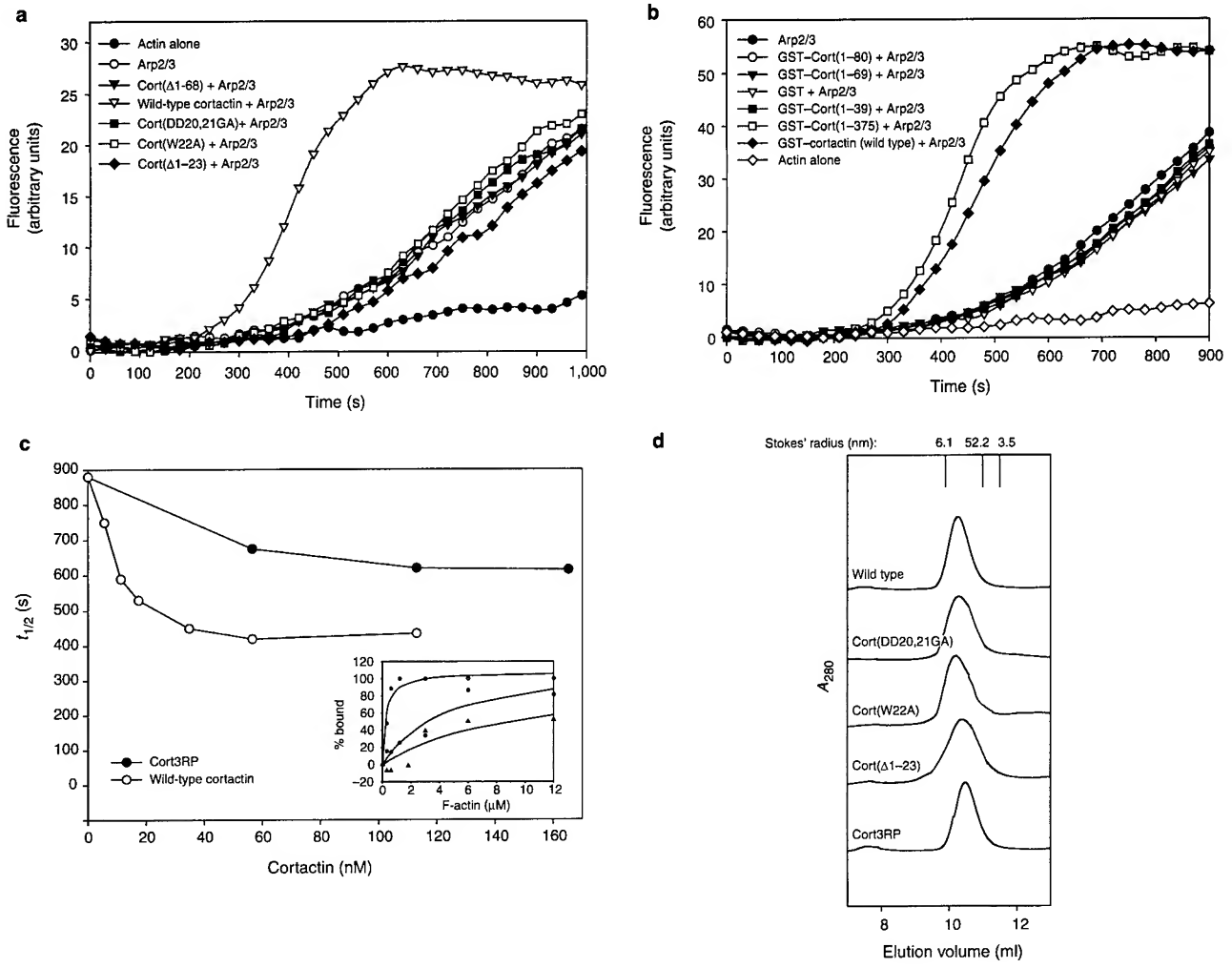

Figure 4 **Requirement of F-actin binding for cortactin to stimulate the Arp2/3 complex a**, Polymerization of pyrene-labelled actin monomers induced by cortactin deletion or point mutants. Conditions were as follows: 1.5 μM 10% pyrene-labelled actin monomer, 80 nM Arp2/3 complex; 50 nM wild-type cortactin, 150 nM Cort(Δ1–68), 50 nM Cort(Δ1–23), 50 nM Cort(DD20,21GA) and 50 nM Cort(W22A). **b**, Actin polymerization induced by GST–cortactin fragments. Conditions were as follows: 1.5 μM 10% pyrene-labelled actin monomer, 40 nM Arp2/3 complex, 80 nM GST–Cort(1–80), 80 nM GST–Cort(1–69), 80 nM GST–Cort(1–39), 80 nM GST–Cort(1–375) and 80 nM GST-tagged wild-type cortactin. **c**, Mutation at the F-actin-binding (tandem repeat) domain reduces activation of the Arp2/3 complex. Cort3RP, which lacks the first three repeats, was analysed for polymerization of 1.5 μM 10% pyrene-labelled actin monomers at various concentrations in the presence of 80 nM Arp2/3 complex. Activity at each concentration, as measured by the time taken to induce half-maximal stimulation ($t_{1/2}$), was compared with the maximal activity of wild-type cortactin. At 57 nM, the activity of Cort3RP exhibited 28% of that of the wild type. Inset, measurement of the affinities of cortactin variants and the Arp2/3 complex for F-actin (see Methods). Open circles, wild-type cortactin; closed circles, Arp2/3 complex; triangles, Cort3RP. **d**, Gel-filtration analysis of cortactin mutants (see Methods). Elution volumes were compared to those of BSA, catalase and ferritin.

polymerization requires an acidic domain that interacts directly with the Arp2/3 complex. However, the repeat domain is distinct from the WH2 domain of the WASP family. The former shows an ability to bind to F-actin[33], whereas the latter has a strong affinity for monomeric actin[25,28,30,34,35]. Thus, it is unlikely that cortactin would be able to shuttle G-actin to the Arp2/3 complex, as proposed for WASP-family proteins[25,30]. Conversely, binding to F-actin is essential for cortactin to activate the Arp2/3 complex. Deletion or partial deletion of the repeat domain can abolish or significantly reduce actin polymerization. On the other hand, Cort(1–375), which contains the Arp2/3- and F-actin-binding domains only, is able to activate the Arp2/3 complex as efficiently as WT-cortactin. Because the affinity of cortactin for F-actin is much higher (~20-fold) than that for the Arp2/3 complex and the affinity of the Arp2/3 complex for F-actin is lower than that for cortactin, the presence of cortactin would probably promote the association of the Arp2/3 complex with F-actin. Interaction of the Arp2/3 complex with F-actin has been proposed to be important for the nucleation of dendritic actin filaments[22,36]. Indeed, preformed actin filaments can reduce the lag required for WASP-mediated activation of the Arp2/3 complex[23,37] Thus, we postulate that cortactin promotes actin polymerization by enhancing F-actin-mediated activation of the Arp2/3 complex.

At a low concentration of the Arp2/3 complex (10 nM), the activity of cortactin was not apparent unless small amounts of GST–VCA were present (Fig. 3d). However, cortactin itself was unable to stimulate GST–VCA-mediated actin polymerization by more than 30% in the presence of either 10 nM (Fig. 3d) or higher concentrations (data not shown) of the Arp2/3 complex. Because cortactin binds to the Arp2/3 complex through an acidic motif, which is similar to those used by GST–VCA, it is likely that cortactin binds to the same site of the Arp2/3 complex as GST–VCA. Thus, the slight increase in the rate of actin polymerization in the presence of both cortactin and GST–VCA is more likely to be due to an additive, rather than a synergistic, effect. However, cortactin could function in concert with

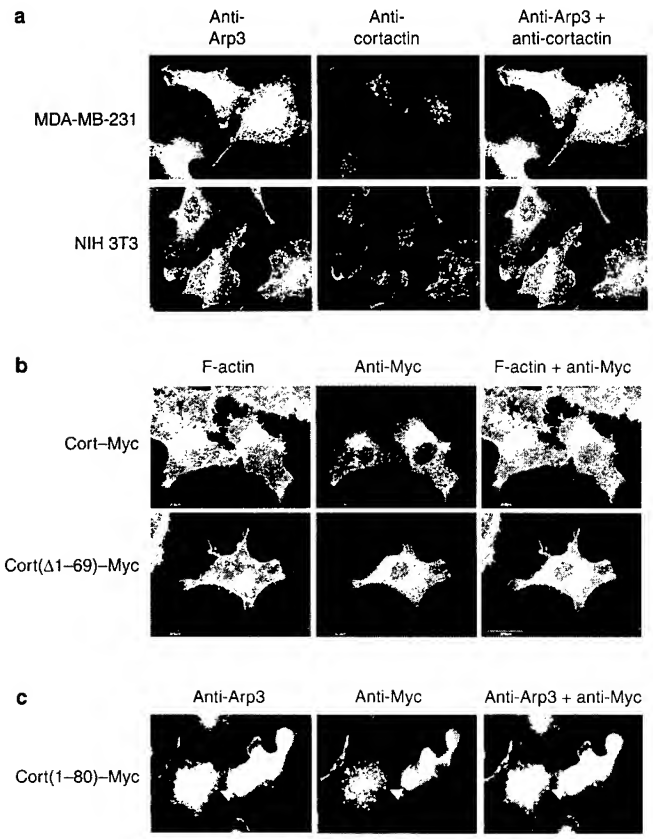

Figure 5 **Requirement of interaction with the Arp2/3 complex for localization of cortactin with actin patches. a**, Co-localization of cortactin with the Arp2/3 complex. MDA-MB-231 or NIH 3T3 cells were plated onto a glass cover slip pre-coated wth fibronectin (1 μg ml^{-1}) and incubated overnight. Cells were stained with an anti-cortactin monoclonal antibody (4F11) and an anti-Arp3 polyclonal antibody. Stained cells were examined by confocal scanning microscopy. **b**, Interaction with the Arp2/3 complex is required for localization of cortactin in F-actin-enriched patches of breast-cancer cells. Plasmids encoding wild-type cortactin–Myc and Cort(Δ1–68)–Myc were transiently transfected into MDA-MB-231 cells grown at log phase and plated on fibronectin-coated glass cover slips. After 2 days, cells were stained with 9E-10 anti-Myc antibody or with phalloidin for F-actin, and were examined by confocal microscopy. Arrows indicate representative particulate sites. **c**, Binding to the Arp2/3 complex is sufficient to localize cortactin within particular structures. A plasmid encoding Cort(1–80)–Myc was transiently transfected into MDA-MB-231 cells, which were then subjected to double staining with anti-Arp3 (green) and anti-Myc (red) antibodies. Arrows indicate representative particulate sites showing co-localization of Arp2/3 and Cort(1–80)–Myc. Note the diffused distribution of endogenous Arp2/3 and Cort(1–80)–Myc in the cytoplasm of two cells overexpressing Cort(1–80)–Myc.

WASP proteins in other ways. For example, an activated WASP-like protein could take over cortactin to interact with F-actin-associated Arp2/3 complex and to warrant rapid formation of branched actin filaments in response to extracellular stimuli. Future studies will be focused on the determination of the specific functions of these two types of molecule in the regulation of actin polymerization within cells.

In contrast to the activation of GST–VCA, we propose that the activity of cortactin is more intimately dependent upon an intrinsic activity of the Arp2/3 complex, which is influenced primarily by its concentration. However, we cannot rule out the possibility that other cellular factors that might be co-purified in the preparation of the Arp2/3 complex can also contribute to its apparent intrinsic activity. This unique feature may explain the recently reported failure to detect the activity of cortactin in the presence of very low concentrations of the Arp2/3 complex[38]. However, the concentrations of cortactin and the Arp2/3 complex in the cell are in the micromolar range (~2.0 μM for cortactin and ~2.9 μM for the Arp2/3 complex in MDA-MB-231 cells, data not shown). Thus, it is likely that nucleation of actin polymerization mediated by cortactin and the Arp2/3 complex is physiologically relevant.

Maximal activation of the Arp2/3 complex by cortactin occurs at a concentration that is far below its K_d value for the Arp2/3 complex (50 nM compared with 1 μM). The exact reason for this apparent discrepancy is not clear. The possibility that the Arp2/3 complex may be partially denatured in preparation seems unlikely because the same preparation was able to respond effectively to GST–VCA (Fig. 3). The discrepancy may be also partially explained by limitation of the sites at which cortactin can bind to F-actin. It is known that cortactin binds to F-actin subunits with a ratio of roughly 1:15, as shown using pre-formed F-actin[11,33]. These sites could be further restricted by the possibility that only certain binding sites, such as those near to the ends of actin filaments, are able to activate the Arp2/3 complex[37]. Another possibility is that cortactin may not always associate stably with the Arp2/3 complex, given the fact that the affinity is weak (K_d 1 μM). Because the Arp2/3 complex itself is also able to bind to F-actin, albeit weakly, the transient interaction of cortactin with the Arp2/3 complex would be sufficient to make the Arp2/3 complex competent to initiate new actin polymerization from an existing filament.

In the cell, cortactin is dominantly localized within F-actin-rich peripheral areas and punctate structures[12,33]. We found that in MDA-MB-231 cells plated on fibronectin-coated dishes, cortactin co-localizes with F-actin and the Arp2/3 complex in giant particulate structures. The association of cortactin with the Arp2/3 complex seems to be profound because the majority (~80%) of sites of cortactin immunostaining co-localized with those of the Arp3 complex (Figs 5a and 6c). Thus, cortactin is likely to have a general function in the regulation of actin polymerization nucleated by the Arp2/3 complex. The co-localization of cortactin with the Arp2/3 complex is apparently the result of a direct association of these two complexes, as it requires the Arp2/3-binding domain of cortactin (Fig. 5b). Interestingly, Cort(Δ1–68)–Myc, which lacks the Arp2/3-binding motif, seems to be capable of localizing to peripheral regions (Fig. 6b) independently of association with the Arp2/3 complex. Thus, activation of these two separate actin-rich compartments may be different. In contrast, Cort(1–80)–Myc, which contains the Arp2/3-binding domain only, is able to associate with the Arp2/3 complex within the particulate structures of MDA-MB-231 cells (Figs 5c and 6b). The fact that Cort(1–80) is unable to associate with F-actin indicates that the interaction of the Arp2/3 complex with F-actin may not be entirely dependent on cortactin within the particular structure. However, the localization of this mutant in actin patches seems only to occur in cells in which the level of the mutant is low. In cells in which the mutant is overexpressed, it was distributed with the Arp2/3 complex throughout the cytoplasm (Fig. 5c), indicating that the overexpressed mutant is able to alter the function of the endogenous Arp2/3 complex as well as its association with particulate structures.

The nature of the particulate structures is unknown. When MDA-MB-231 cells are plated on extracellular matrix, cortactin is accumulated within the invadopodium, a cortical protrusion on the ventral side of cells that is implicated in degradation of and penetration into the extracellular matrix[14]. Further studies will be required to determine whether the interaction of cortactin with the Arp2/3 complex is necessary for formation of invadopodia and for tumour invasion. Actin and cortactin-rich particulate structures are also abundant in other types of cell, such as osteoclasts[39]. In osteoclasts, these structures are called podosomes and are used to seal off regions of bone where bone resorption occurs[40]. Thus, actin polymerization mediated by the Arp2/3 complex and cortactin may have a general function in the formation of dynamic, protrusive structures through which cells interact with the extracellular matrix or with surrounding cells in which extensive proteolysis takes place. □

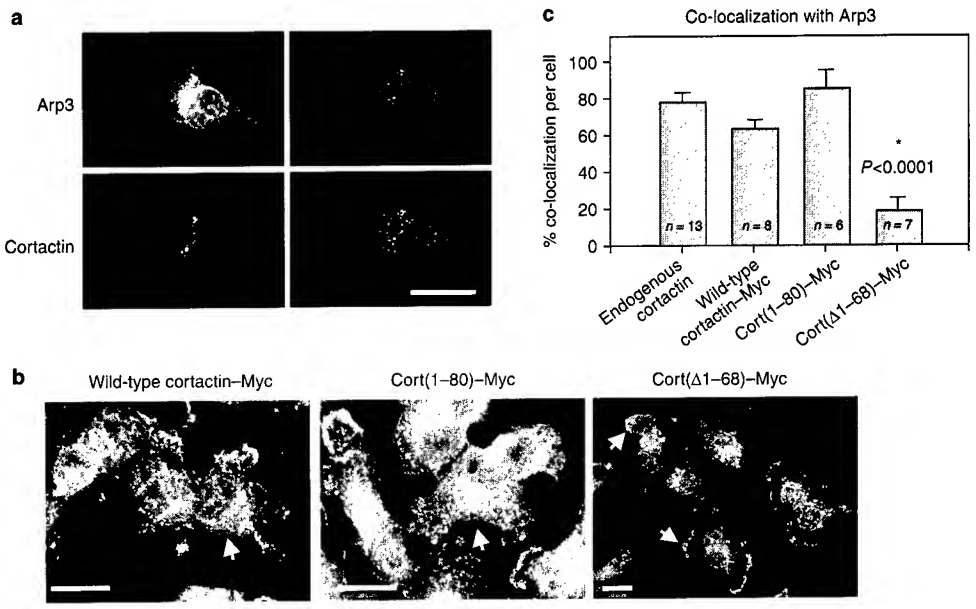

Figure 6 **Quantification of the co-localization of cortactin variants with the Arp2/3 complex.** All quantitative analysis was done on the basis of cells with an apparent normal morphology, without rounding up. **a**, MDA-MB-231 cells were cultured on fibronectin-coated cover slips overnight, and then fixed and double-stained for Arp3 (green) and cortactin (red). Left column, immunolabelled cells exhibit intense punctate staining in a perinuclear region. Right column, binary images identifying these punctate sites of labelling. Scale bar represents 20 μm. **b**, MDA-MB-231 cells were transiently transfected with wild-type cortactin–Myc, Cort(1–80)–Myc or Cort(Δ1–69)–Myc and double-stained for Myc (red) and Arp3 (green). Arrows indicate cells with anti-Myc labelling of exogenous cortactin. Co-localization of cortactin–Myc and Arp3 in intracellular particles (yellow) is seen for both wild-type cortactin and the Cort(1–80)–Myc, but not for Cort(Δ1–68)–Myc. **c**, Quantification of the co-localization of cortactin–Myc variants and endogenous cortactin with Arp3 in MDA-MB-231 cells. *P* refers to the difference between Cort(Δ1–68)–Myc and wild-type cortactin–Myc.

Methods

Antibodies.

Polyclonal antibody against Arp3 was prepared using the human-Arp3-derived peptide YEEIGP-SIVRHNPVFGVMS and was affinity-purified as described[25]. Monoclonal anti-cortactin antibody (4F11) was from Upstate Biotechnology.

Preparation of the Arp2/3 complex.

Bovine Arp2/3 complex was purified using a modified procedure as described[25]. Briefly, 100 g of frozen bovine brain was minced with a Waring blender in buffer Q (100 ml of 20 mM Tris pH 8.0, 100 mM NaCl, 5 mM $MgCl_2$, 5 mM EGTA and 1 mM dithiothreitol (DTT)) supplemented with 50 μg ml^{-1} phenylmethylsulphonyl fluoride, 5 μg ml^{-1} leupeptin and 1 μg ml^{-1} aprotinin. The minced tissue was further homogenized using a Dounce homogenizer and was clarified by centrifugation at 5,000*g* for 60 min at 4 °C. The supernatant was subjected to chromatography in a 100-ml Sepharose Q column equilibrated with buffer Q. The flow-through containing the Arp2/3 complex was collected, supplemented with 0.1 mM ATP and fractionated on a GST–VCA glutathione–sepharose column equilibrated with buffer B (50 mM Tris pH 7.5, 25 mM KCl, 1 mM $MgCl_2$ 0.5 mM EDTA, 1 mM DTT and 0.1 mM ATP). After washing with 0.2 M KCl in buffer B, the Arp2/3 complex was eluted with buffer B containing 0.2 M $MgCl_2$. The protein was then dialysed against buffer B and concentrated using a Centriprep 10 cartridge. The concentrated Arp2/3 complex was stored in buffer B containing 30% glycerol at –80 °C. Protein concentration was determined by the Bradford method (Bio-Rad protein assay), using BSA as a standard. Concentrations in mg ml^{-1} were converted to molar concentrations on the basis of the equivalence of 1 mg ml^{-1} to 14 μM cortactin, 23 μM actin and 4.6 μM Arp2/3 complex.

Analysis of interaction of the Arp2/3 complex and cortactin variants.

GST or GST-tagged cortactin variants (5 μg), immobilized on glutathione beads, were mixed with 10 pmol of purified Arp2/3 complex in buffer A (100 μl of 50 mM Tris pH 8.0, 150 mM NaCl and 1% Triton X 100), and incubated for 2 h at 4 °C on a rotating wheel. Beads were rinsed three times with buffer A and were then boiled in 2 × SDS sample buffer. The Arp2/3 complex was detected by immunoblotting using a polyclonal anti-Arp3 antibody after resolution by SDS–PAGE.

Construction of cortactin mutants.

All numbers used here are based on the amino-acid sequence of murine cortactin[3]. The deletion cortactin mutants Cort(Δ1–23), Cort(Δ1–38), Cort(Δ1–68), Cort(1–39), Cort(1–69) and Cort(1–80) were generated by mutagenesis and polymerase chain reaction (PCR; PfuTurbo polymerase, Stratagene), using the murine cortactin complementary DNA (pXZ112) as a template[3]. The point mutants Cort(W22A) and Cort(DD20,21GA) were generated by site-directed mutagenesis using the Quickchange site-directed mutagenesis kit (Stratagene). All constructs, except for the three-repeat deletion mutant (pCort3RP), were first generated as *Eco*RI–*Sal*I fragments and then subcloned into the pUC19 plasmid. The resulting plasmids served as the master plasmids from which the inserts were excised and further cloned either into pGEX4T-2 (Amersham Pharmacia), for expression of bacterial GST-fusion proteins, or into pCMV-Tag5B (Stratagene), for mammalian expression of C-terminal Myc-tagged proteins. Inserts in the master plasmids were verified by DNA sequencing. To construct pCort3RP, the DNA sequence encoding the first three repeats was deleted by PCR using the ExSite kit (Stratagene) and was further cloned into pGEX-2T. The primers used were 5′-TCCAAAGGTTTTGGTGGC and 5′-AGCCTTGGGTTCCGTTTC. The plasmid encoding histidine (His)-tagged cortactin was prepared as follows: a murine cortactin cDNA was constructed into the *Bam*HI–*Sal*I sites of pTrcHis2 A vector (Invitrogen) with the aid of PCR using primers 5′-CGGGGATCCGTGGAAAGCCTCTGCAGGCCATC and 5′-CCGGTCGACCTGCGCAGCTC-CACATAGTTGG. The resulting plasmid was transformed into XL-1 Blue *E. coli* strain (Stratagene).

Purification of cortactin derivatives.

Detailed methods for purifying GST–cortactin derivatives and GST-free proteins have been described[41]. To prepare His–cortactin proteins, bacteria were grown at 37 °C in a shaker (051–473, Reuce, Ashedille, North Carolina) at 240 r.p.m. When the density of the culture reached log phase, with an absorbance at 600 nm of 0.4–0.6, 1 mM isopropylthio-β-D-galactoside (IPTG) was added. Bacteria were then shifted to a shaker at 30 °C, incubated for a further 3 h and collected by centrifugation at 3,000*g* for 20 min. The bacterial pellet was stored at –80 °C. To purify His–cortactin, the bacterial pellet was thawed at room temperature, resuspended in lysis buffer (50 mM NaH_2PO_4 pH 8.0, 300 mM NaCl and 10 mM imidazole), and sonicated with an ultrasonic processor (Heat Systems-Ultrasonics, Inc.) at power setting at 3 with 20 pulses per cycle up to a total of 10 cycles. The lysate was added with Triton X-100 to a final concentration of 2%, and the mixture was left on ice for 10 min. Lysate was clarified by centrifugation at 15,000*g* for 20 min at 4 °C. The supernatant was mixed with nickel–nitrilotriacetic acid (Ni–NTA) metal affinity beads (Qiagen) and incubated at 4 °C for 1 h in a rotator tube (Scientific Equipment Products, Baltimore, Maryland). Beads were washed extensively with lysis buffer, and His–cortactin was eluted in 50 mM NaH_2PO_4 pH 8.0, 300 mM NaCl, 20 mM imidazole and 0.05% Tween-20. Eluted fractions were combined, loaded to a Mono-Q column on a Waters 600 pump in elution buffer (50 mM Tris pH 7.5, 1 mM DTT and 1 mM EGTA) and eluted with elution buffer against a 0–1 M KCl gradient at 1 ml min^{-1}. The concentration of the principal peak was determined by the Bradford method using BSA as a standard. All purified proteins were stored at –80 °C.

Measurement of the affinity of cortactin for the Arp2/3 complex.

Purified Arp2/3 complex (4 nM) was incubated with various amounts of immobilized GST–Cort(1–80) for 90 min at 4 °C in binding buffer (5 mM Tris pH 7.5, 1 mM EGTA, 0.1 mM $CaCl_2$, 0.5 mM DTT, 3 mM NaN_3, 50 mM KCl, 2 mM $MgCl_2$, 0.2 mM ATP, 0.2 mg ml^{-1} BSA and 0.1% Tween-20). After incubation, samples were centrifuged at 800*g* in a microcentrifuge for 10 s; supernatants were then fractionated by SDS–PAGE using 12% (*w*/*v*) SDS and immunoblotted using polyclonal anti-Arp3 antibody. The densities of Arp3 bands shown by the blot, which represented unbound Arp3, were scanned and quantified with NIH image software (version 1.62). The amounts of Arp3 depletion by different concentrations of cortactin was used to fit a single rectangular hyperbola using Sigma plot version 5.0, and K_d values were calculated on the basis of $V = V_{max}C/(K_d + C)$, where V is the depletion of Arp3 proteins in the supernatant and C is the concentration of samples to be tested. The same procedure was also used to measure the affinity for GST–VCA.

Actin polymerization.

Rabbit skeletal-muscle monomeric actin labelled with pyrene with 10% efficiency and non-labelled monomeric actin were from Cytoskeleton Inc. Labelled actin was mixed with non-labelled G-actin at ratio of 1:10 in G-actin buffer (5 mM Tris–HCl pH 8.0, 0.2 mM $CaCl_2$, 0.5 mM DTT and 0.2 mM ATP) and centrifuged at 200,000*g* for 2 h. To analyse actin polymerization, the Arp2/3 complex, cortactin or other testing protein was added to 200 µl of 1.5 × polymerization buffer (7.5 mM Tris buffer pH 7.5, 1.5 mM EGTA, 0.15 mM $CaCl_2$, 0.75 mM DTT, 4.5 mM NaN_3, 75 mM KCl, 3 mM $MgCl_2$ and 0.3 mM ATP). Polymerization was initiated by adding 100 µl of stock G-actin solution at 8.4 µM. The final concentration of G-actin in the polymerization reaction was 2.8 µM. In some experiments, 1.5 µM G-actin was used. Actin polymerization was monitored by measuring the increase in pyrene fluorescence using an LS50B fluorometer (Perkin Elmer, Norwalk, Connecticut) with filters for excitation at 365 nm and emission at 407 nm (15-nm and 10-nm bandwidth, respectively). The concentration of barbed ends was derived from measurement of the rate of elongation using $R = K_+(A)(ends)$, where R is the rate of elongation, K_+ is the association rate constant (10 $\mu M^{-1}\ s^{-1}$), A is the concentration of actin monomer, and *ends* is the concentration of growing filament ends[23].

Gel-filtration analysis.

Purified GST-free cortactin proteins were dissolved in elution buffer (50 mM Tris–HCl pH. 7.4, 134 mM KCl and 1 mM $MgCl_2$) at 0.5 mg ml^{-1}. Fifty microlitres of each sample solution was applied to a Superose 12 (Pharmacia) column on a Waters 600 pump. Samples were eluted in elution buffer at 0.5 ml min^{-1}. Eluted proteins were monitored using a Waters 2487 Dural absorbance detector. The standards used to calibrate the column were BSA, catalase and ferritin, with Stokes' radii of 35 nm, 52.5 nm and 61 nm, respectively. The sizes of eluted samples were predicated on the basis of a chart in which the Stoke's radii of the standards were plotted against the elution volume.

G-actin-binding assay.

Monomeric G-actin powder was from Cytoskeleton Inc. G-actin powder was dissolved at a final concentration of 230 µM in G-actin buffer. Before immediate analysis, G-actin was diluted to 1.4 µM in G-actin buffer and then centrifuged at 200,000*g* for 3 h at 4 °C to remove any F-actin. Supernatants were then supplemented with 2 mM $MgCl_2$ and 50 mM KCl. The reconstituted G-actin solution (200 µl) was then added to 5 µl glutathione beads bound to individual GST–cortactin derivatives; the final concentration of GST–cortactin proteins in the reactions was 2 µM. Mixtures of G-actin and cortactin proteins were incubated at 4 °C in a rotator. After 1 h, glutathione beads were precipitated, and the insoluble pellets were analysed further by immunoblotting with monoclonal anti-actin antibody 5C5 (Sigma).

F-actin-binding assay.

Cortactin or the Arp2/3 complex (80 nM) was mixed with F-actin at concentrations of 0.3–12.0 µM in 1 × polymerization buffer at room temperature for 30 min. The reaction was centrifuged at 200,000*g* for 30 min, and the presence of cortactin and Arp3 in the supernatant was detected by immunoblotting using antibodies against cortactin and Arp3.

Fluorescence microscopy.

MDA-MB-231 cells were transiently transfected with plasmids encoding cortactin–Myc proteins with a Superfect transfection kit according to the manufacturer's protocol. Cells were plated on a glass cover slip precoated with fibronectin at 1 µg ml^{-1}. After 24 h cells were fixed with 4% formaldehyde in PBS for 10 min and permeabilized with 0.5% Triton X-100 for 5 min. Treated cells were incubated for 1 h with a monoclonal anti-mMyc antibody (9E10) at 2 µg ml^{-1} in PBS containing 5% BSA, and then with rhodamine-conjugated goat anti-mouse antibody at 14 µg ml^{-1} in the same buffer for 30 min. For F-actin staining, fluorescein isothiocyanate (FITC)-labelled phalloidin was added at a final concentration of 1 µM. Between each step, three washes with PBS were carried out.

To quantify the efficiency of co-localization, images were collected using a ×60 1.4 NA Olympus PlanApo lens on a Fluoview laser-scanning confocal microscope with 20% laser intensity, confocal aperture set at 3 and using Argon (488 nm) and Krypton (568 nm and 647 nm) lasers. All images were collected at the same zoom and photomultiplier settings to allow direct comparison of staining patterns. Green and red images were collected separately with excitation at 488 nm and at 568 nm, respectively, to avoid channel crosstalk from FITC to rhodamine images; for presentation, red and green images were merged. Co-localization of Arp3 and cortactin (endogenous, labelled with monoclonal antibody 4F11, or exogenous, labelled with anti-Myc 9E10) was quantified using Optimas 5.2 image-analysis software. Briefly, matching green and red images of individual cells were opened sequentially. Fluorescence thresholds were applied to each image to exclude diffuse labelling in the cytoplasm. Punctate sites of positive staining were identified and each image was converted to binary form. Matching binary images derived from Arp3 and cortactin images were then subjected to an 'and' operation, resulting in the identification of sites containing both Arp3 and cortactin staining. These sites were scored as well as the total number of Arp3-positive sites per cell. Anti-Myc labeling was not detected in non-transfected cells adjacent to transfected cells. The following equation was used to determine percentage co-localization per cell: % co-localization = (no. punctate sites containing both Arp3 and cortactin) × 100/(no. punctate sites containing Arp3). Means ± s.e.m. were determined and plotted using SigmaPlot software.

RECEIVED 16 JUNE 2000; REVISED 14 NOVEMBER 2000; ACCEPTED 30 NOVEMBER 2000; PUBLISHED 9 FEBRUARY 2001.

1. Schuuring, E. D., Verhoeven, E., Litvinov, S. & Michalides, R. J. A. M. The product of the EMS1 gene, amplified and overexpressed in human carcinomas, is homologous to a v-src substrate and is located in cell-substratum contact sites. *Mol. Cell Biol.* **13**, 2891–2898 (1993).
2. Wu, H., Reynolds, A. B., Kanner, S. B., Vines, R. R. & Parsons, J. T. Identification and characterization of a novel cytoskeleton-associated pp60src substrate. *Mol. Cell Biol.* **11**, 5113–5124 (1991).
3. Zhan, X. *et al.* Murine cortactin is phosphorylated in response to fibroblast growth factor-1 on tyrosine residues late in the G1 phase of the BALB/c 3T3 cell cycle. *J. Biol. Chem.* **268**, 24427–24431 (1993).
4. Schuuring, E. The involvement of the chromosome 11q13 region in human malignancies: cyclin D1 and EMS1 are two new candidate oncogenes. *Gene* **159**, 83–96 (1995).
5. Maruyama, S. *et al.* Physical and functional association of cortactin with Syk in human leukemic cell line K562. *J. Biol. Chem.* **271**, 6631–6635 (1996).
6. Kim, L. & Wong, T. W. Growth factor-dependent phosphorylation of the actin-binding protein cortactin is mediated by the cytoplasmic tyrosine kinase FER. *J. Biol. Chem.* **273**, 23542–23548 (1998).
7. Gallet, C. *et al.* Tyrosine phosphorylation of cortactin associated with Syk accompanies thromboxane analogue-induced platelet shape change. *J. Biol Chem* **274**, 23610–23616 (1999).
8. Liu, M., Qin, Y., Tanswell, A. K. & Post, M. Mechanical stress induces $pp60^{src}$ activation and translocation to cytoskeleton in fetal rat lung cells. *J. Biol. Chem.* **271**, 7066–7071 (1996).
9. Kapus, A., Szaszi, K., Sun, J., Rizoli, S. & Rotstein, O. D. Cell shrinkage regulates Src kinases and induces tyrosine phosphorylation of cortactin, independent of the osmotic regulation of Na^+/H^+ exchangers. *J. Biol. Chem.* **274**, 8093–8102 (1999).
10. Li, Y., Liu, J. & Zhan, X. The role of cortactin and Src in the H_2O_2-mediated injury of human endothelial cells. *J. Biol. Chem.* **275**, 37187–37193 (2000).
11. Huang, C. *et al.* Down regulation of the F-actin crosslinking activity of cortactin by c-Src. *J. Biol. Chem.* **272**, 13911–13915 (1997).
12. Huang, C., Liu, J., Haudenschild, C. C. & Zhan, X. The role of tyrosine phosphorylation of cortactin in the locomotion of endothelial cells. *J. Biol. Chem.* **273**, 25770–25776 (1998).
13. Kitamura, D., Kaneko, H., Miyagoe, Y., Ariyasu, T. & Watanabe, T. Isolation and characterization of a novel human gene expressed specifically in the cells of hematopoietic lineage. *Nucleic Acids Res.* **17**, 9367–9379 (1989).
14. Bowden, E. T., Barth, M., Thomas, D., Glazer, R. I. & Mueller, S. C. An invasion-related complex of cortactin, paxillin and PKCmu associates with invadopodia at sites of extracellular matrix degradation. *Oncogene* **18**, 4440–4449 (1999).
15. Dehio, C., Prevost, M. C. & Sansonetti, P. J. Invasion of epithelial cells by *Shigella flexneri* induces tyrosine phosphorylation of cortactin by a pp60c-src-mediated signalling pathway. *EMBO J.* **14**, 2471–2482 (1995).
16. Fawaz, F. S., van Ooij, C., Homola, E., Mutka, S. C. & Engel, J. N. Infection with *Chlamydia trachomatis* alters the tyrosine phosphorylation and/or localization of several host cell proteins including cortactin. *Infect. Immun.* **65**, 5301–5308 (1997).
17. Cantarelli, V. V., Takahashi, A., Akeda, Y., Nagayama, K. & Honda, T. Interaction of enteropathogenic or enterohemorrhagic *Escherichia coli* with HeLa cells results in translocation of cortactin to the bacterial adherence site. *Infect. Immun.* **68**, 382–386 (2000).
18. Pollard, T. D., Blanchoin, L. & Mullins, R. D. Molecular mechanisms controlling actin filament dynamics in nonmuscle cells. *Annu. Rev. Biophys. Biomol. Struct.* **29**, 545–576 (2000).
19. Welch, M. D., Iwamatsu, A. & Mitchison, T. J. Actin polymerization is induced by Arp2/3 protein complex at the surface of *Listeria monocytogenes*. *Nature* **385**, 265–269 (1997).
20. Svitkina, T. M. & Borisy, G. G. Arp2/3 complex and actin depolymerizing factor/cofilin in dendritic organization and treadmilling of actin filament array in lamellipodia. *J. Cell Biol.* **145**, 1009–1026 (1999).
21. Blanchoin, L. *et al.* Direct observation of dendritic actin filament networks nucleated by Arp2/3 complex and WASP/Scar proteins. *Nature* **404**, 1007–1011 (2000).
22. Mullins, R. D., Heuser, J. A. & Pollard, T. D. The interaction of Arp2/3 complex with actin: nucleation, high affinity pointed end capping, and formation of branching networks of filaments. *Proc. Natl Acad. Sci. USA* **95**, 6181–6186 (1998).
23. Machesky, L. M. *et al.* Scar, a WASp-related protein, activates nucleation of actin filaments by the Arp2/3 complex. *Proc. Natl Acad. Sci. USA* **96**, 3739–3744 (1999).
24. Winter, D., Lechler, T. & Li, R. Activation of the yeast Arp2/3 complex by Bee1p, a WASP-family protein. *Curr. Biol.* **9**, 501–504 (1999).
25. Egile, C. *et al.* Activation of the CDC42 effector N-WASP by the *Shigella flexneri* IcsA protein promotes actin nucleation by Arp2/3 complex and bacterial actin-based motility. *J. Cell Biol* **146**, 1319–1332 (1999).
26. Yarar, D., To, W., Abo, A. & Welch, M. D. The Wiskott–Aldrich syndrome protein directs actin-based motility by stimulating actin nucleation with the Arp2/3 complex. *Curr. Biol.* **9**, 555–558 (1999).
27. Skoble, J., Portnoy, D. A. & Welch, M. D. Three regions within ActA promote Arp2/3 complex-mediated actin nucleation and *Listeria monocytogenes* motility. *J. Cell Biol.* **150**, 527–538 (2000).
28. Machesky, L. M. & Insall, R. H. Scar1 and the related Wiskott–Aldrich syndrome protein, WASP, regulate the actin cytoskeleton through the Arp2/3 complex. *Curr. Biol.* **8**, 1347–1356 (1998).
29. Uversky, V. N. & Ptitsyn, O. B. 'Partly folded' state, a new equilibrium state of protein molecules: four-state guanidinium chloride-induced unfolding of beta-lactamase at low temperature. *Biochemistry* **33**, 2782–2791 (1994).
30. Rohatgi, R. *et al.* The interaction between N-WASP and the Arp2/3 complex links Cdc42-dependent signals to actin assembly. *Cell* **97**, 221–231 (1999).
31. Mullins, R. D. & Pollard, T. D. Structure and function of the Arp2/3 complex. *Curr. Opin. Struct. Biol.* **9**, 244–249 (1999).
32. Carson, M., Weber, A. & Zigmond, S. H. An actin-nucleating activity in polymorphonuclear leukocytes is modulated by chemotactic peptides. *J. Cell Biol.* **103**, 2707–2714 (1986).
33. Wu, H. & Parsons, J. T. Cortactin, an 80/85-kilodalton pp60(src) substrate, is a filamentous actin-binding protein enriched in the cell cortex. *J. Cell Biol.* **120**, 1417–1426 (1993).
34. Miki, H. & Takenawa, T. Direct binding of the verprolin-homology domain in N-WASP to actin is essential for cytoskeletal reorganization. *Biochem. Biophys. Res. Commun.* **243**, 73–78 (1998).
35. Higgs, H. N., Blanchoin, L. & Pollard, T. D. Influence of the C terminus of Wiskott–Aldrich syndrome protein (WASp) and the Arp2/3 complex on actin polymerization. *Biochemistry* **38**, 15212–15222 (1999).
36. Mullins, R. D., Stafford, W. F. & Pollard, T. D. Structure, subunit topology, and actin-binding activity of the Arp2/3 complex from *Acanthamoeba*. *J. Cell Biol.* **136**, 331–343 (1997).
37. Pantaloni, D., Boujemaa, R., Didry, D., Gounon, P. & Carlier, M-F. The Arp2/3 complex branches filament barbed ends: functional antagonism with capping proteins. *Nature Cell Biol* **2**, 385–391 (2000).
38. Weed, S. A. *et al.* Cortactin localization to sites of actin assembly in lamellipodia requires interactions with F-actin and the Arp2/3 complex. *J. Cell Biol.* **151**, 29–40 (2000).
39. Hiura, K., Lim, S. S., Little, S. P., Lin, S. & Sato, M. Differentiation dependent expression of tensin and cortactin in chicken osteoclasts. *Cell Motil. Cytoskeleton* **30**, 272–284 (1995).
40. Blair, H. C., Teitelbaum, S. L., Ghiselli, R. & Gluck, S. Osteoclastic bone resorption by a polarized vacuolar proton pump. *Science* **245**, 855–857 (1989).
41. Huang, C. & Zhan, X. Proteolysis of cortactin by calpain in platelets and *in vitro*. *Methods Mol. Biol.* **144**, 289–295 (2000).

ACKNOWLEDGMENTS:
This work was supported by grants from the National Institutes of Health, the American Heart Association and the Department of Army.
Correspondence and requests for materials should be addressed to X.Z.

THE JOURNAL OF BIOLOGICAL CHEMISTRY
Vol. 275, No. 47, Issue of November 24, pp. 37187–37193, 2000
Printed in U.S.A.

Tyrosine Phosphorylation of Cortactin Is Required for H_2O_2-mediated Injury of Human Endothelial Cells*

Received for publication, June 19, 2000, and in revised form, August 8, 2000
Published, JBC Papers in Press, August 21, 2000, DOI 10.1074/jbc.M005301200

Yansong Li, Jiali Liu, and Xi Zhan‡

From the Department of Experimental Pathology, Holland Laboratory, American Red Cross, Rockville, Maryland 20855

Injury of endothelial cells induced by reactive oxygen species plays an important role in the development of early stages of vascular diseases such as hypertension and atherosclerosis. Exposure of human umbilical vein endothelial cells to hydrogen peroxide (H_2O_2), a common form of reaction oxygen species, triggers a series of intracellular events, including actin cytoskeletal reorganization, cytoplasm shrinkage, membrane blebbing and protein-tyrosine phosphorylation. The effect of H_2O_2 on endothelial cells is dramatically enhanced when a survival pathway involving extracellular signal-regulated kinase is blocked by PD098059. In contrast, the injury of endothelial cells mediated by H_2O_2 is inhibited by PP2, a selective specific inhibitor for protein-tyrosine kinase Src. Cortactin, a filamentous actin (F-actin)-associated protein, becomes phosphorylated at tyrosine residues upon stimulation by H_2O_2 in a manner dependent on the activity of Src. The level of tyrosine phosphorylation of cortactin is correlated with the formation of membrane blebs. Overexpression of wild-type cortactin tagged with green fluorescent protein in endothelial cells via a retroviral vector substantiates the H_2O_2-induced morphological changes, whereas overexpression of a green fluorescent protein-cortactin mutant deficient in tyrosine phosphorylation renders endothelial cells resistant to H_2O_2. The functional role of cortactin in H_2O_2-mediated shape changes was also evaluated in NIH 3T3 cells. Stable 3T3 transfectants expressing wild-type cortactin in the presence of either H_2O_2/PD098059 or H_2O_2 alone at 200 μM exhibited a dramatic shape change characterized by rounding up or aggregation. However, the similar changes were not detected with cells overexpressing a cortactin mutant deficient in tyrosine phosphorylation. These data demonstrate an important role of the Src/cortactin-dependent actin reorganization in the injury of endothelial cells mediated by reactive oxygen species.

The injury of endothelial cells underling the lumen of blood vessels contributes significantly to the development of atherosclerosis and hypertension. Numerous studies have shown that exposure to local reactive oxygen species is one of the main causes for the injury of endothelial cells. Reactive oxygen species can be derived from the dismutation of superoxide anion or from the products of activated neutrophils or macrophages that accumulate in the blood vessel wall as a consequence of ischemia and reperfusion injury (1–3). Cancer cells also produce reactive oxygen species *in vivo*, which may contribute to the damage of endothelium during the metastatic process (4). Hydrogen peroxide (H_2O_2) is known to be one of the common forms of reactive oxygen species and can easily penetrate the plasma membrane and affect neighboring cells as well as H_2O_2-producing cells (5). One of the prominent events within endothelial cells upon exposure to H_2O_2 is the formation of plasma membrane blebs (6). The surface blebbing of endothelial cells promotes platelets to adhere to the injured endothelium as well as leukocytes to block capillary lumens, which would lead ultimately to cardiac, brain, lung, kidney, and liver failure. Although the mechanism of the formation of membrane blebs is not fully understood, it appears to be intimately associated with the reorganization of the actin cytoskeleton that are mediated by cytoskeleton binding or cross-linking proteins. For example, cells deficient in an actin filament cross-linking protein, ABP-280, show prolonged blebbing (7). Similarly, redistribution of filamin, another F-actin cross-linking protein, is one of the early events in H_2O_2-mediated endothelial cell injury (8).

H_2O_2 triggers signal transduction within cells in a similar manner as growth factors (9, 10). Exposure to H_2O_2 induces a rapid increase in tyrosine phosphorylation of a various proteins, including Src- and Syk-related non-receptor protein-tyrosine kinases (11), and enhances the kinase activity of Src in endothelial cells (12). The implication of protein-tyrosine phosphorylation in H_2O_2-mediated signal transduction is further strengthened by the findings that non-selective tyrosine kinase inhibitors such as genistein and herbimycin A can abolish the response of cells to H_2O_2 (13, 14). In addition to protein-tyrosine kinases, H_2O_2 also induces the activity of extracellular signal-regulated kinase (Erk),[1] a member of the mitogen-activated protein kinase family (15). Induction of Erk may represent a surviving pathway because selective inhibition of Erk by PD098059, can increase apoptosis induced by H_2O_2 (9, 15).

Cortactin, a cortical actin-associated protein that is widely expressed in most adherent cells (17), is a prominent substrate of protein-tyrosine kinase Src *in vivo* and *in vitro* (18, 19). The protein sequence of cortactin is featured by six and a half tandem repeats of a unique 37-amino acid sequence and a Src homology 3 (SH3) domain at the carboxyl terminus. Between the repeat and the SH3 domain, there is an α-helical structure

* This work was supported in part by National Institutes of Health Grant R01 HL52753-07, Department of Defense Grant DAMD17-98-1-8278, and American Heart Association Established Investigator Grant 0040135N (to X. Z.). The costs of publication of this article were defrayed in part by the payment of page charges. This article must therefore be hereby marked "*advertisement*" in accordance with 18 U.S.C. Section 1734 solely to indicate this fact.

‡ To whom correspondence should be addressed: Dept. of Experimental Pathology, Holland Laboratory, American Red Cross, 15601 Crabbs Branch Way, Rockville, MD 20855. Tel.: 301-738-0568; Fax: 301-738-0879; E-mail: zhanx@usa.redcross.org.

[1] The abbreviations used are: Erk, extracellular signal-regulated kinase; F-actin, filamentous actin; FGF, fibroblast growth factor; FITC, fluorescein isothiocyanate; GFP, green fluorescent protein; HUVE, human umbilical vein endothelial; PCR, polymerase chain reaction; SH3, Src homology 3; wt, wild type; FBS, fetal bovine serum; DMEM, Dulbecco's modified Eagle's medium; PBS, phosphate-buffered saline.

followed by a proline-rich region. Our previous studies have determined that Src targets cortactin primarily at three residues (Tyr-421, Tyr-466, and Tyr-482) between the proline-rich and the SH3 domain (20). *In vitro*, cortactin binds to and cross-links F-actin into meshworks (18). The F-actin cross-linking activity of cortactin can be dramatically reduced upon tyrosine phosphorylation mediated by Src (18). The role of Src in the function of cortactin was also appreciated during the study of Src-deficient (Src−/−) cells in which cortactin fails to respond to FGF-1 for tyrosine phosphorylation and shows less association with polarized lamellipodia. Concomitant with low levels of tyrosine phosphorylation of cortactin, Src−/− cells are less motile compared with normal cells and resistant to FGF-1-mediated shape changes (19). These data suggest that tyrosine phosphorylation of cortactin plays an important role in the dynamic change of the actin cytoskeleton induced by growth factors. In the study presented here, we examined the role of cortactin and Src in the injury of endothelial cells induced by H_2O_2. We found that H_2O_2 induces a significant increase in tyrosine phosphorylation of human endothelial cortactin in a manner dependent on the activity of Src. Furthermore, overexpression of wild-type cortactin enhances the response of endothelial cells to H_2O_2, whereas overexpression of a cortactin mutant deficient in tyrosine phosphorylation significantly reduces the H_2O_2-mediated injury of endothelial cells. Thus, this study demonstrates that the signal pathway involving Src and cortactin is implicated in the injury of endothelial cells.

EXPERIMENTAL PROCEDURES

Reagents—H_2O_2, dimethyl sulfide (Me_2SO), and heparin were purchased from Sigma. PP2, SB203580, and PD098059 were from Calbiochem. LipofectAMINE and G418 were purchased from Life Technologies, Inc. Protein A-Sepharose CL-4B and ECL Western blotting kits were from Amersham Pharmacia Biotech.

Antibodies—Monoclonal anti-phosphotyrosine antibody (4G10) and monoclonal anti-cortactin antibody 4F11 were purchased from Upstate Biotechnology, Inc. (Lake Placid, NY). Antibodies against Erk (both type 1 and type 2 forms) were from Promega (Madison, WI). Polyclonal cortactin antibodies were prepared as described previously (21).

Cell Culture—Human vein umbilical endothelial (HUVE) cells were purchased from Clonetics (Walkersville, MD). HUVE cells were grown in medium M199 supplemented with 10% (v/v) fetal bovine serum (FBS), heparin and human recombinant FGF-1 (10 ng/ml) in cell culture dishes coated with fibronectin (5 $\mu g/cm^2$). Cells with passages less than 15 were used in this study. NIH 3T3 cells and cortactin transfectants were cultured in Dulbecco's modified Eagle's medium (DMEM) (Fisher Scientific, Pittsburgh, PA) supplemented with 10% (v/v) calf serum and antibiotics.

Construction and Preparation of Cortactin Viruses—A plasmid encoding green fluorescent protein (GFP)-cortactin was prepared as following. A DNA fragment encoding cortactin coding sequence was generated by polymerase chain reaction (PCR) using a cDNA clone encoding murine cortactin as the template (21). The primers used in PCR were CATTGTGTCGACTGGAAAGCCTCTGCA and CATGCTGGATCCCTACTGCCGCAGCTCC. The PCR product was inserted into the *Sal*I and *Bam*HI sites of pEGFP-C1 (CLONTECH, Palo Alto, CA). The resulting plasmid was named pJQ-7. The encoding sequence of GFP-cortactin was further inserted into *Age*1 and *Not*I sites in a retroviral plasmid MGIN (a gift of Robert Hawley, Holland Laboratory). The *Age*1 and *Not*I sites were introduced with PCR using primers GCGCTACCGGTCGCCACC and ACGTCCGCGGCCGCCTACTGCCGCAGCTC. The final resulting plasmid was named pJL-6.

To prepare GFP-$Cort_{F421F466F482}$, the sequence spanning the mutation sites in the plasmid pCH17 (18) was amplified with PCR using primers GACAAGAATGCATCCACCTTT and ACGTCCGCGGCCGCCTACTGCCGCAGCTC. The PCR product was inserted into the unique sites *Nsi*I and *Not*I sites on pJL-6. The resulting plasmid was named pJL-12.

Preparation of Viruses—Retrovirus packaging cells (293GPG) were the gift of Mehrdad Tondravi (Holland Laboratory) and maintained in DMEM supplemented with 10% FBS, 1 mM minimal essential medium, sodium pyruvate, 2 mM L-glutamine, antibiotics, 1 $\mu g/ml$ tetracycline, 2 $\mu g/ml$ puromycin, and 0.3 mg/ml G418. Packaging cells (1×10^6) were transfected with MGIN viruses using Superfect transfection reagent (Qiagen Inc., Valencia, CA). To harvest viruses, the transfectants were grown in DMEM containing 10% FBS, 1 mM sodium pyruvate, and 2 mM L-glutamine. The medium of the transfectants was collected at 48, 72, and 96 h after transfection and filtered through a 0.45-μm filter (Gelman Sciences, Ann Harbor, MI). The virus medium was stored at −70 °C.

Viral Infection—HUVE cells were plated at density of 1×10^5 in 35-mm dishes. On the next day, the medium was replaced with 1 ml of viral supernatant containing 8 $\mu g/ml$ Polybrene. After 24 h of incubation, the culture medium was changed to M199 containing 10% FBS, 10 ng/ml FGF-1, and 10 $\mu g/ml$ heparin. Expression of GFP proteins was monitored by fluorescent microscopy. To increase the efficiency of infection, the cells were infected with viruses for two or three times.

Fluorescence-activated Cell Sorting Analysis and Sorting—Infected HUVE cells were trypsinized. The suspended cells (2×10^6) were washed one time with PBS supplemented with 2% FBS. The washed cells were then resuspended in PBS plus 2% FBS and sorted in a fluorescent-activated cell sorting system (Beckton Dickinson, Franklin Lakes, NJ) according to light scatter and fluorescence intensity.

Phosphotyrosine Immunoblot Analysis—Cells were extracted in lysis buffer (50 mM Tris-HCl, pH 7.4, containing 1% Nonidet P-40, 0.25% sodium deoxycholate, 150 mM NaCl, 1 mM EDTA, 1 mM PMSF, 1 $\mu g/ml$ aprotinin, leupeptin, pepstatin, 2 mM Na_3VO_4, and 1 mM NaF). The extracts were centrifuged at 14,000 × rpm for 10 min at 4 °C. The clarified supernatants were immunoprecipitated with polyclonal cortactin antisera 2719 (21). The immunoprecipitates were resolved in a SDS-polyacrylamide gel electrophoresis (7.5%, w/v), transferred to a nitrocellulose membrane, and further blotted with a monoclonal phosphotyrosine antibody (4G10). In some experiments, the blot membrane was stripped and re-blotted with monoclonal cortactin antibody 4F11 as described previously (22).

Analysis of Activated Mitogen-activated Protein Kinases—Cells were lysed in 0.5 ml of 2× SDS sample buffer. The cell lysates were analyzed in 10% SDS-polyacrylamide gel electrophoresis and transferred to a nitrocellulose membrane. The membrane was blotted with either active Erk antibody or Erk antibody.

Immunofluorescent Microscopy—Cells were plated on glass coverslips pre-coated with fibronectin. After treatment, the cells were fixed with 3.7% formaldehyde and permeabilized with 0.5% Triton X-100 in PBS for 5 min. The permeabilized cells were incubated with a monoclonal cortactin antibody 4F11 at the concentration of 0.2 $\mu g/ml$ in PBS containing 5% bovine serum albumin for 1 h. The cells were then incubated for 1 h with rhodamine-conjugated goat anti-mouse IgG (Pierce) at the concentration of 5 $\mu g/ml$ and fluorescein isothiocyanate (FITC)-labeled phalloidin at the concentration of 1 μM. Between each step, three washes with PBS were applied. After staining with antibodies, the cells were mounted on a glass slide and inspected under a laser confocal scanning or fluorescent microscope.

RESULTS

H_2O_2 Induces Tyrosine Phosphorylation of Cortactin—In an attempt to study the mechanism by which oxygen radicals induce the injury of endothelial cells, we examined tyrosine phosphorylation of cortactin in HUVE cells upon exposure to H_2O_2. Cortactin was immunoprecipitated from the lysates of HUVE cells treated with H_2O_2 for 1 h at concentrations up to 2 mM. The precipitates were further immunoblotted with a phosphotyrosine antibody. As shown in Fig. 1*A*, H_2O_2 induced tyrosine phosphorylation of cortactin in a dose-dependent manner. Significant increase in the tyrosine phosphorylation of cortactin was apparent in the presence of 1.4 mM H_2O_2, and reached a maximal level at 2 mM. To evaluate the function of tyrosine phosphorylation of cortactin induced by H_2O_2, we examined morphological changes of endothelial cells treated with H_2O_2 at different concentrations by analyzing actin filaments stained with FITC-labeled phalloidin. As shown in Fig. 1*B*, cells treated with H_2O_2 exhibited significant cytoskeletal reorganization and shape changes characterized by formation of membrane blebbing and cytoplasm shrinkage. However, these changes only occured when cells were treated with H_2O_2 at high doses (greater than 1.6 mM) when phosphorylation of cortactin was apparent. Thus, the apparent morphological

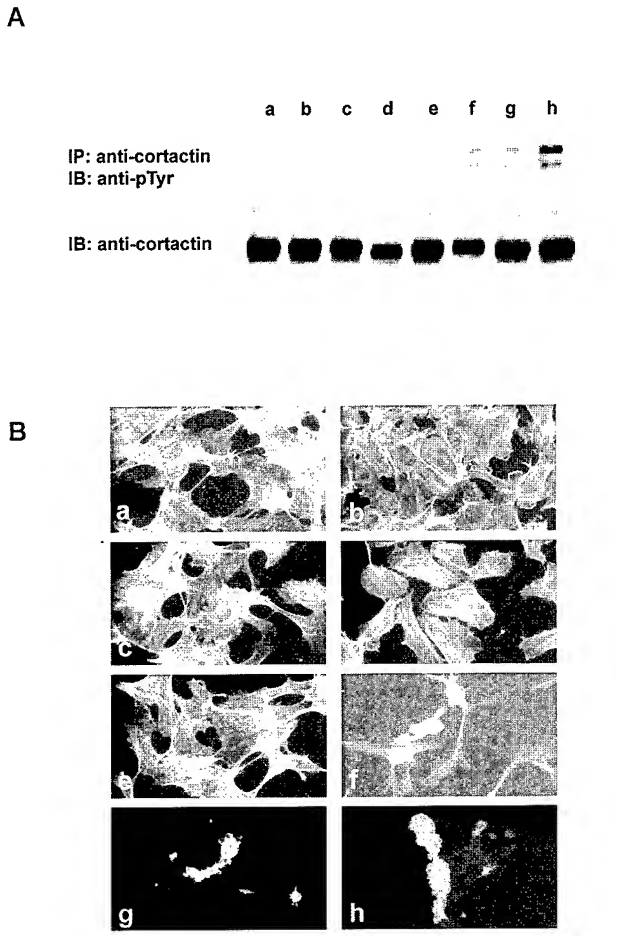

FIG. 1. **H_2O_2 induces tyrosine phosphorylation of cortactin and shape changes of endothelial cells.** *A*, confluent HUVE cells were treated with H_2O_2 for 1 h at concentrations indicated. The resulting cell lysates were immunoprecipitated with a cortactin polyclonal antibody. The immnoprecipitates were then immunoblotted with monoclonal antibodies against either phosphotyrosine or cortactin. *B*, the H_2O_2 treated cells were stained with FITC-labeled phalloidin as described under "Experimental Procedures." Stained cells were examined by immunofluorescent microscopy. Concentrations of H_2O_2 used in the experiment were: *a*, 0; *b*, 0.1 mM; *c*, 0.5 mM; *d*, 1.0 mM; *e*, 1.4 mM, *f*, 1.6 mM; *g*, 1.8 mM; and *h*, 2.0 mM.

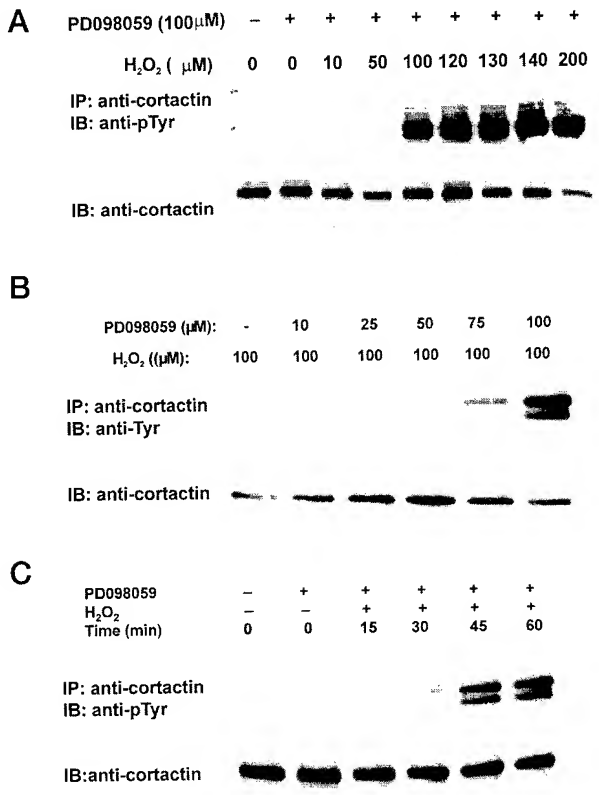

FIG. 2. **Erk inhibitor enhances H_2O_2-mediated tyrosine phosphorylation of cortactin.** HUVE cells were treated with PD098059 for 1 h prior to exposure to H_2O_2. After treatment, cells were lysed and the resulting cell lysates were immunoprecipitated with a cortactin polyclonal antibody and further immunoblotted with phosphotyrosine or cortactin antibodies. *A*, cells were treated with 100 μM PD098059 and H_2O_2 at various concentrations. *B*, cells were treated with various amounts of PD098059 and 100 μM H_2O_2. *C*, cells were treated with 100 μM H_2O_2 and 100 μM PD098059 for various times.

changes were correlated with increase in the levels of tyrosine phosphorylation of cortactin.

Although high doses of H_2O_2 were required to induce morphological changes that correlates with cortactin tyrosine phosphorylation, the conditions also exerted a toxic effect on cells, as indicated by increase in cell detachment from culture dishes (data not shown). To reduce the cytotoxicity of H_2O_2, we attempted to search for less harsh conditions using lower concentrations of H_2O_2. It has been reported that H_2O_2 induced a protective pathway involving Erk, and inhibition of Erk can enhance the response of cells to apoptotic signals (23–27). Thus, we examined the response of cells to H_2O_2 in the presence of PD098059, a specific inhibitor for the activation of Erk (28). As shown in Fig. 2*A*, the presence of 100 μM PD098059 enhanced dramatically the increase in tyrosine phosphorylation of cortactin even at 50 μM H_2O_2. Similarly, titration of different amounts of PD098059 indicated that the inhibitor at 50 μM is sufficient to induce tyrosine phosphorylation of cortactin in the presence of 100 μM H_2O_2 (Fig. 2*B*). A time-course study further demonstrated that the tyrosine phosphorylation of cortactin in the presence of both H_2O_2 and PD098059 was readily detected at 30 min after treatment and reached to a maximal level at approximately 45 min (Fig. 2*C*).

Concomitant with increased cortactin tyrosine phosphorylation, inhibition of ERK also potentiated the morphologic response of cells to H_2O_2. There were no apparent shape changes when cells were exposed to either H_2O_2 alone at 100 μM (Fig. 3*A*, *c*) or PD098059 alone (data not shown), although careful examination revealed a slight increase in the formation of stress fibers in the cells treated with H_2O_2 alone (Fig. 3*A*, *d*). In contrast, cells treated with H_2O_2 plus PD098059 showed dramatic shape changes characterized by formation of membrane blebbings. (Fig. 3*A*, *e* and *f*). The H_2O_2-induced shape changes in the presence of PD098059 appeared to require the activity of Src because these changes did not occur when cells were pretreated with PP2, a selective inhibitor of Src (Fig. 3*A*, *g* and *h*). PP2 also inhibited the shape changes induced by H_2O_2 alone at 2 mM (data not shown). The effect of H_2O_2 on the shape changes of HUVE cells was also quantified by measuring the numbers of cells forming membrane blebs and cytoplasm shrinkage (Fig. 3*B*). Based on these criteria, H_2O_2 alone at 100 μM induced shape changes in 18% of cells, whereas H_2O_2 plus PD098059 was able to induce changes in nearly 45% of cells. The shape changes were significantly reduced by more than 50% in the presence of PP2.

PD098059 enhances the effect of H_2O_2 at the concentrations that also inhibit activation of Erk, as determined by immunoblot with an antibody specifically against active Erk (Fig. 4, *lanes 3* and *4*; data not shown). However, the inhibition of Erk does not appear to be necessary for the H_2O_2-induced injury of endothelial cells. First, shape changes of HUVE cells could

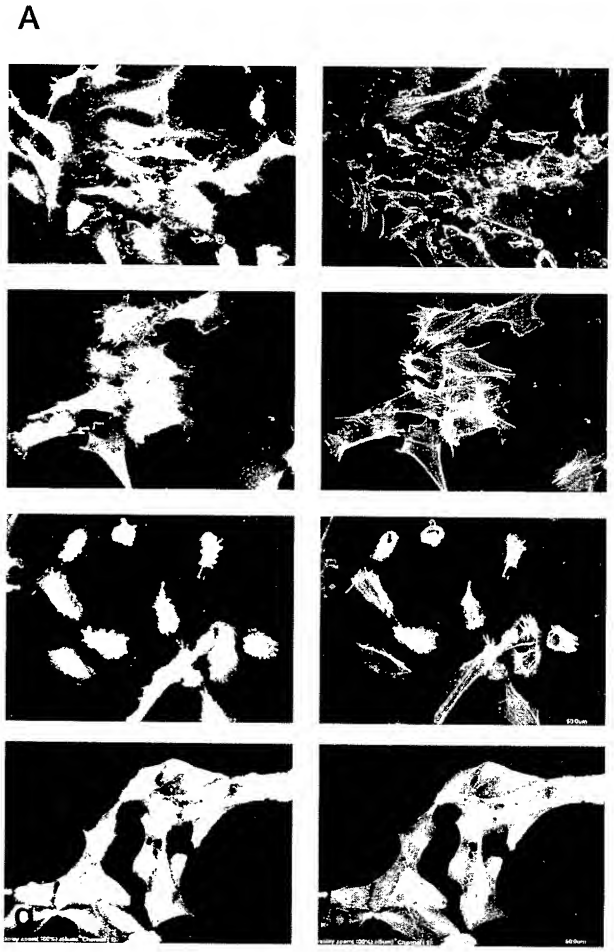

FIG. 3. **PD098059 enhances H_2O_2-mediated morphological changes of endothelial cells in an Src-dependent manner.** *A*, microscopic analysis of HUVE cells. Cells grown on fibronectin-coated glass coverslips were pretreated with 0.2% Me_2SO (*a–d*) or 100 μM PD098059 (*e–h*) for 1 h, or 20 μM PP2 (*g* and *h*) for 20 min. The cells were further added with 100 μM H_2O_2 (*c–h*) for 1 h. Treated cells were then stained with either a rhodamine-conjugated cortactin antibody (*a*, *c*, *e*, and *g*) or FITC-conjugated phalloidin (*b*, *d*, *f*, and *h*). The stained cells were visualized by confocal fluorescent microscopy. *B*, quantification of H_2O_2 plus PD098059-induced shape changes. Treated cells with apparent shape changes as characterized by forming membrane blebbing and cytoplasm shrinkage were counted under a fluorescent microscope. The means ± standard deviation from three independent experiments are shown.

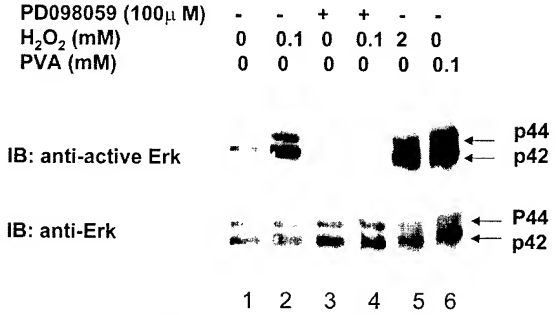

FIG. 4. **Inhibition of Erk is not necessary for H_2O_2-mediated injury of endothelial cells.** HUVE cells were pretreated with 100 μM PD098059 for 1 h and then added with 100 μM H_2O_2 for 10 min. In addition, cells were treated with peroxide vanadate (the mixture of vanadate and H_2O_2) for 10 min (*lane 6*). The activity of mitogen-activated protein kinase was analyzed, as described under "Experimental Procedures."

be also induced when cells treated with H_2O_2 at high doses (greater than 1.6 mM) in the absence of PD098059 (Fig. 1*B*), the condition under which Erk was also activated (Fig. 4, *lane 5*). Second, when cells were treated with H_2O_2 at a low concentration (100 μM) plus vanadate, a mixture (peroxide vanadate) that can efficiently increase the tyrosine phosphorylation of cortactin and induce shape changes of HUVE cells (data not shown) was also able to induce efficiently the activation of Erk (Fig. 4, *lane 6*). Thus, inhibition of Erk potentiates the effect of H_2O_2 but is not required for shape changes. In contrast, H_2O_2-induced shape changes of endothelial cells are more intimately associated with the increase in tyrosine phosphorylation of cortactin. Because the condition where cells are exposed to PD098059 and H_2O_2 at low concentrations appeared to be milder and causes less cell detachment compared with high concentrations of H_2O_2, it was used in the rest of experiments described below.

Expression of Cortactin Mutant Confers Cells Resistant to H_2O_2-mediated Shape Change–To further evaluate the role of tyrosine phosphorylation of cortactin in the injury of endothelial cells, we constructed several retroviruses encoding a green fluorescent protein (GFP)-tagged wild-type cortactin and a cortactin mutant $Cort_{F421F466F482}$, which is deficient in tyrosine phosphorylation (20). To ensure that most cells to be analyzed express GFP-cortactin proteins, infected cells were sorted based on GFP by a flow cytometry system. After sorting, 80% cells exhibited green under a fluorescent microscope. GFP-cortactin proteins were also evaluated by immunoblot, which demonstrated comparative levels of GFP-cortactin proteins with endogenous cortactin (Fig. 5). Furthermore, the GFP-wt-cortactin behaved similarly to endogenous cortactin because it could be phosphorylated in response to H_2O_2 as efficiently as

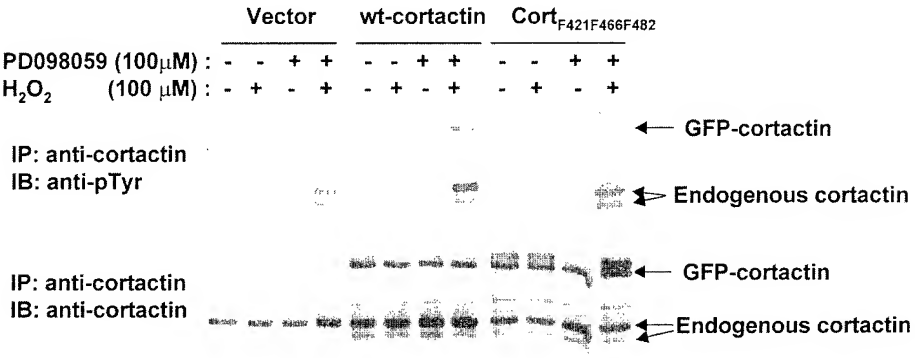

FIG. 5. **Analysis of tyrosine phosphorylation of GFP-cortactin variants in HUVE cells.** HUVE cells were infected with viruses encoding GFP-wt-cortactin, GFP-Cort$_{F421F466F482}$, and GFP only as described under "Experimental Procedures." Infected cells were pretreated with either Me_2SO (0.2%) or PD098059 (100 μM) for 1 h, followed by treatment with H_2O_2 (100 μM) for an additional 1 h. The cells were lysed, immunoprecipitated with a cortactin antibody, and immunoblotted with a monoclonal phosphotyrosine antibody. The same blot was stripped and reprobed with a monoclonal cortactin antibody (4F11). The positions for GFP-cortactin and endogenous cortactin were indicated.

the endogenous cortactin. In contrast, the mutant GFP-Cort$_{F421F466F482}$ was unable to be phosphorylated under the same conditions, which confirmed our previous conclusion that Tyr-421, Tyr-466, and Tyr-482 are the primary sites for Src *in vivo* (20).

The cells expressing different forms of GFP-cortactin variants respond differentially to H_2O_2. The GFP-wt-cortactin expressors developed significant shape changes as early as 30 min after treatment (Fig. 6*A*, *e* and *h*). Because the similar changes in control cells expressing GFP only were not observed until 1 h after treatment, the susceptibility of cells to H_2O_2 appeared to be enhanced by overexpression of GFP-wt-cortactin. In contrast, cells expressing Cort$_{F421F466F482}$ showed little difference in morphology compared with untreated cells either by 30 min or by 1 h of treatment (Fig. 6*A*, *f* and *i*), indicating that the mutant acts in a dominant negative fashion.

The activities of cortactin variants were also evaluated in NIH 3T3 cells stably transfected with Myc-tagged cortactin proteins (20). Like endothelial cells, overexpression of Myc-wt-cortactin enhanced the response of NIH 3T3 cells to H_2O_2 because the expressors could develop a dramatic shape change as characterized by rounding up and aggregation either in the presence of H_2O_2 plus PD098059 or H_2O_2 alone at 200 μM. Under the same conditions, no apparent changes were observed with control cells expressing vector only. In contrast to cells expressing Myc-wt-cortactin, no significant changes were observed with cells overexpressing Myc-Cort$_{F421F466F482}$ in the presence of either H_2O_2 alone or H_2O_2 plus PD098059. These data confirm that overexpression of cortactin enhances H_2O_2-induced shape changes in a tyrosine phosphorylation-dependent manner.

DISCUSSION

In this study, we provide evidence that tyrosine phosphorylation of cortactin is required for H_2O_2-induced shape changes in human endothelial cells. First, either H_2O_2 alone at high concentrations (more than 1.6 mM) or H_2O_2 at a low concentrations (100 μM) in the presence of PD098059, a selective inhibitor for Erk, induces a significant increase in tyrosine phosphorylation of cortactin. Tyrosine phosphorylation of cortactin appears to be one of the major events induced by H_2O_2, as indicated by analyzing total phosphotyrosyl proteins (data not shown). Second, the level of tyrosine phosphorylation of cortactin is correlated with the shape changes induced by H_2O_2. The conditions that induce high levels of tyrosine phosphorylation of cortactin are also able to induce shape changes of endothelial cells. These conditions include high concentrations of H_2O_2, H_2O_2 plus PD098059, and H_2O_2 plus vanadate. In addition, tyrosine phosphorylation induced by H_2O_2 is time-dependent and plateaus at 45 min (Fig. 2*C*). This kinetics of tyrosine phosphorylation of cortactin is correlated with shape changes induced by H_2O_2 (data not shown). Third, tyrosine phosphorylation of cortactin is dependent upon the activity of Src. Treatment of cells with a selective Src inhibitor PP2 can abrogate tyrosine phosphorylation of cortactin (data not shown) as well as the shape changes induced by H_2O_2 (Fig. 3). Finally, overexpression of a cortactin mutant deficient in tyrosine phosphorylation can significantly inhibit shape changes induced by H_2O_2 either in endothelial cells or in NIH 3T3 cells (Figs. 6 and 7).

Cortactin, a prominent substrate of Src, is a potent filament actin-binding protein. *In vitro*, cortactin also exhibits a potent activity to cross-link actin filaments into a filamentous meshwork (21). Importantly, this F-actin cross-linking activity can be down regulated upon tyrosine phosphorylation mediated by Src. Thus, tyrosine phosphorylation of cortactin likely constitutes an important mechanism by which Src or its-related protein-tyrosine kinases regulate the dynamics of the actin cytoskeleton. Consistent with the role of tyrosine phosphorylation of cortactin in cell shape changes, cells such as Src−/− cells in which cortactin is deficient in tyrosine phosphorylation are more resistant to shape changes induced by extracellular stimuli compared with cells with elevated tyrosine phosphorylation of cortactin (19). Similarly, non-phosphorylated cortactin tend to accumulate within the cytoplasm. Thus, the cortactin mutant deficient in tyrosine phosphorylation likely acts as a dominant negative fashion (20). Conversely, cells overexpressing wild-type cortactin increase susceptibility to H_2O_2 (Figs. 6 and 7).

Upon exposure to H_2O_2, many endothelial cells develop extensive membrane blebs. Similar morphological changes were also observed in cells expressing high levels of cortactin. For example, tumor cells with high levels of cortactin expression due to gene amplification often develop large spherical membrane protrusions.[2] Furthermore, transient transfection of GFP-wt-cortactin, which led to expression of extreme high levels of expression, can also result in apoptosis-like membrane blebbing.[3] Membrane blebbing may involve a mechanism similar to the formation of membrane protrusions, lamellipodia, and filopodia (29). In normal cells, cortactin is mainly associated with cell cortical structures, including lamellipodia, membrane ruffles, and punctate-like protrusions. Within these

[2] E. Schuuring, personal communication.
[3] X. Zhan, unpublished result.

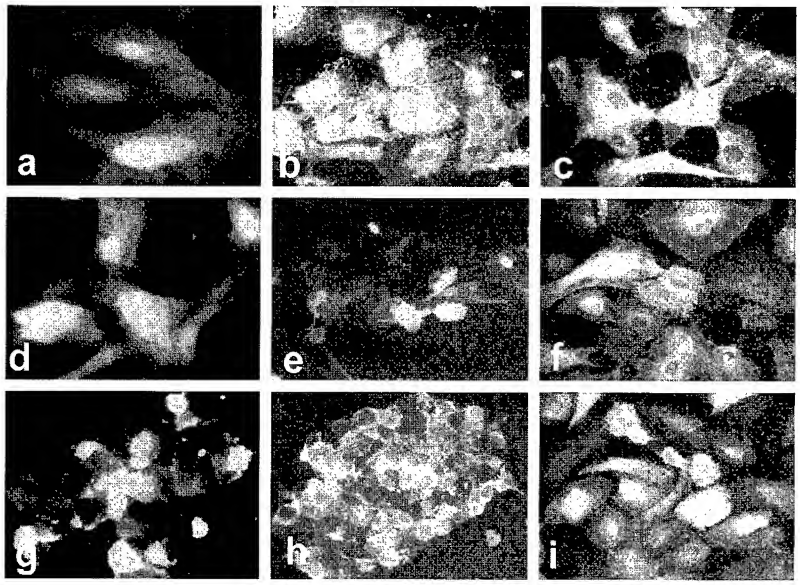

FIG. 6. **Analysis of cell shape changes in endothelial cells expressing GFP-cortactin variants.** HUVE cells were infected with GFP-cortactin viruses as described in the legend of Fig. 5. The infected cells were examined under a fluorescent microscope. *a*, *d*, and *g*, GFP only; *b*, *e*, and *h*, GFP-wt-cortactin; *c*, *f*, and *i*, GFP-Cort$_{F421F466F482}$. *a–c*, without treatment; *d–f*, treated with 100 μM H_2O_2 and 100 μM PD098059 for 30 min; *g–i*, treated with H_2O_2 and PD098059 at the same concentrations for 1 h.

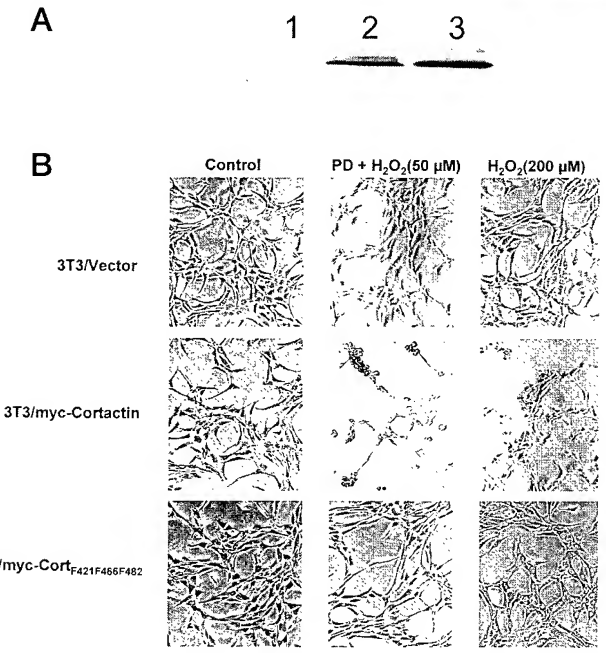

FIG. 7. **Overexpression of wild-type cortactin potentiates the response of NIH/3T3 cells to H_2O_2-mediated shape changes.** *A*, stable NIH/3T3 transfectants expressing Myc-wt-cortactin and Myc-Cort$_{F421F466F482}$ were analyzed for the expression of Myc-cortactin proteins by immunoblotting total lysates using monoclonal antibody 9E10 against the Myc epitope. *Lane 1*, cells expressing vector only; *lane 2*, cells expressing Myc-wt-cortactin; *lane 3*, cells expressing Myc-Cort$_{F421F466F482}$. *B*, NIH/3T3 transfectants expressing Myc-cortactin variant as indicated were grown on fibronectin-coated glass coverslips and treated for 1 h with either 0.2% Me_2SO as control or 100 μM PD098059. The cells were then treated with H_2O_2 at concentrations as indicated. The cells were inspected under a phase-contrast light microscope.

structures, cortactin co-localizes with F-actin (20, 30). We found that H_2O_2-induced blebs are rich in cortactin (Fig. 3), suggesting that locally concentrated cortactin may be implicated in the formation of membrane blebs. The primary driving force to form membrane protrusions is the actin polymerization occurring underneath the plasma membrane (31). One possibility is that cortactin could be directly implicated in actin polymerization. Evidence to support this possibility is our recent finding that cortactin is a potent activator of Arp2/3, a protein complex that is responsible for the nucleation of actin polymerization.[4] Cortactin may also contribute to membrane blebbing through its regulation of F-actin cross-linking. It has been postulated that the flow of the cortical actin gel is a determining factor in the formation of membrane blebs (7). The rate of flow of the actin gel is inversely regulated by the activity of F-actin cross-linking proteins. Thus, tyrosine-phosphorylated cortactin, which has a significant lower F-actin cross-linking activity than non-phosphorylated cortactin (18), would increase the flow of the actin gel and eventually favor a tuned balance toward the formation of membrane blebs. Indeed, human melanoma cell lines deficient in an actin filament cross-linking protein, ABP-280, show prolonged and extensive membrane blebbing (7).

The effect of H_2O_2 on the shape changes in endothelial cells can be dramatically enhanced by PD098059, a chemical that specifically inhibits the activity of Erk 1/2. However, the role of activation of Erk in the oxidant-mediated injury of endothelial cells is still not clear. Because the activation of Erk is implicated in the signal pathways of growth factors, Erk may represent a survival factor for cells to antagonize the effect of H_2O_2 (15). Although our data appear to be consistent with this view, we did not find an intimate correlation of the activity of Erk either with phosphorylation of cortactin nor with shape changes. Exposure to H_2O_2 at high concentrations or H_2O_2 at low concentrations in the presence of vanadate can increase tyrosine phosphorylation of cortactin and shape changes as well (Fig. 4).[5] These treatments also induce significant increase in the activity of Erk (Fig. 4). Thus, inhibition of Erk by PD098059 is not necessary either for the H_2O_2-mediated tyrosine phosphorylation of cortactin or for cell shape changes. It appears that inhibition of Erk only affects tyrosine phosphorylation of cortactin when cells expose to low concentrations of H_2O_2. One explanation is that inhibition of Erk may potentiate the activation of Src related kinases by H_2O_2. It has been shown that extracellular H_2O_2 can activate the intracellular Ras pathway (32). Recent studies also demonstrated that Ras can further activate both Src via Ral and Erk via Raf independently (16, 33). Thus, it is possible that inhibition of the activation of Erk pathway would favor the pathway by which Ras/Ral

[4] T. Uruno, J. Liu, B. Zhang, X. Fan, and X. Zhan, personal communication.

[5] Y. Li, unpublished data.

activates Src and leads to apparent increase in the tyrosine phosphorylation of cortactin.

In summary, the data presented in this study demonstrate an important role of Src and cortactin in H_2O_2-induced shape changes of endothelial cells. The future studies using small antagonists for cortactin may reveal a novel approach to target specifically at the actin cytoskeleton and protect endothelium from reactive oxygen species.

Acknowledgments—We thank Susette Mueller for confocal microscopic analysis, Mehrdad Tondravi for the help of virus preparation, and Teresa Hawley for the use of the fluorescent cell sorting system. We also thank Takehito Uruno and Peijing Zhang for critical reading.

REFERENCES

1. Hull, D. S., Green, K., Thomas, L., and Alderman, N. (1984) *Invest. Ophthalmol. Vis. Sci.* **25,** 1246–1253
2. Schror, K., Thiemermann, C., and Ney, P. (1988) *Naunyn Schmiedebergs Arch. Pharmacol.* **338,** 268–274
3. Sacks, T., Moldow, C. F., Craddock, P. R., Bowers, T. K., and Jacob, H. S. (1978) *J. Clin. Invest.* **61,** 1161–1167
4. Orr, F. W., Wang, H. H., Lafrenie, R. M., Scherbarth, S., and Nance, D. M. (2000) *J. Pathol.* **190,** 310–329
5. Nakamura, H., Nakamura, K., and Yodoi, J. (1997) *Annu. Rev. Immunol.* **15,** 351–369
6. Hinshaw, D. B., Sklar, L. A., Bohl, B., Schraufstatter, I. U., Hyslop, P. A., Rossi, M. W., Spragg, R. G., and Cochrane, C. G. (1986) *Am. J. Pathol.* **123,** 454–464
7. Cunningham, C. C. (1995) *J. Cell Biol.* **129,** 1589–1599
8. Hastie, L. E., Patton, W. F., Hechtman, H. B., and Shepro, D. (1998) *J. Cell. Biochem.* **68,** 511–524
9. Peus, D., Vasa, R. A., Meves, A., Pott, M., Beyerle, A., Squillace, K., and Pittelkow, M. R. (1998) *J. Invest Dermatol.* **110,** 966–971
10. Berk, B. C. (1999) *Thromb. Haemost.* **82,** 810–817
11. Natarajan, V., Scribner, W. M., Al Hassani, M., and Vepa, S. (1998) *Environ. Health Perspect.* **106,** 1205–1212
12. Abe, J., Takahashi, M., Ishida, M., Lee, J. D., and Berk, B. C. (1997) *J. Biol. Chem.* **272,** 20389–20394
13. Carbajal, J. M., and Schaeffer, R. C., Jr. (1998) *Biochem. Cell Biol.* **249,** 461–466
14. Barchowsky, A., Munro, S. R., Morana, S. J., Vincenti, M. P., and Treadwell, M. (1995) *Am. J. Physiol.* **269,** L829–L836
15. Guyton, K. Z., Liu, Y., Gorospe, M., Xu, Q., and Holbrook, N. J. (1996) *J. Biol. Chem.* **271,** 4138–4142
16. Goi, T., Shipitsin, M., Lu, Z., Foster, D. A., Klinz, S. G., and Feig, L. A. (2000) *EMBO J.* **19,** 623–630
17. Zhan, X., Haudenschild, C. C., Ni, Y., Smith, E., and Huang, C. (1997) *Blood* **89,** 457–464
18. Huang, C., Ni, Y., Gao, Y., Wang, T., Haudenschild, C. C., and Zhan, X. (1997) *J. Biol. Chem.* **272,** 13911–13915
19. Liu, J., Huang, C., and Zhan, X. (1999) *Oncogene* **18,** 6700–6706
20. Huang, C., Liu, J., Haudenschild, C. C., and Zhan, X. (1998) *J. Biol. Chem.* **273,** 25770–25776
21. Zhan, X., Hu, X., Hampton, B., Burgess, W. H., Friesel, R., and Maciag, T. (1993) *J. Biol. Chem.* **268,** 24427–24431
22. Wu, H., Reynolds, A. B., Kanner, S. B., Vines, R. R., and Parsons, J. T. (1991) *Mol. Cell. Biol.* **11,** 5113–5124
23. Levy-Toledano, S., Grelac, F., Caen, J. P., and Maclouf, J. (1995) *Thromb. Haemost.* **73,** 857–861
24. Kuroda, K., Ozaki, Y., Qi, R., Asazuma, N., Yatomi, Y., Satoh, K., Nomura, S., Suzuki, M., and Kume, S. (1995) *J. Immunol.* **155,** 4427–4436
25. Yanaga, F., Poole, A., Asselin, J., Blake, R., Schieven, G. L., Clark, E. A., Law, C. L., and Watson, S. P. (1995) *Biochem. J.* **311,** 471–478
26. Aikawa, R., Komuro, I., Yamazaki, T., Zou, Y., Kudoh, S., Tanaka, M., Shiojima, I., Hiroi, Y., and Yazaki, Y. (1997) *J. Clin. Invest.* **100,** 1813–1821
27. Huot, J., Houle, F., Rousseau, S., Deschesnes, R. G., Shah, G. M., and Landry, J. (1998) *J. Cell Biol.* **143,** 1361–1373
28. Alessi, D. R., Cuenda, A., Cohen, P., Dudley, D. T., and Saltiel, A. R. (1995) *J. Biol. Chem.* **270,** 27489–27494
29. Hagmann, J., Burger, M. M., and Dagan, D. (1999) *J. Cell. Biochem.* **73,** 488–499
30. Wu, H., and Parsons, J. T. (1993) *J. Cell Biol.* **120,** 1417–1426
31. Mitchison, T. J., and Cramer, L. P. (1996) *Cell* **84,** 371–379
32. Lander, H. M., Ogiste, J. S., Teng, K. K., and Novogrodsky, A. (1995) *J. Biol. Chem.* **270,** 21195–21198
33. Spaargaren, M., and Bischoff, J. R. (1994) *Proc. Natl. Acad. Sci. U. S. A.* **91,** 12609–12613

Cancer Research

CORTACTIN POTENTIATES BONE METASTASIS OF BREAST CANCER CELLS

Yansong Li[1], Mehrdad Tondravi[2], Jiali Liu[1], Elizabeth Smith[1], Christian C. Haudenschild[1], Michele Kaczmarek[2] and Xi Zhan[1,3]

1: Department of Experimental Pathology

2: Department of Hematpoiesis
Holland Laboratory, American Red Cross
15601 Crabbs Branch Way, Rockville, MD 20855
Telephone: (301) 738-0568
Fax: (301) 738-0352
E-mail: zhanx@usa.redcross.org

3: Department of Anatomy and Cell Biology
The George Washington Universtiy, Washington D.C. 20037

Key words: Cortactin, breast cancer cell, metastasis, tyrosine phosphorylation, and actin cytoskeleton

Running title: Overexpression of cortactin induces metastasis

Acknowledgment: We thank Teresa Hawley for the use of fluorescent cell sorting system and Robert Hawley for the supply of MGIN viral vector. We also thank Nick Greco for the help in culturing bone marrow endothelial cells.

Footnotes: This study was supported in part by the National Health of Institute Grant RO1 HL52753-07, Department of Defense Grant DAMD 17-98-18278 and American Heart Association Established Investigator Grant 0040135N (to X. Z.).

ABSTRACT

Gene amplification of the chromosome 11q13 in breast cancer and squamous carcinomas in the head and neck results in frequent overexpression of cortactin, a prominent substrate of Src-related tyrosine kinases in the cell cortical areas. To investigate the role of cortactin in tumor progression, we analyzed MDA-MB-231 breast cancer cells overexpressing green fluorescent protein (GFP) tagged murine cortactin and a cortactin mutant deficient in tyrosine phosphorylation under the control by a retroviral vector. Injection of MDA-MB-231 cells overexpressing GFP-cortactin into nude mice through cardiac ventricles caused bone osteolysis at a frequency higher than cells expressing the vector alone by approximately 85%, whereas injection of cells overexpressing the mutant deficient in tyrosine phosphorylation induced osteolytic metastases 74% less than the control group. Interestingly, the cells expressing either GFP-cortactin or the mutant did not show significant differences in growth in vitro or when injected subcutaneously in vivo. On the other hand, the cells overexpressing GFP-cortactin, but not the mutant, acquired an enhanced capability for transendothelial invasion and endothelial cell adhesion by more than 60%. These data suggest that cortactin contributes to tumor metastasis by enhancing the interaction of tumor cells with endothelial cells and the invasion of tumor cells into bone tissues.

INTRODUCTION

Breast cancer cells are known to spread preferentially to bone tissues and develop ultimately osteolytic metastasis[1,2]. Bone metastasis is a major cause of the decline in the quality of life of patients due to uncontrollable bone pain, pathological fractures, hypercalcemia, and nerve compression syndromes[3]. In spite of these well recognized clinical syndromes, the mechanism that causes breast tumors to target on bone tissue remains unclear. Breast cancer is frequently associated with gene amplification at the chromosome 11q13, resulting in overexpression of cortactin (EMS1)[4], a cortical actin-associated protein that is a prominent substrate of the protein tyrosine kinase Src[5,6]. Gene amplification of cortactin is also frequently found in other types of cancer including head and neck squamous carcinoma and bladder cancer[7,8]. While the precise role of cortactin in tumor progression remains unclear, amplification and overexpression of cortactin appear to be intimately associated with patients with poor prognosis or relapse[9], indicating that overexpression of cortactin may contribute to a late stage of tumor progression.

Cortactin is accumulated in peripheral structures of cells including lamellipodia and membrane ruffles where cortical actin is enriched[10]. In MDA-MB-231 breast cancer cells plated on extracellular matrix cortactin is enriched in invadopodia, a type of membrane protrusions that participates in degradation of and invasion into the matrix[11]. The protein sequence of cortactin is featured by six and half tandem copies of a unique 37-amino-acid repeat and a Src homology 3 (SH3) domain at the carboxyl terminus. Our previous studies have determined that Src-mediated tyrosine phosphorylation primarily occurs at residues Tyr-421, Tyr-466 and Tyr-482, which lie between the repeat domain and the SH3. *In vitro*, cortactin binds to and cross-links F-actin into meshwork. The F-actin cross-linking activity of cortactin can be reduced upon tyrosine

phosphorylation mediated by Src[5]. Inhibition of tyrosine phosphorylation of cortactin by a selective Src inhibitor reduces the response of endothelial cells to hydrogen peroxide-mediated cell injury[12]. Likewise, overexpression of a cortactin mutant that is deficient in tyrosine phosphorylation can compromise cell shape changes induced by reactive oxygen species, whereas overexpression of wild-type cortactin results in enhancement of the injury response to hydrogen peroxide[12]. The role of cortactin in the cytoskeletal reorganization is further highlighted by a recent finding that cortactin binds to Arp2/3 complex and activates Arp2/3 complex-mediated actin polymerization[13]. Thus, cortactin appears to act as a signaling molecule in the regulation of the dynamics of actin cytoskeleton in a tyrosine phosphorylation dependent manner.

Although the biochemical and cellular function of cortactin and its relationship with poor prognosis in a subset of cancers suggest that cortactin may play a role in tumor metastasis, direct evidence is lacking. In the present study, we examined the metastatic ability of MDA-MB-231 breast cancer cells overexpressing wild-type cortactin and a cortactin mutant with defect in tyrosine phosphorylation. We show here that overexpression of wild-type cortactin promoted the metastatic potential of tumor cells, whereas overexpression of the phosphorylation deficient cortactin mutant inhibited metastasis. In addition, we show that cortactin influences the interaction of tumor cells with endothelial cells. Thus, our study provides direct evidence first time for the role of cortactin in tumor metastasis.

MATERIALS AND METHODS

Reagents

Unless stated otherwise, all chemicals were purchased from Sigma Chemical Co. (St. Louis, MO). Lipofectamine and G418 were purchased from Life Technologies Inc. (Rockville, MD). Protein A Sepharose CL-4B and ECL western blotting kits were from Amersham Pharmacia (Piscataway, NJ). Monoclonal anti-phosphotyrosine antibody (4G10) and monoclonal anti-cortactin antibody (4F11) were purchased from Upstate Biotechnology, Inc. (Lake Placid, NY). Polyclonal cortactin antibody was prepared as previously described[14].

Cell Culture

MDA-MB-231 cells were grown in Dulbecco's modified Eagle's medium (DMEM) supplemented with 10% (vol/vol) fetal bovine serum (FBS). Human bone marrow endothelial cells (BMEC), gifted from Malcolm Moore at Sloan-Kettering, were maintained in Iscove's Modified Dublecco's Medium (IMDM, GiBcoBRL) supplemented with 20% FBS, 1x antibiotic-antimycotic solution, and 2 mM L-Glutamine in a 75-cm^2 tissue culture flask (Corning).

Construction and Preparation of Cortactin Virus

Retrovirus encoding GFP-cortactin and GFP-$Cort_{F421F466F482}$ were constructed and prepared as previously described[12]. The viral vector (MGIN) was a gift of Robert Hawley (Holland Laboratory) and was previously described[15].

Viral Infection

MDA-MB-231 cells were plated at a density of $1x10^5$ in 35-mm dishes. On the next day, the medium was replaced with 1 ml of viral supernatant containing 8 μg/ml of polybrene. After 48 h of incubation, the culture medium was replaced with DMEM containing 10% FBS. Expression of GFP proteins was monitored by fluorescence microscopy. To increase the

efficiency of infection, the cells were re-infected with virus for two or three times, and the infected cells were enriched further by fluorescence activated cell sorting (FACS).

FACS Analysis

MDA-MB-231 cells ($2x10^6$) infected with cortactin viruses were trypsinized, washed and suspended in phosphate basic saline (PBS) supplemented with 2% FBS. The suspended cells were sorted in a FACS system (Beckton Dickinson, Franklin Lakes, NJ) according to light scatter and fluorescence intensity. Sorted cells with expression efficiencies from 85% to 98% were used for further analysis.

Phosphotyrosine Immunoblot Analysis

Cells were extracted in lysis buffer (50 mM Tris-HCl, pH7.4, containing 1% NP-40, 0.25% sodium deoxycholate, 150 mM NaCl, 1mM EDTA, 1 mM PMSF, 1 μg/ml aprotinin, 1 μg/ml leupeptin, 1 μg/ml pepstatin, 2mM Na_3VO_4, and 1mM NaF). The extracts were centrifuged at 14,000 x rpm for 10 min at 4°C in a microcentrifuge. The clarified supernatants were immunoprecipitated with 5 μg polyclonal cortactin antisera [14]. The immunoprecipitates were resolved by SDS-polyacrylamide gel electrophoresis (PAGE) (7.5%, w/v), transferred to a nitrocellulose membrane, and further blotted with a monoclonal phosphotyrosine antibody (4G10). To measure the expression levels of cortactin, the blot membrane was stripped and re-blotted with monoclonal cortactin antibody (4F11).

Cell Growth Assay

MDA-MB-231 cells were seeded on Day 0 in a 12-well plate at a density of 0.4×10^5 cells per well in DMEM supplemented with 10% of FBS and 1 x antibiotic-antimycotic solution (Life Technologies). At the times from day 1 to 6, cells were trypsinized and counted with a

hemocytometer under a phase-contrast light microscope. Quadrupled simples were analyzed for each time point.

Colony formation assay

Cells were trypsinized and resuspended in DMEM plus 10% FBS. The suspended cells (500) were mixed with 1 ml 0.4% top agarose (Sea-plaque, FMC Corp. Bioproducts, Rockland, ME) in DMEM plus 10% FBS. The mixture was plated onto a 35-mm petri dish containing 1 ml 0.6% bottom agarose in the same culture medium and incubated at 37°C, 5% CO_2. After two weeks, colonies were examined under a fluorescent microscope (Olympus 70-S1F2) equipped with a RT Slider digital camera (Diagnostic Instruments, Inc.). To count the colonies, each dish was divided into 18 zones with a marker and the cell image in each zone was captured by the digital camera. The colonies with diameters greater than 100 μm were counted and averaged based on the 18 images. For each cell line, four independent dishes were examined.

Tumorigenicity of MDA-MB-231 cells in the mammary fat pad of nude mice

All animal works described here were performed according to protocols approved by Institutional Animal Care And Use Cmmittee in Holland Laboratory. Tumorigenicity of MDA-231 cells was determined based on a modified method [16]. Briefly, cells (2×10^6) were suspended in 0.2 ml 50% (v/v) Matrigel (Collaborative Research, Bedford, MA) in PBS. Female nude mice (4-wk-old) were anesthetized with ketamine (30 μg/gram) and xylazine (1.5 μg/gram). The mammary fat pad of a mouse was exposed by a skin incision of right lateral thorax, and the cells were inoculated into the tissue using a 23-gauge needle. For each cell sample, 8 mice were analyzed. Four weeks after injection, the animals were sacrificed, and the tumors were removed and weighed.

Analysis of adhesion of MDA-MB-231 cells to* human bone marrow endothelial *cells

The procedure was based on a modified method as described[17]. Briefly, human bone marrow endothelial cells (a gift of Malcolm Moore at Sloan-Kettering) were plated on fibronectin-coated 2-well Lab-TeK chamber slides (Nunc Inc. Naperville, IL) at a density of 2×10^5 per well. After cells were confluent, MDA-MB-231 cells expressing GFP-cortactin variants were trypsinized, resuspended in DMEM containing 0.1% BSA and 1 mM $CaCl_2$, and plated over the monolayers of endothelial cells that had been washed with PBS twice immediately prior to plating. The cells were incubated at 37°C for 4 h in a CO_2 incubator. Non-attached cells were removed by three washes with PBS. Attached cells were fixed with 3.7% formaldehyde for 30 min. Cells adhered to endothelial cells were inspected under a fluorescent microscope equipped with a digital camera and quantified by counting green cells based on 5 random digital images of high power fields (HPF) taken at 200 x magnification. The average number of adhered cells and the standard derivation were calculated based on three independent experiments.

Analysis of Transendothelial Invasion by Tumor Cells

Transendothelial invasion of MDA-MB-231 cells was analyzed based on a modified method as described[18]. Briefly, human bone marrow endothelial cells (3×10^5) were plated on a fibronectin-coated polycarbonate membrane insert (with 6.5 mm in diameter and 8.0 μm pores) in a Transwell apparatus (Costar, Cambridge, MA) and maintained in IMDM containing 20% FBS, 1 x antibiotic-antimycotic solution, and 2 mM L-glutamine. After cells reached to confluence, MDA-MB-231 cells expressing GFP-cortactin variants were trypsinized and resuspended in DMEM containing 10% FBS. The suspended cells (3×10^4) were seeded on the monolayer of endothelial cells and incubated for 20 h at 37°C in a CO_2 incubator. After incubation, the insert was washed with PBS. The cells on the upper surface of the insert were

removed by wiping with a cotton swab. The cells migrated to the lower surface of the insert were fixed with 3.7% formaldehyde and subjected to fluorescence microscopic inspection. Green cells were counted based on five HPF digital images randomly taken at 200 x magnification. The average of cell number and the standard derivation were calculated based on duplicated experiments.

Intracardiac Injections of MDA-MB-231 Cells in Nude Mice.

Subconfluent MDA-MB-231 cells were fed with DMEM containing 10% FBS 24 h before injection. The cells were trypsinized, immediately suspended in DMEM containing 0.2 mg/ml soybean trypsin inhibitor, and washed twice with PBS. The washed cells were finally resuspended in cold PBS at a density of 2.5×10^6 cells/ml on ice. Female BALB/c-nu/nu mice at ages of 4 to 5 weeks (National Cancer Institute, Frederick, MD) were anesthetized with ketamine (30 μg/gram) and xylazine (1.5 μg/gram). The suspended cells ($5x10^5$) were injected into the heart left ventricle of animals with a 27-gauge needle. The injected animals were housed in a pathogen-free environment for 5 to 10 weeks. Body weights of animals were measured using a digital Sartorius weigher (The Scale People, Inc. Beltsville, MD). Experiments were repeated twice, and each involving 5 animals for each cell sample.

Statistical analysis

Statistical evaluation of the difference among each group was performed by Mann-Whitney test using GraphPad InStat software. All data shown were the mean ± standard deviation.

Determination of Bone Metastases by X-radiography

Tumors in bone were examined by X-ray radiographs 5 weeks after injection. Animals were anesthetized and placed in a transparent board in prone and lateral positions. The board was

placed against an X-ray film (22 x 27 mm; X-OMAT AR; Kodak, Rochester, NY) and exposed to X-ray at 30 kv for 10 seconds in a Fixitron radiographic inspection unit (Model 43855A). Exposed films were developed using an automatic film processor (Kodak RP X-OMAT). Radiographs of bones were evaluated for the presence of tumor foci.

Histological Examinations

Animals were sacrificed with CO_2. The Lung, heart, liver, kidney, spleen, pancreas, forelimbs and hindlimbs were incised and fixed with 10% formalin. The bone tissues were decalcified in Cal-Ex II solution (Fisher Scientific) for 24 hours. All tissues were embedded in paraffin. Histological sections were prepared by a standard conventional processing and stained with Hematoxylin-Eosin (H & E). Micrographs were taken with a Nikon microscope equipped with a digital camera (Cool Snap) and further processed using Adobe photoshop software.

RESULTS

Preparation of MDA-MB-231 cells infected with retrovirus carrying GFP-cortactin variants

To examine the role of cortactin in tumor progression, wild-type cortactin and a tyrosine phosphorylation deficient cortactin mutant[19] were tagged at their N-termini by green fluorescent protein (GFP) in a retroviral vector MGIN as described previously[12], yielding fusion proteins GFP-cortactin and GFP-$Cort_{F421F466F482}$, respectively. The viruses carrying GFP-cortactin and GFP-$Cort_{F421F466F482}$ were used to infect MDA-MB-231 cells. The infected cells were further enriched up to 85% by FACS based on the expression of GFP. Expression of GFP-cortactin proteins was further quantified with immunoblot analysis. As shown in Figure 1, both GFP-cortactin and GFP-$Cort_{F421F466F482}$ were expressed at a level nearly 2-fold higher than endogenous cortactin. The epitope GFP did not seem to affect the specificity of tyrosine phosphorylation of cortactin because GFP-cortactin, but not GFP-$Cort_{F421F466F482}$, was able to be phosphorylated in response to a mixture of hydrogen peroxide and sodium vanadate (Figure 1). The similar response was also described with either endogenous cortactin or small epitopes such as Myc tagged cortactin proteins[19].

Overexpression of GFP-cortactin variants did not affect the growth of breast cancer cells.

To study the effect of cortactin on cell proliferation, the growth of MDA-MB-231 cells infected with GFP-cortactin viruses in either normal culture medium, or soft agarose, or the mammary fat pad of nude mice was evaluated. All these assays did not detect any significant differences among cells expressing GFP-cortactin, GFP-$Cort_{F421F466F482}$, and GFP only (Figure 2A, B, and C), indicating that cortactin and its mutant deficient in tyrosine phosphorylation have no significant effect on cell growth.

Overexpression of GFP-cortactin potentiates bone metastases

MDA-MB-231 cells infected with GFP-cortactin variants were also evaluated for their metastatic ability by an experimental bone metastasis assay involving injection of the cells into the left ventricles of nude mice[20]. After 5 weeks of injection, the animals bearing GFP-cortactin cells developed apparent cachexia (loss of muscle, fat, and body weight). These animals had an average body weight 25% less than that of control animals injected with cells expressing the viral vector only (Figure 3A). In contrast, the average body weight of mice bearing GFP-$Cort_{F421F466F482}$ was about 20% higher than that of the control animals.

The tumors that had metastasized into bone tissues were examined by X-ray radiography, which revealed tumor-induced bone lesions as radio-lucent foci (Figure 3C). As summarized in Figure 3B, the mice bearing GFP-cortactin cells developed an average of 7 tumors per animal, whereas the mice bearing GFP only developed an average of less 4 tumors per animal. In contrast, the mice injected with GFP-$Cort_{F421F466F482}$ cells showed much less potential for bone metastasis with only one tumor per animal. This result is consistent with our previous finding that the mutant acts in a dominant negative manner within cells[12]. Tumors grown in other tissues were also examined by histological analysis. Most tumor metastases were found within bone tissues, a few in the lung and one in the adrenal gland (Table 1). No tumors were found in the heart, kidney, spleen, liver and pancreas.

Overexpression of GFP-cortactin variants modulates transendothelial invasion of MDA-MB-231 cells

We also attempted to examine whether the enhancement of tumor metastases manifested by overexpression of cortactin could be due to an increase in invasion through endothelial cells[21]. Tumor cells were placed on the monolayer of human bone marrow endothelial cells (BMEC)

grown in the top chamber of Transwell, a modified Boyden chamber apparatus. After 20 h, the cells migrated through the membrane on the bottom chamber were examined by fluorescent microscopy. As shown in Figure 4A, GFP-cortactin cells exhibited a motility 70% higher than that of the control cells, whereas the motility of GFP-$Cort_{F421F466F482}$ cells was 45% lower than that of the control cells (Figure 4A).

The apparent cortactin-induced increase in transendothelial invasion could be the result of increase in their adhesions to endothelial cells. The adhesive abilities of tumors cells were evaluated by measuring the numbers of cells that were able to attach to the monolayer of BMEC 4 h after plating. As shown in Figure 4B, GFP-cortactin cells enhanced by approximately 62% the adhesive affinity for endothelial cells compared to cells expressing the viral vector alone, whereas GFP-$Cort_{F421F466F482}$ cells adhered to BMEC cells with an efficiency 40% lower than the control cells.

DISCUSSION

Metastasis is a multi-stage process and requires tumor cell invasion into lymphatic and blood circulation systems, adhesion to endothelium, transendothelial invasion and migration, and finally colonization in distant tissues[22]. While the detailed molecular mechanism for each process remains unclear, tumor invasion requires the formation of protrusions projected from the membrane surface of tumor cells[23]. These pseudopods, which are also called invadopodia[24], may facilitate either the action of proteinases for the degradation of extracellular matrix around the tumors or penetration of cells into contact regions between endothelial cells, eventually enabling the entire cells to invade through the endothelial layer[23]. Thus, a molecule that is implicated in the formation of cellular protrusions and cell adhesion to endothelial cells would be likely a good candidate for playing a role in metastasis. The study described here provides first evidence that cortactin, a cell protrusion associated protein, is able to enhance tumor metastasis *in vivo*. Overexpression of wild-type cortactin in MDA-MB-231 cells enhanced significantly the frequency of bone metastasis of the cells in nude mice (Figure 3). This result was consistent with the reports that overexpression of cortactin via gene amplification is often associated with poor prognosis of cancer patients[9,25].

Cortactin could play a role in early stages of tumor progression because its phosphorylation level is known to be up-regulated by oncogenes and growth factors[26,27]. However, cells overexpressing either wild-type or tyrosine phosphorylation deficient cortactin variants showed a similar growth rate to control cells expressing the vector only as analyzed by growth curve, colony formation in soft agarose and growth in the mammary fat pad (Figure 2). This result agrees with our previous finding that the Src(-/-) cells, in which tyrosine phosphorylation of cortactin is impaired, exhibit a similar response as normal cells to FGF for

cell growth[6]. Thus, overexpression of cortactin via gene amplification may serve as a pathogenic mechanism in the late stages of tumor development, rather contribute directly to the primary tumor progression, which is known to involve many genes responsible for the cell cycle regulation[28]. However, the pathological function of cortactin may be implemented in concert with oncogenes that are involved in the cell growth. In this regard, it is worth to note that cortactin is frequently co-amplified in cancers with cyclin D1, an important regulator of the cell cycle[4].

Overexpression of cortactin can increase by 62 to 70% in transendothelial invasion as well as adhesion to endothelial cells (Figure 4). Adhesion of tumor cells to endothelial cell is known to be an important step in tumor metastasis and may determine the rate of cell transendothelial invasion[29]. Indeed, highly metastatic colorectal cancer cells also tend to have higher affinities for endothelial cells than poorly metastatic cells [30]. However, the mechanism by which overexpression of cortactin facilitates the interaction of tumor cells with endothelial cells is not clear. It may involve the activation of cell surface proteins implicated in cell adhesions via alteration of the actin cytoskeleton underneath the plasma membrane, which is required for the function of cell- to-cell or cell-to-extracellular matrix[31]. The actin cytoskeleton is a dynamic structural entity and undergoes constantly assembly or disassembly[32]. The assembled actin filaments can be further cross-linked to form either actin bundles or actin meshwork. Cortactin may alter the cytoskeleton by its ability to promote actin assembly via activation of Arp2/3, a protein complex that plays a vital role in the nucleation of actin assembly[13], and the ability to cross-link actin filaments in a manner dependent reversibly on its tyrosine phosphorylation[5]. Cortactin also contains a carboxyl terminal SH3 domain, which is known to bind to various

membrane associated proteins, including ZO1, a junction associated protein[33]. Thus, cortactin may link a cell adhesion molecule either directly or indirectly via its SH3 domain.

TABLE LEGEND

Table 1. The frequency of metastasis of MDA-MB-231 cells into the organs of mice. The internal organs of the mice infected with GFP-cortactin virus were incised and fixed. The resulting paraffin sections were examined for the presence of tumor cells. The data were compiled from 10 animals in each group.

FIGURE LEGENDS

Figure 1. Analysis of the expression of GFP-cortactin proteins in MDA-MB-231 cells.

MDA-MB-231 cells were infected with viruses encoding GFP-Cortactin, GFP-$Cort_{F421F466F482}$ and GFP. Infected cells were treated with 100 μM of pervanadate (100 μM hydrogen peroxide and 100 μM sodium vanadate) for 1 h. The cells were lysed, immunoprecipitated with polyclonal cortactin antibody and further immunoblotted with a monoclonal phosphotyrosine antibody (4G10). The same blot was stripped and reprobed with a monoclonal cortactin antibody (4F11). The positions for GFP-cortactin and endogenous cortactin were indicated by arrows.

Figure 2. Analysis of the effect of cortactin on the growth of MDA-MB-231 cells.

(**A**) MDA-MB-231 cells infected with cortactin viruses were plated in a 12-well plate at a density of 0.4×10^5/well in DMEM medium supplemented with 10% FBS. At day 1, 2, 3, 4, 5 and 6, cells were harvested and counted with a hemocytometer. The data represent the mean of four independent experiments. (**B**) MDA-MB-231 cells were mixed with 0.4% soft agarose and plated to 35 mm dishes at the density of 500 cells/dish. After 14 days of incubation, colonies developed in the soft agarose with sizes greater than 100 μm in diameter were counted. Data shown are the mean ± standard derivation (n=4). (**C**) Cells ($2x10^6$) were suspended in the mixture of PBS and Matrigel (1:1) were injected into the mammary fat pad of nude mice (8 mice per cell sample). Four weeks after injection, the tumors were removed and weighed. Values shown are the mean ± standard derivation (n=8). No significant differences were detected among each group by Mann-Whitney test ($p>0.05$).

Figure 3. Analysis of bone metastases of MDA-MB-231 cells expressing GFP-cortactin proteins.

MDA-MB-231 cells infected with cortactin viruses were injected into the left ventricle of nude mice as described in the Materials and Methods. The experiment was repeated twice. In each experiment 5 animals for each cell sample were analyzed. At 5 weeks after injection, the body weights of the mice were measured (**A**) and further examined by X-ray radiograph (**B**). All data shown represent the mean ± standard deviation (n=10). Representative radiography for each group was also shown (**C**). The bone lesions at the joints between femurs and tibiae in high magnification were indicated by arrows in the bottom panel **C**.

Figure 4. Cortactin potentiates the transendothelial invasion and adhesion of MDA-MB-231 cells. (**A**). 3×10^4 of MDA-MB-231 cells expressing cortactin variants were seeded over confluent human bone marrow endothelial cells (BMEC). After 20 h, the cells migrated through the endothelium layer were counted. The numbers shown represent the mean ± standard deviation of three independent experiments. (**B**) MDA-MB-231 cells expressing cortactin variants (2×10^5) were plated on the monolayer of BMEC. After 4 h, adhered cells were photographed under a fluorescent microscope. The data shown are the mean ± standard deviation of three independent experiments.

References

1. Cifuentes, N. and Pickren, J. W. Metastases from carcinoma of mammary gland: an autopsy study. J Surg.Oncol., *11*: 193-205, 1979.

2. Elte, J. W., Bijvoet, O. L., Cleton, F. J., van Oosterom, A. T., and Sleeboom, H. P. Osteolytic bone metastases in breast carcinoma pathogenesis, morbidity and bisphosphonate treatment. Eur.J Cancer Clin.Oncol., *22*: 493-500, 1986.

3. Coleman, R. E. and Rubens, R. D. The clinical course of bone metastases from breast cancer. Br.J Cancer, *55*: 61-66, 1987.

4. Schuuring, E., Verhoeven, E., Mooi, W. J., and Michalides, R. J. Identification and cloning of two overexpressed genes, U21B31/PRAD1 and EMS1, within the amplified chromosome 11q13 region in human carcinomas. Oncogene, *7*: 355-361, 1992.

5. Huang, C., Ni, Y., Wang, T., Gao, Y., Haudenschild, C. C., and Zhan, X. Down-regulation of the filamentous actin cross-linking activity of cortactin by Src-mediated tyrosine phosphorylation. J Biol.Chem., *272*: 13911-13915, 1997.

6. Liu, J., Huang, C., and Zhan, X. Src is required for cell migration and shape changes induced by fibroblast growth factor 1. Oncogene, *18*: 6700-6706, 1999.

7. Bringuier, P. P., Tamimi, Y., Schuuring, E., and Schalken, J. Expression of cyclin D1 and EMS1 in bladder tumours; relationship with chromosome 11q13 amplification. Oncogene, *12*: 1747-1753, 1996.

8. Williams, M. E., Gaffey, M. J., Weiss, L. M., Wilczynski, S. P., Schuuring, E., and Levine, P. A. Chromosome 11Q13 amplification in head and neck squamous cell carcinoma. Arch.Otolaryngol.Head Neck Surg., *119*: 1238-1243, 1993.

9. Rodrigo, J. P., Garcia, L. A., Ramos, S., Lazo, P. S., and Suarez, C. EMS1 gene amplification correlates with poor prognosis in squamous cell carcinomas of the head and neck [In Process Citation]. Clin.Cancer Res., *6*: 3177-3182, 2000.

10. Wu, H. and Parsons, J. T. Cortactin, an 80/85-kilodalton pp60src substrate, is a filamentous actin-binding protein enriched in the cell cortex. J Cell Biol., *120*: 1417-1426, 1993.

11. Bowden, E. T., Barth, M., Thomas, D., Glazer, R. I., and Mueller, S. C. An invasion-related complex of cortactin, paxillin and PKCmu associates with invadopodia at sites of extracellular matrix degradation. Oncogene, *18*: 4440-4449, 1999.

12. Li, Y., Liu, J., and Zhan, X. Tyrosine phosphorylation of cortactin is required for H2O2-mediated of injury of human endothelial cells. J Biol.Chem., 275: 37187-37193, 2000.

13. Uruno, T., Liu, J., Zhang, P., Egile, C., Li, R., Mueller, S. C., and Zhan, X. Activation of Arp2/3 complex-mediated actin polymerization by cortactin. Nature Cell Biology, 3: 259-266, 2001.

14. Zhan, X., Hu, X., Hampton, B., Burgess, W. H., Friesel, R., and Maciag, T. Murine cortactin is phosphorylated in response to fibroblast growth factor-1 on tyrosine residues late in the G1 phase of the BALB/c 3T3 cell cycle. J Biol.Chem., *268*: 24427-24431, 1993.

15. Cheng, L., Du, C., Murray, D., Tong, X., Zhang, Y. A., Chen, B. P., and Hawley, R. G. A GFP reporter system to assess gene transfer and expression in human hematopoietic progenitor cells. Gene Ther., *4*: 1013-1022, 1997.

16. Price, J. E., Polyzos, A., Zhang, R. D., and Daniels, L. M. Tumorigenicity and metastasis of human breast carcinoma cell lines in nude mice. Cancer Res., *50*: 717-721, 1990.

17. Cohen, M. C., Mecley, M., Antonia, S. J., and Picciano, P. T. Adherence of tumor cells to endothelial monolayers: inhibition by lymphokines. Cell Immunol., *95*: 247-257, 1985.

18. Okada, T., Okuno, H., and Mitsui, Y. A novel in vitro assay system for transendothelial tumor cell invasion: significance of E-selectin and alpha 3 integrin in the transendothelial invasion by HT1080 fibrosarcoma cells. Clin.Exp.Metastasis, *12*: 305-314, 1994.

19. Huang, C., Liu, J., Haudenschild, C. C., and Zhan, X. The role of tyrosine phosphorylation of cortactin in the locomotion of endothelial cells. J Biol.Chem., *273*: 25770-25776, 1998.

20. Mbalaviele, G., Dunstan, C. R., Sasaki, A., Williams, P. J., Mundy, G. R., and Yoneda, T. E-cadherin expression in human breast cancer cells suppresses the development of osteolytic bone metastases in an experimental metastasis model. Cancer Res., *56*: 4063-4070, 1996.

21. De Bruyn, P. P., Michelson, S., and Thomas, T. B. The migration of blood cells of the bone marrow through the sinusoidal wall. J Morphol., *133*: 417-437, 1971.

22. Weiss, L., Orr, F. W., and Honn, K. V. Interactions of cancer cells with the microvasculature during metastasis. FASEB J, *2*: 12-21, 1988.

23. Voura, E. B., Sandig, M., Kalnins, V. I., and Siu, C. Cell shape changes and cytoskeleton reorganization during transendothelial migration of human melanoma cells. Cell Tissue Res., *293*: 375-387, 1998.

24. Mueller, S. C. and Chen, W. T. Cellular invasion into matrix beads: localization of beta 1 integrins and fibronectin to the invadopodia. J.Cell Sci, *99 (Pt 2)*: 213-225, 1991.

25. Meredith, S. D., Levine, P. A., Burns, J. A., Gaffey, M. J., Boyd, J. C., Weiss, L. M., Erickson, N. L., and Williams, M. E. Chromosome 11q13 amplification in head and neck squamous cell carcinoma. Association with poor prognosis. Arch.Otolaryngol.Head Neck Surg., *121*: 790-794, 1995.

26. Garfinkel, S., Hu, X., Prudovsky, I. A., McMahon, G. A., Kapnik, E. M., McDowell, S. D., and Maciag, T. FGF-1-dependent proliferative and migratory responses are impaired in senescent human umbilical vein endothelial cells and correlate with the inability to signal

tyrosine phosphorylation of fibroblast growth factor receptor-1 substrates. J Cell Biol., *134*: 783-791, 1996.

27. Zhan, X., Plourde, C., Hu, X., Friesel, R., and Maciag, T. Association of fibroblast growth factor receptor-1 with c-Src correlates with association between c-Src and cortactin. J Biol.Chem., *269*: 20221-20224, 1994.

28. Nishida, N., Fukuda, Y., Komeda, T., Kita, R., Sando, T., Furukawa, M., Amenomori, M., Shibagaki, I., Nakao, K., and Ikenaga, M. Amplification and overexpression of the cyclin D1 gene in aggressive human hepatocellular carcinoma. Cancer Res., *54*: 3107-3110, 1994.

29. Nicolson, G. L. Metastatic tumor cell attachment and invasion assay utilizing vascular endothelial cell monolayers. J Histochem.Cytochem., *30*: 214-220, 1982.

30. Sawada, H., Wakabayashi, H., Nawa, A., Mora, E., Cavanaugh, P. G., and Nicolson, G. L. Differential motility stimulation but not growth stimulation or adhesion of metastatic human colorectal carcinoma cells by target organ- derived liver sinusoidal endothelial cells. Clin.Exp.Metastasis, *14*: 308-313, 1996.

31. Pavalko, F. M. and Otey, C. A. Role of adhesion molecule cytoplasmic domains in mediating interactions with the cytoskeleton. Proc.Soc.Exp.Biol.Med., *205*: 282-293, 1994.

32. Stossel, T. P. On the crawling of animal cells. Science, *260*: 1086-1094, 1993.

33. Katsube, T., Takahisa, M., Ueda, R., Hashimoto, N., Kobayashi, M., and Togashi, S. Cortactin associates with the cell-cell junction protein ZO-1 in both Drosophila and mouse. J Biol.Chem., *273*: 29672-29677, 1998.

Table 1

	Bone	Lung	Adrenal gland	Kidney	Spleen	Liver	Heart	Pancreas
MDA/GFP	30	5	0	0	0	0	0	0
MDA/GFP-wt-Cortactin	57	4	0	0	0	0	0	0
MDA/GFP-$Cort_{F421F466F482}$	9	0	1	0	0	0	0	0

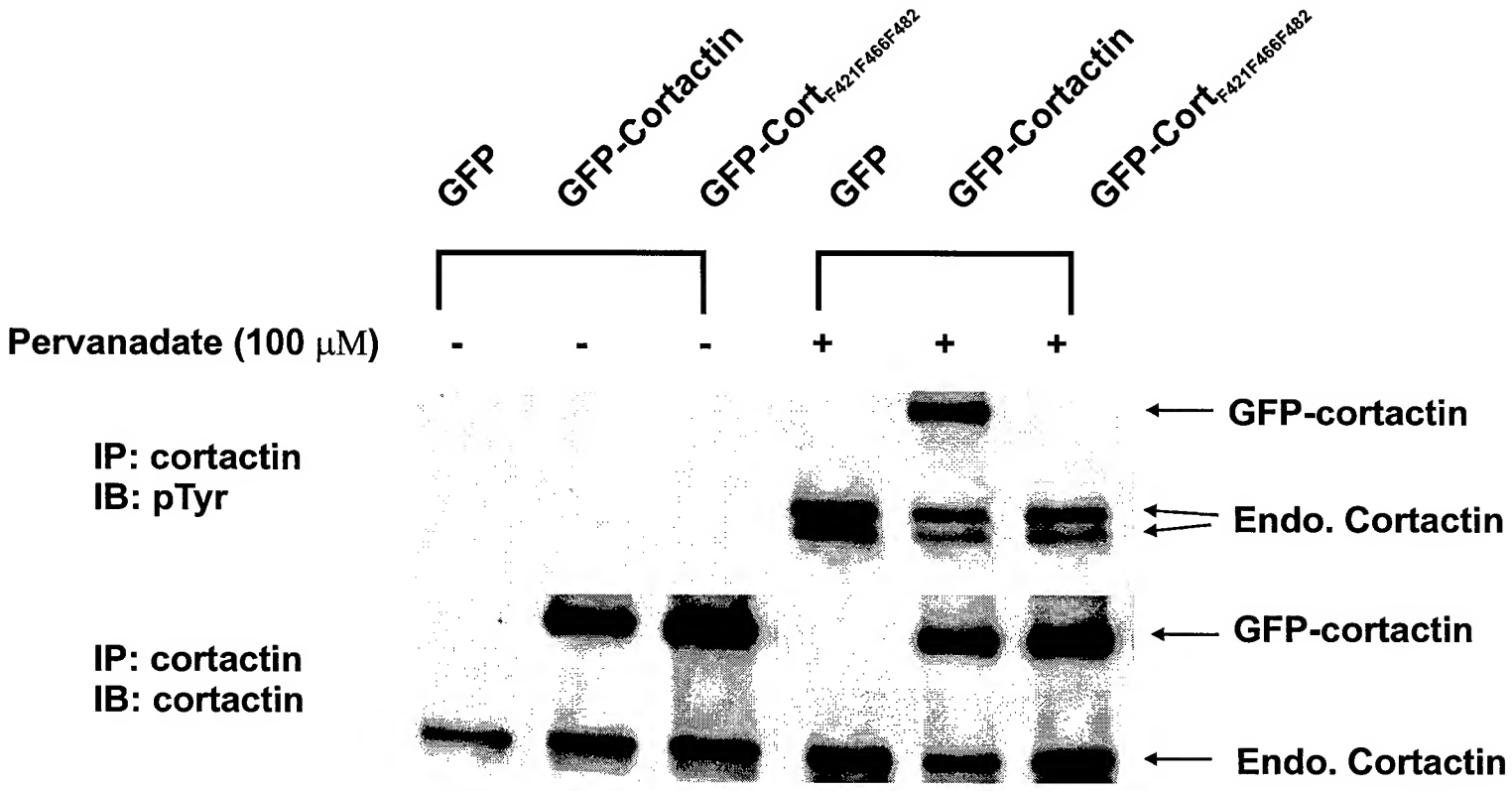
GFP
GFP-Cortactin
GFP-Cort$_{F421F466F482}$
GFP
GFP-Cortactin
GFP-Cort$_{F421F466F482}$
Pervanadate (100 μM)
- - - + + +
IP: cortactin
IB: pTyr
GFP-cortactin
Endo. Cortactin
IP: cortactin
IB: cortactin
GFP-cortactin
Endo. Cortactin

Figure 1

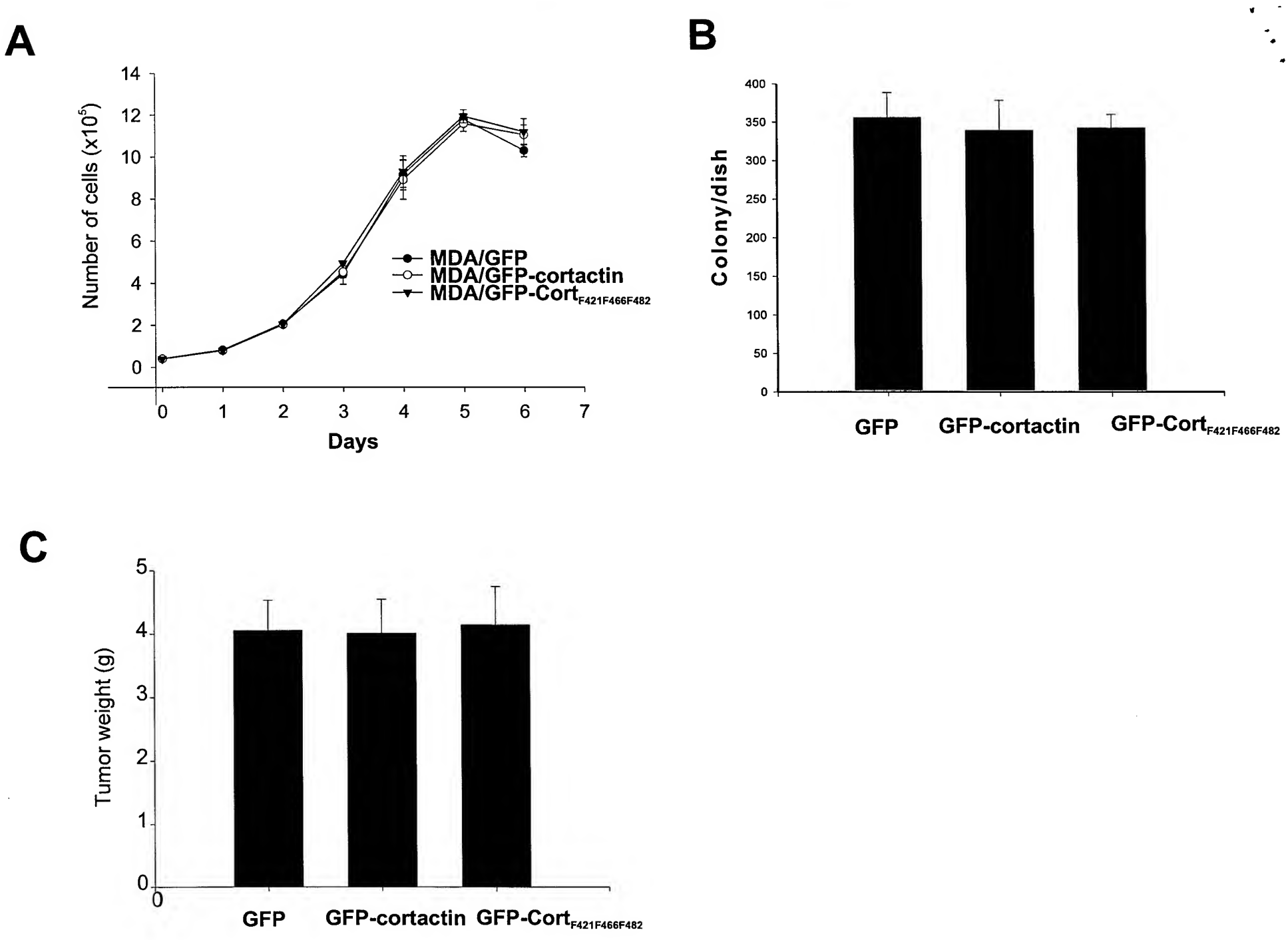
A
Number of cells (x10^5)
14
12
10
8
6
4
2
0
0 1 2 3 4 5 6 7
Days
MDA/GFP
MDA/GFP-cortactin
MDA/GFP-Cort F421F466F482
B
Colony/dish
400
350
300
250
200
150
100
50
0
GFP
GFP-cortactin
GFP-Cort F421F466F482
C
Tumor weight (g)
5
4
3
2
1
0
0
GFP
GFP-cortactin
GFP-Cort F421F466F482

Figure 2

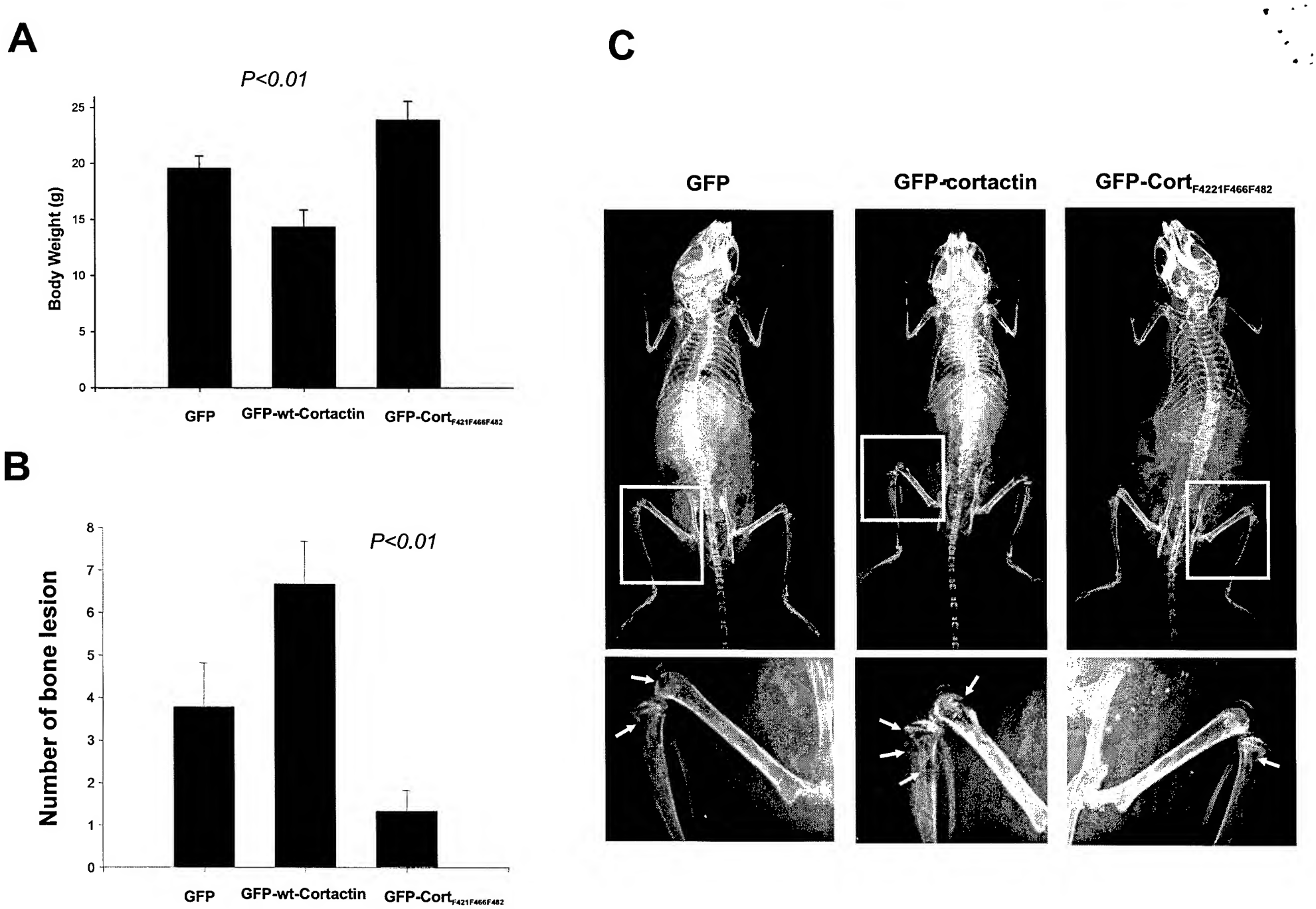
A
P<0.01
Body Weight (g)
25
20
15
10
5
0
GFP
GFP-wt-Cortactin
GFP-Cort F421F466F482
B
P<0.01
Number of bone lesion
8
7
6
5
4
3
2
1
0
GFP
GFP-wt-Cortactin
GFP-Cort F421F466F482
C
GFP
GFP-cortactin
GFP-Cort F4221F466F482

Figure 3

A

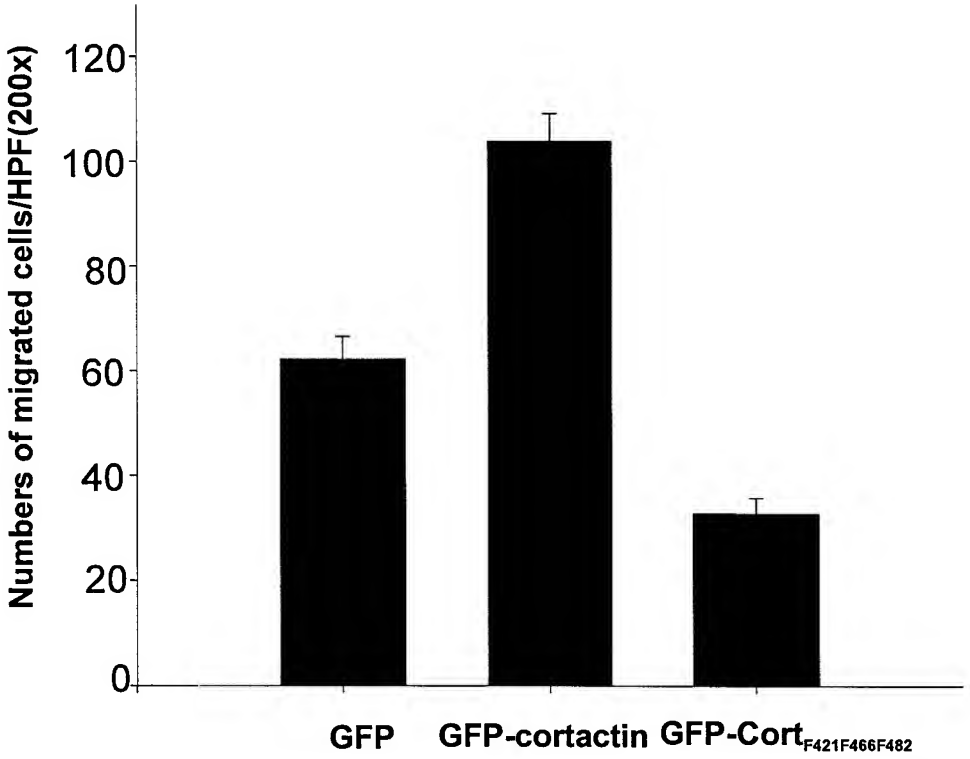
Numbers of migrated cells/HPF(200x)
120
100
80
60
40
20
0
GFP
GFP-cortactin
GFP-Cort$_{F421F466F482}$

B

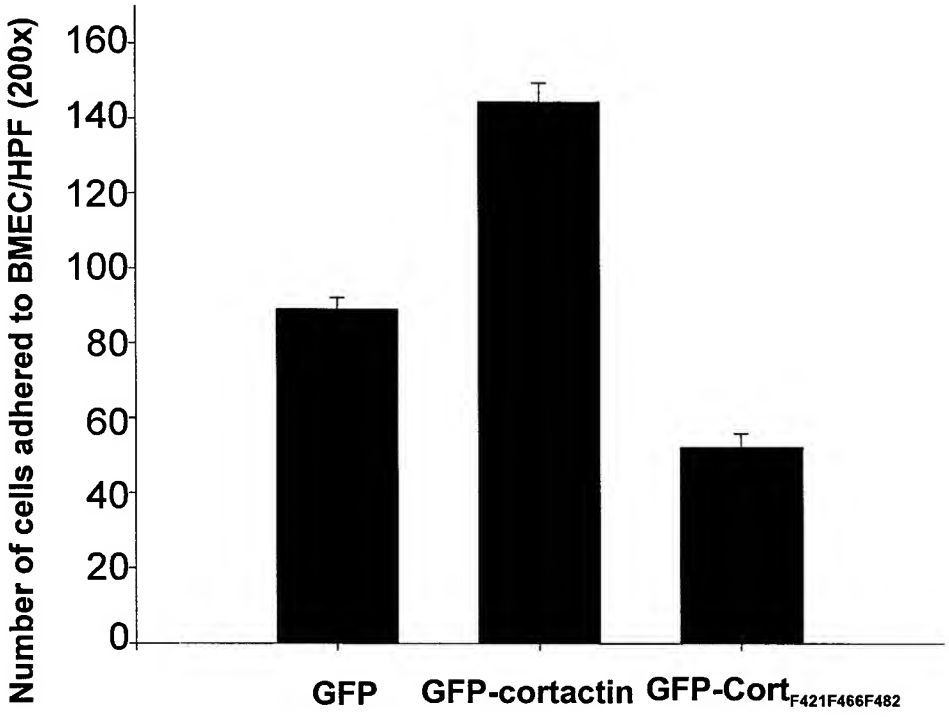
Number of cells adhered to BMEC/HPF (200x)
160
140
120
100
80
60
40
20
0
GFP
GFP-cortactin
GFP-Cort$_{F421F466F482}$

Figure 4